# DOUBLE LAYER INTERACTION MODEL AND PARTICLE CONCENTRATION EFFECT IN WATER

by

Jianzhong Guo, M. Sc.

A Thesis

submitted to the School of Graduate Studies

in Partial Fulfilment of the Requirements

for the Degree

Doctor of Philosophy

McMaster University

PARTICLE CONCENTRATION EFFECT

DOCTOR OF PHILOSOPHY (1995)
(Geochemistry)

McMASTER UNIVERSITY
Hamilton, Ontario

TITLE: Double Layer Interaction Model and Particle Concentration Effect in Water

AUTHOR: Jianzhong Guo, B.Sc. (Tianjin University)
M. Sc. (Nankai University)

SUPERVISOR: Professor J. R. Kramer

NUMBER OF PAGES: X, 187

## ABSTRACT


The observation that an increase in particle concentration increases the solute concentration has been noted by a number of investigators. This phenomenon is very important to re-suspension of particles and contaminant release and diagenesis. Various reasons for this effect have been proposed. This study investigates the role of repulsive forces acting among particles when they are close to one another (e.g. double layers overlap).

The approach was to assess all possible forces theoretically. The only significant long range force is the columbic force which is shown to increase the solute concentration. A double layer interaction (DLI) model was developed based on this theory. The predicted ionic strength effect is the same as has been observed experimentally. The model gives limits for the particle concentration effect.

In other experiments, a Couette device was also constructed to examine the impact of inter-particle collision on adsorption.

Environmental implications of the particle concentration effect are that desorption (of contaminants) can occur up to 30% for clay sized particles in fresh water (ionic strength less than 0.1 m/l).

**ACKNOWLEDGEMENTS**

I would like to express my appreciation to all those who helped make this work possible.

I am particularly grateful to:

My supervisor committee, Dr. J. R. Kramer, Dr. Y. K. Chau and Dr. A. Hitchcock, for their guidance, encouragement, financial support and patience.

McMaster University, the Department of Geology.

The staff of the Department of Geology for their technical and administrative assistance.

My fellow graduate students, for their help and advice.

## TABLE OF CONTENTS

## LIST OF FIGURES

## LIST OF TABLES

# 1. INTRODUCTION

## 1.1 Significance of Adsorption in the Environment

Most chemical reactions that occur in natural waters take place at phase discontinuities. One of the most fundamental and significant interactions in the aquatic environment is the adsorption of contaminants onto suspended particles. In many natural systems, the behaviour of contaminants is profoundly affected by the presence of particle surfaces. The degree of partitioning between dissolved and adsorbed components can significantly alter the fate of contaminant species, including transportation, settling, resuspension, chemical transformation and biological uptake.

Suspended particles in a natural body of water consist predominantly of inorganic colloids, such as clays, oxides, metal hydroxides etc., organic colloidal matter of detrital origin, and living microorganisms. Most of the clay minerals have physical dimensions smaller than 1 to 2 $\mu m$. Many solid phases have specific surface energies higher than 0.1 $J \cdot m^{-2}$. Hence for particles that have specific surface areas of a few hundred $m^2 g^{-1}$, the total surface energy is of the order of 100 $J \cdot g^{-1}$.

The study of adsorption onto suspended particles is complicated. Even in single and reasonably well defined systems the interfacial and colloidal properties involve many variables and represent complex physical and chemical interactions. During the last decade, significant advances have been made in applying the concepts and mathematical formalism of coordination chemistry to metal-particle interactions. Current knowledge about aqueous surface chemistry has come primarily from studies of equilibrium metal adsorption in model laboratory systems. Models that require the use of highly detailed information have been developed for the oxide-solution interface. Such models are useful heuristic devices for probing our understanding of the basic physical-chemical nature of metal-particle interactions. Also, these models are being used increasingly to predict the transport of toxic and radioactive pollutant species in ground and surface waters, and to assess human and animal health risks.

Among the many models developed for describing the interactions that take place at the oxide-solution interface, surface complexation models are regarded to be the more realistic. Nevertheless, several observations of adsorption cannot currently be accounted for in such deterministic models. These effects include surface site heterogeneity [Benjamin & Leckie, 1981], nonadditivity in multiple-adsorbent systems [Honeyman, 1984], slow sorption kinetics [Kurbatov & Wood 1952; Hingston 1981; Li et al. 1984; Santschi 1984; Nyffeler et al 1984, 1986], and anomalous effects due to particle concentration [Atkinson et al. 1972; Enfield et al. 1976; O'Connor & Connolly 1980; Voice et al. 1983; Gschwend & Wu 1985; Di Toro et al. 1986]. Particle concentration effects is the topic of this research and thesis.

## 1.2 Phenomenon of Particle Concentration Effect

In an adsorption experiment, the distribution of the adsorbate between the adsorbed phase and the aqueous phase for linear partitioning is defined by the apparent partition coefficient as

where $q_e$ and $C_e$ are the adsorbed and the aqueous equilibrium concentrations of the

$$K_p = \frac{q_e}{C_e} \tag{1.1}$$

adsorbate respectively. From basic thermodynamic principles, one can show that the partition coefficient is a function of system variables such as pH, temperature, type of adsorbent and adsorbate etc., but should be indifferent to the amount of adsorbent used in the adsorption experiment. This presumption has been challenged by numerous observations collectively described as the "particle concentration effect" [Lotse et al. 1968; Grover and Hance 1970; O'Connor and Connolly 1980; Di Toro et al. 1985, 1986]. In these studies, the partition coefficient decreases when the concentration of the adsorbent is increased above a threshold level, and the level depends upon other factors.

### 1.3 Objective of the Research

The study of the particle concentration effect on adsorption has been rather controversial. Some researchers do not agree that the phenomenon actually exists, dismissing it as a procedural artifact. While Di Toro [1986] reported the effect for various systems (metal and organics adsorption onto clay, quartz and glass beads, etc.), others (e.g. McKinley & Jenne [1991]) failed to observe the phenomenon at all.

This research focuses on the following questions:

1. Is the particle concentration effect merely an experimental artifact, or is it real and occurs ubiquitously?

if the answer is yes,

2. What is the mechanism and what are the important factors and

parameters?

3. How can one model the process mathematically?

and 4. What are the environmental implications of the particle concentration effect in adsorption?

As developed later, this research concentrates on a laboratory study with a well defined synthetic system. Natural systems appear to be too complex to analyze mechanistically and with rigour. For example, one of the major problems that hampers the study of the particle concentration effect in natural systems is the difficulty of a defintive liquid/solid phase separation. Natural sediments have a large size distribution. The smaller-sized fractions can not be separated well by methods such as filtration and centrifugation. Depending on the situation, a portion of the colloids may remain in the solution phase after the solid-liquid separation procedure. These colloidal particles carry surface adsorbed substances. This fraction of colloidal particles may be responsible for the particle concentration effect phenomenon.

## 1.4 Hypotheses Offered to Explain the Phenomenon

Hypotheses on the particle concentration effect may be categorized into "positive" and "negative" types. The "negative" theories declare that the particle concentration effect is simply due to experimental artifacts. The "positive" types, on the other hand, suggest that some "intrinsic" explainable factor(s) exist(s).

The "negative" concept has been explained as follows:

*(1) Kinetic effects [Karickhoff 1984]:*

Equilibrium is reached more slowly at higher particle concentration. Karickhoff found equilibrium conditions at high particle concentration only after days. If sufficient time is not allowed for the higher particle concentrations, the loading per unit weight of particle will be lower than for the condition of low particle concentration. This conjecture, rational as it may be, can readily be tested. Therefore non-equilibrium is highly unlikely as a fundamental explanation for the particle effect. Furthermore specific studies can and should always be assessed for achievement of steady state/equilibrium.

*(2) Aggregation of the adsorbent [Grover and Hance 1970]:*

Particles may tend to aggregate, reducing surface area available to adsorption, at higher particle concentrations. This concept might explain some conditions, depending on the properties of the adsorbent and the adsorbate. Some adsorbents aggregate easier than others. For example, adsorption of organics may be susceptible to aggregation because of steric effects, but metal ions are probably too small to be affected by such aggregation, since surfaces within an aggregation are still accessible to them.

*(3) The existence of a third adsorption phase [Griffin and Au 1977; Carter and Suffet 1982; Voice et al. 1983; Curl and Keolelan 1984; Morel and Gschwend 1987]:*

This is the most popular explanation of the particle concentration effect. Particle adsorbents are postulated to release fine colloids or ligands into solution. A significant portion of the sorbates will be associated with this "third phase" either by adsorption or complexation. Separation of the "third phase" from the solution and the solid is virtually impossible. Therefore the portion of the sorbate associated with the "third phase" will be detected and included as part of the solution phase concentration. When a series of adsorption experiments is conducted using different amounts of particles, more "third phase" will be released into the solution when more solids are added into the system. After solid-liquid separation, the concentration of the "third phase" in the liquid phase will be higher as compared with the case of low particle concentration (Figure 1.1). In other words, because of the inability to separate the colloid completely from the solution, the apparent equilibrium of sorbate partition will appear to shift to the solution side when more solids are added into the system.

*(4) No particle effect [McKinley and Jenne 1989]:*

Through their systematic experiments on adsoprtion of heavy metals on iron oxy-hydroxide, McKinley and Jenne observed no particle concentration effect. They conclude that the effect is an experimental artifact which can be avoided if experiments are carefully controlled.

The "positive" hypotheses try to correlate the phenomenon with some sort of inter-particle interaction. Presently, there are three basic theories:

*(1)* Di Toro [1986] was the first to speculate that inter-particle interactions are an inherent reason for the particle concentration effect. He developed an empirical model which works fine for experimental curve-fitting. He did not specify the mechanism of the particle concentration effect in detail. Di Toro has done studies on adsorption of both organics and heavy metals on sediments or glass beads. Some of his data may be questionable, however, because the experiments were conducted under conditions of supersaturation with respect to the sorbate.

*(2)* Mackay and Powers [1987] suggest that inter-particle collisions may play a role in the desorption of loosely adsorbed hydrophobic organics. Figure 1.2 illustrates the mechanism of this theory schematically. The adsorbed concentration on the particle

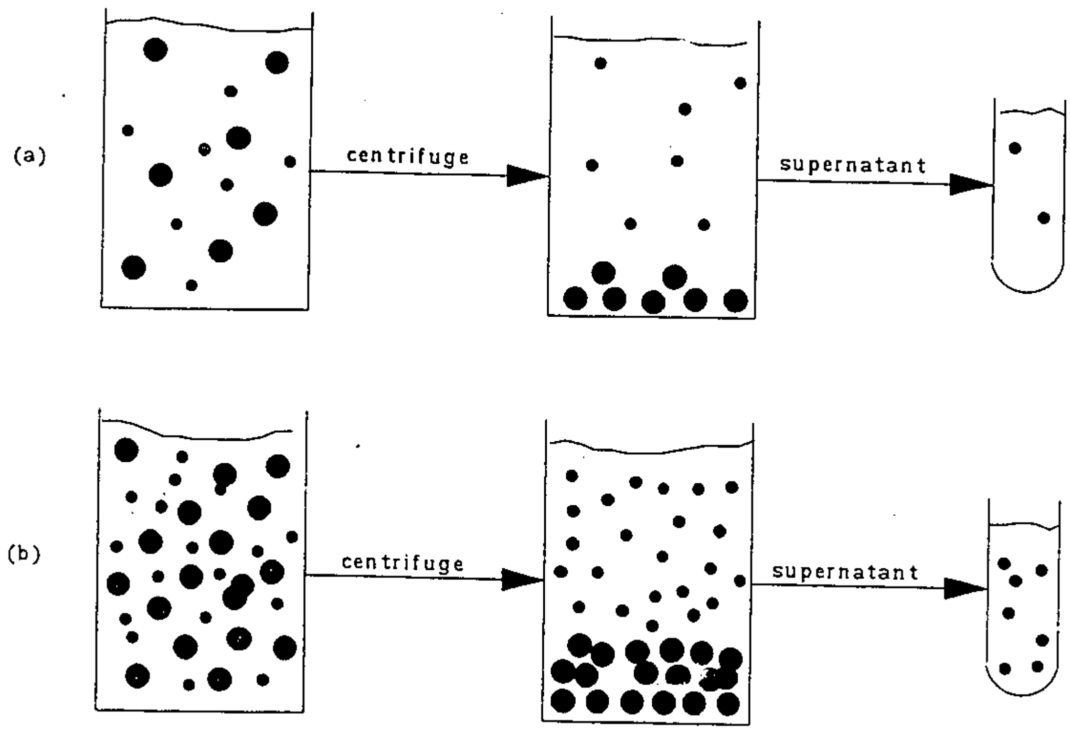


Fig.1.1 Schematic of the "third adsorption phase" theory
(a) low particle concentration
(b) high particle concentration

accumulates until a collision happens. The collision will "shake off" at least part of the adsorbed sorbates back into the solution and the accumulation starts again until the next collision. The process is at dynamic equilibrium, and the amount of adsorption is limited by the frequency of collision. Increasing particle concentration will result in increasing frequency of collision. The accumulation of the sorbates on the particle will decrease, because the next collision comes earlier than that for low particle concentrations.

*(3)* the double layer interaction theory, proposed here in the following section.

**1.5 Proposing the Double Layer Interaction Theory**

As presented in Section 1.4, negative hypotheses dismiss the particle concentration effect as operational artifacts. Certainly these negative explanations can be operative under certain conditions to create an artificial particle concentration effect. Through these processes, desorption or shift of the adsorption equilibrium will never happen. Showing the validity of a negative theory in a specific case, however, does not automatically negate the potential for a real particle concentration effect.

Higher particle concentration implies stronger interparticle interaction, i.e., shorter interparticle distances and increased frequency of interparticle collision. Existing "positive" theories tend to bridge interparticle interaction with the particle concentration. Unfortunately these hypotheses are either not specific or questionable. Di Toro [1986] suggested interparticle interaction as the cause of the phenomenon, yet no particular mechanism was proposed. The collision theory of Mackay and Powers [1987] can not explain the fact that some of the studies on particle concentration effect failed to observe the phenomenon (to be discussed later).

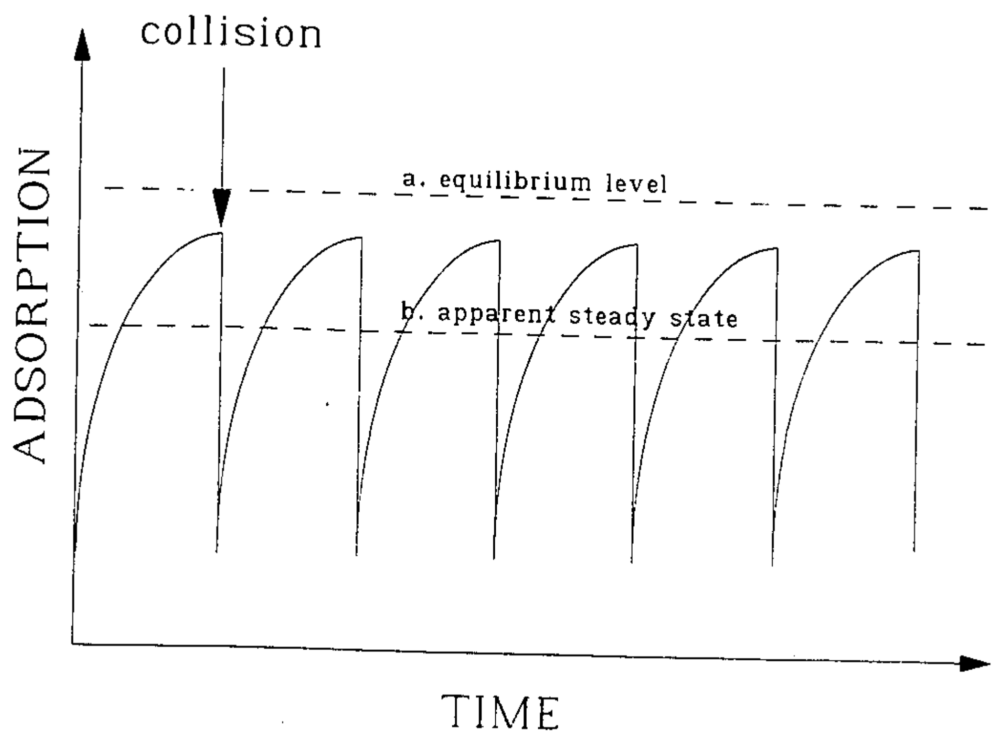


Fig.1.2 proposed hypothesis of collision effect on adsorption

An analysis of Di Toro's experiments shows that the particle concentration effect appears to be a function of ionic strength, with the particle effect diminishing with increasing ionic strength. Simultaneously the electric double layer will decrease as ionic strength increases. A parallel change is the decrease in thickness of the electric double layer, which is also a function of ionic strength. It is well known that double layers of particles interact when particles are close to each other. The interaction is mostly electrostatic in nature and the interaction can be long-range when ionic strength is low. Electrostatic force plays an important role in adsorption. It is speculated that the interaction of double layers of adsorbent particles reduces adsorption, causing the particle concentration effect. A double layer interaction (DLI) model is developed along this line of reasoning and is tested by both a theoretical and an experimental study.

The particle concentration effect has been observed on both inorganic and organic adsorbates. Therefore the DLI theory must be general enough to explain many types of adsorption.

# 2. MODELLING THE PARTICLE CONCENTRATION EFFECT

In order to mechanistically explain and model the particle concentration effect on adsorption, it is necessary to explore the various possible adsorption mechanisms and subsequently to analyze the impact of interparticle interactions based on the mechanisms.

## 2.1 Adsorption Theories in General

Adsorption can be broadly classified into chemical and physical mechanisms. In principle, an adsorption process is chemical if there is transfer or sharing of electron(s) between sorbent and sorbate. Otherwise, it is physical adsorption.

### 2.1.1 Physical Adsorption

Contrasted to "bonding", any attraction forces between adsorbent and sorbate, such as dispersion forces, electrostatic forces, can result in physical adsorption. Usually physical adsorption is

(1) non-specific

(2) non-stoichiometric

(3) lower in adsorption energy

(4) multiple-layered, when sorbates are excessive

(5) reversible

### 2.1.2 Chemical Adsorption

The sorbate is attached to the adsorbent by means of chemical bonding. Chemical adsorption is often characterized as

(1) specific

(2) stoichiometric

(3) high adsorption energy

(4) single layer adsorption only

(5) poorly reversible

## 2.2 The Choice of the Adsorption Model

### 2.2.1 Classic Adsorption Models

Gouy and Chapman [Parks 1975; Grahame 1947] independently developed adsorption models. By assuming that ions can be represented by point charges, they derived theoretical expressions for surface charge, interfacial concentrations of potential determining ions and surface potential. The Gouy-Chapman model considers only electrical interactions, it cannot account for specific adsorption, i.e., adsorption involving chemical, dispersion or other non-electrostatic bonding. Also, the point-charge model of ions leads to unrealistically large ionic concentrations near the interface. Stern [Grahame 1947] refined the theory by including a term to account for specific adsorption and suggesting that ions retain their hydration sphere during adsorption and therefore can approach the surface no nearer than the dimesnion of their hydrated radii. Grahame altered Stern's treatment slightly by suggesting that only specifically adsorbed ions lose their hydration spheres and can approach to a distance equal to their unhydrated radii.

As modified, the Gouy-Chapman-Stern-Grahame (GCSG) adsorption model is still an oversimplification in that it treats the charge in the double layer as diffuse rather than discrete, and lumps all non-electrostatic terms into a single specific adsorption potential. The model does an adequate job of predicting electrical phenomena at many solid/liquid interfaces. When the model is applied to the metal oxide/aqueous solution interface, anomalies arise. The observed surface charge is considerably greater than that predicted, and the electrokinetic potential and colloidal stability do not bear the same relationship to surface charge as in model systems [Lyklema 1971; Ahmed 1972; Hunter & Wright 1971].

### 2.2.2 Surface Complexation Models

Yates [1975] was able to resolve many of the anomalies by assuming that adsorbed ions form interfacial ion pairs with a discrete charged surface. His model considers adsorption only of the potential determining ions and the specifically adsorbed metal. Schindler and Stumm and their co-workers further developed the idea [Schindler et al. 1976 a; b; Stumm et al. 1970]. Their model is based on chemical adsorption, the oxide surface is treated analogous to an amphoteric, polyprotic acid which can form covalent bonds with the sorbate. Davis and co-workers [1978 a;b;c] have synthesized and refined aspects of both models into a generalized model that can account for adsorption of trace metals and bulk electrolyte ions and for electrokinetic phenomena. This model is referred to as the Stanford Generalized Model for Adsorption (SGMA).

### 2.2.3 Physical Adsorption Model

James and Healy developed a model [1972 a;b;c;] in which adsorption is viewed as a physical process. The ions retain their inner hydration spheres, and a single layer of water molecules separates the sorbate from the surface. The extent of adsorption is governed by a combination of columbic, solvation and chemical terms.

### 2.2.4 The Choice of Adsorption Model

As noted, the fundamental conceptual difference between physical and surface complexation models is whether the adsorption induces chemical bonding or physical attraction. Both physical and chemical models can adequately describe much of the published trace metal adsorption data. In the meantime, all of the models have serious deficiencies when applied over wide ranges of sorbate concentration.

Surface complexation models have been the most popular and successful adsorption models. Nevertheless they do not account for "anomalous" effects such as the particle concentration effect. In the surface complexation model, the mechanism of adsorption is considered as chemical bonding. Chemical bonds are strong and short ranged, they can not theoretically accommodate the influence of the concentration of adsorbent particles. With the physical adsorption approach, however, it becomes possible to correlate the decrease of adsorption with change in the adsorption environment. In this study, therefore, the physical adsorption mechanism is explored.

### 2.2.5 Combination of Adsorption Forces

Physical adsorption in an aquatic solution may be caused by the following forces or effects [Ruthven 1984; James and Healy 1972 ]:

(1) columbic

(2) dispersive

(3) repulsive

(4) polarization

(5) hydrophobic

(6) solvation effect

An adsorption process usually results from the combination of these forces. Depending on the conditions, one or more of the forces may predominate.

There are other interactions involved, but their magnitude is small compared to the above listed interactions. The sorbate-sorbate interaction, for instance, can be neglected if the concentration of the sorbate is relatively low. Namely, the adsorption is carried on in the "Henry's Law range" where the relation between bulk and adsorbed concentration is linear [Ruthven 1984]. Also because of the low coverage of the solid surface, the influence of the adsorbed sorbates on the interparticle forces [Everett and Radke 1975] is also negligible.

*(1) The Columbic Force*

Generally speaking, the surface of a particle in an aqueous solution is charged. The uneven distribution of electric charges at the phase boundary originates for one of the following reasons:

a. chemical reactions at the surface

b. lattice imperfections at the solid surface and isomorphous replacement within the lattice

c. adsorption of surfactant ions

This distribution of electric charge is usually idealized as an electrochemical double layer. One layer of the double layer is envisaged as a fixed charge or surface charge attached to the solid surface, while the other layer is distributed more or less diffusely in the liquid in contact with the surface. The net charge of the system remains zero, i.e., the liquid layer contains an excess of counter ions, opposite in sign to the fixed charge and usually a deficit of co-ions of the same sign as the fixed charge. These counterions are electrostatically attracted by the charged surface, yet because of thermal motion, tend to become more evenly distributed through the solution.

The surface charge of particles plays an important role in adsorption. Not only does the electrostatic force contribute substantially to the adsorption of ionic and polar sorbates, but also the electrostatic field can induce a dipole in non-polar sorbates and subsequently enhance their adsorption. The Columbic force is generally the dominating force in a physical adsorption of ionic or polar sorbate in aquatic systems.

*(2) Dispersion Force*

The dispersion force is an attractive force due to the interaction of sorbate and adsorbent atoms. From the perspective of long-term statistical averages, electron clouds of atoms are distributed in a spherical symmetry. At certain times, however, greater or lesser deviations from spherical symmetry may occur, the centre of the positive and negative charges of the atom will differ, and a dipole will be formed. The behaviour of this dipole, which is variable in time, is similar to the motion of a harmonic oscillator. When two such oscillators approach each other, the minimum energy corresponds to a state in which the motion of the oscillating dipoles is in phase. Since the energy of two dipoles that interact in this way is less than their energy at an infinite distance between them, the logical consequence is that the two oscillators are influenced by attractive forces. These forces are called London or dispersion forces. Dispersion force is the second most important force in physical adsorption.

*(3) Repulsive Force*

The repulsive energy arises from the finite size of the nucleus and interactions of electron clouds. Nuclei are positively charged and will result in a repulsive force if brought too close to one another. This force opposes adsorption but is quickly attenuated with distance, and is much shorter-ranged as compared to dispersion forces. It is less important than most of the adsorption forces.

*(4) Polarization Force*

The polarity of a molecule is subject to the electrostatic environment. A strong foreign electrostatic field can induce polarity on a non-polar molecule, or enhance existing polarity. Its effect can be important for molecules of large polarizability.

*(5) Hydrophobic Effect*

Hydrophobic substances, e.g., hydrocarbons, tend to reduce their contact with water, and seek environments of less polarity. Such tendency results in the accumulation of organic sorbates at the solid-liquid interface. Here the adsorption is not caused by a particular affinity of these organics to the solid. Rather, it is because of the strong attractive forces between the polar water molecules which must be disrupted when any nonpolar solute is dissolved in water.

*(6) Solvation Effect*

Ionic sorbents such as metal ions in bulk solution are hydrated. An ion is wrapped by two layers of water molecules, which form the primary and secondary hydration sheathe. Before chemical bonding can form, the hydration sheath has to be completely removed. In the case of physical adsorption, it is believed that the sorbates can retain their primary hydration sheath. The physical interpretation of the non-electrostatic term in the Stern and some later models has been in dispute [Grahame 1947; Andersen and Bockris 1964; Levine et al. 1967; Barlow and Mcdonald 1967]. Nevertheless, it is generally agreed that this is a negative term in the case of metal ion adsorption on oxides. In other words, it must oppose adsorption rather than aid it. This is because the columbic term in the model is always favourable for cation adsorption on a surface, as long as it is negatively charged. On the other hand, it has been found experimentally that metal ions will not start to adsorb immediately after the pH has passed the point of zero charge (i.e., after the surface of the solid becomes negatively charged). The adsorption actually begins at a higher pH, when a more negative surface is obtained. Therefore, there must be an interaction that counteracts the columbic force and other adsorption forces, and this interaction is most likely the solvation energy [James and Healy 1972].

In the region adjacent to charged interfaces where electric fields of considerable magnitude exist, the water molecules adsorbed on the interface will undergo partial or complete electrical saturation. The electrical saturation results in the reduction of the dielectric constant of the surface water molecules, from a normal value of 78.5 to as low as 6, if the field is strong enough [Muirhead-Gould & Laidler 1967].

As the hydrated cation approaches the surface of the solid, which in this case is an insulator with a very low dielectric constant, part of the secondary hydration sheath of the cation must be replaced with the interfacial water of very low dielectric constant. Work must be done to remove the secondary solvation sheath. The primary hydration sphere of the cation is not perturbed since it is regarded as electrically saturated.

### 2.3 Calculation of Adsorption Energies

To correlate interparticle interactions of sorbent particles with a desorption effect, it is essential to quantify adsorption energies of all of the significant mechanisms. Given the above concepts on adsorption forces, the overall estimation of a given adsorption system is possible. Instead of adsorption forces, adsorption energies are used in the calculation. Conceptually, energy is the integration of force. Energy is a better term to use here because it is a scalar quantity and therefore directly additive. This is advantageous especially when considering interparticle interaction. Also, it can be directly linked to adsorption quantitatively.

The modelling of the adsorption system has limitations. To minimize the uncertainty inherent in complicated systems and to facilitate the modelling process, relatively simple adsorption systems have been selected.

The first system to be modelled is copper adsorption onto $\alpha$-quartz at pH 6 and

0.001 ionic strength. This system is also one of the systems that was chosen for preliminary experiments on the particle concentration effect. The free energy of adsorption, as mentioned earlier, is the summation of all the energy components listed in Section 2.2.5. In the copper-quartz case, the hydrophobic effect does not exist. Also the interaction among adsorbed sorbates is ignored here. This interaction may be ignored if the adsorption experiment is conducted at low sorbate concentration. Under such sorbate concentration the behaviour of adsorption is linear, indicating no interactions among sorbates.

An important parameter in the calculations is the location of the adsorbed cations, namely the distance between the surface of the cations and the plane of adsorption. Short-range forces are most sensitive to this parameter. Studies on some adsorbed cations have provided evidence that the cations are separated from the surface by at least one layer of water molecules [Cornet and Burwell 1968; Hathaway and Lewis 1969A, 1969B]. This finding suggests that the adsorption is physical, since it precludes the possibility of chemical bonding. If the sorbates were chemically bound to the surface, there would be no water molecules between the surface and the sorbate. In the calculation of the present model, it has been assumed that there is one layer of water molecules between the adsorbed ion and the solid surface. Figure 2.1 shows this assumption.

Information on surface structure of the sorbent (i.e., the topography of the surface and the distribution of different elements on the surface) is needed to perform the calculation. In the case of quartz, the lattice is composed of oxygen and silicon. The detailed data on the surface structure of quartz is adopted from Chem-X, a computer

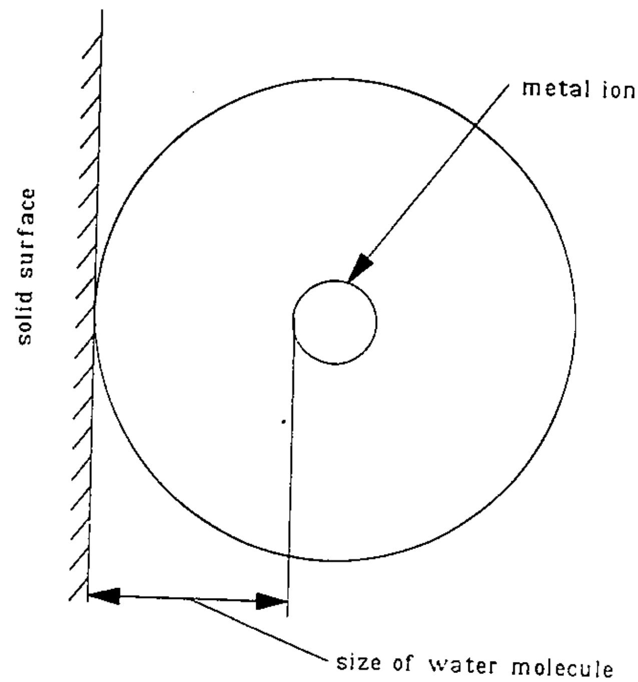


Figure 2.1 location of an adsorbed ion on the surface of solid

program used for mineral lattice information and calculations. Data were generated with Chem-X on the coordinates of the oxygen and silicon atoms in the surface lattices of $\alpha$-quartz. These coordinates were in turn used for the calculation of distances between an adsorbed ion and the surface atoms of the solid.

*(1) Dispersion Energy*

The free energy of adsorption resulting from the dispersion forces may be written in the form [Ruthven 1984]:

$$\Phi_D = -\frac{A_1}{r_{ij}^6} - \frac{A_2}{r_{ij}^8} - \frac{A_3}{r_{ij}^{10}} \tag{2.1}$$

where $A_1$, $A_2$ and $A_3$ are constants, and $r_{ij}$ is the distance between atoms *i* and *j*. From Equation 2.1, it can be seen that the dispersion force decreases rapidly with inter-atomic distance. Therefore, only the first term in equation 2.1 is employed for the calculation of the dispersion energy, since the other terms are usually negligible. In practice, the dispersion energy is calculated as the sum of the pair-wise interactions between a sorbate atom and each sorbent atom that is located within a certain radius from the sorbate atom (Figure 2.2). So the dispersion energy may be rewritten as

$$\Phi'_D = \sum_j -\frac{A_{ij}}{r_{ij}^6} \tag{2.2}$$

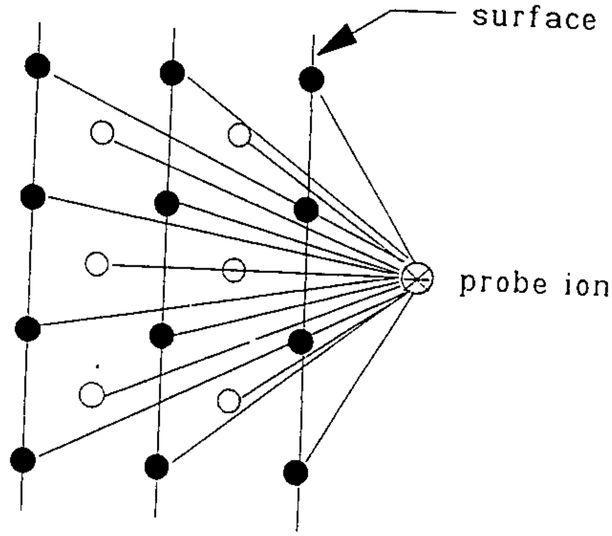


Figure 2.2 pair-wise calculation of dispersion energy between sorbate and sorbent

where $A_{ij}$ is the constant of dispersion potential energy. The constant can be estimated by one of the following expressions [Derrah and Ruthven 1975]:

London:

$$A_L = \frac{3}{2}\,\alpha_i\,\alpha_j\,I \tag{2.3}$$

where

$$\frac{1}{I} = \frac{1}{I_i} + \frac{1}{I_j}$$

or Slater-Kirkwood:

$$A_{s-k} = \frac{3eh\quad \alpha_i\,\alpha_j}{4\pi\sqrt{m}\left(\frac{\sqrt{\alpha_i}}{n_i}\right) + \left(\frac{\sqrt{\alpha_i}}{n_j}\right)} \tag{2.4}$$

or Kirkwood-Müller:

$$A_{K-M} = 6mc^2\,\frac{\alpha_i\,\alpha_j}{\left(\frac{\alpha_i}{x_i} + \frac{\alpha_i}{x_j}\right)} \tag{2.5}$$

where

$\alpha_i$ = polarizability of a sorbent atom

$\alpha_j$ = polarizability of a sorbate atom

c = speed of light in vacuum

h = Planck's constant

i = subscript for sorbent

j = subscript for sorbate

I = ionization potential: 36.83 eV for $Cu^{2+}$, 13.62 eV for $O^{-.5}$, 16.345 eV for $Si^{+1}$

m = electronic mass: 0.511 MeV

$n_i$ = number of electrons of the outermost shell of a sorbate atom: 18 for $Cu^{+2}$

$n_j$ = number of electrons of the outermost shell of a sorbent atom: 6.5 for $O^{-.5}$, 3 for $Si^{+1}$

$x_i$ = diamagnetic susceptibility of the sorbate: $1.993\times10^{-29}$ for copper

$x_j$ = diamagnetic susceptibility of the sorbent: $1.983\times10^{-29}$ for oxygen, $5.534\times10^{-31}$ for silicon

Note that the valences of oxygen and silicon atoms located at the surface of the quartz crystal are different from normal value of -2 and +4, because surface atoms are unsaturated. Instead, here -0.5 and +1 are used respectively, according to Stewart et al. [1980].

*(2) Repulsive Energy*

The repulsive energy arising from the finite size of the atom may be represented as

$$\Phi_R = \frac{B_{ij}}{r_{ij}^{12}} \tag{2.6}$$

in which

$$B_{ij} = \frac{1}{2} A_{ij} r_e^6 \left(1 + \frac{\alpha_i e_j^2 R_e^2}{3 A_{ij}}\right) \tag{2.7}$$

where

$B_{ij}$ = constant of repulsive potential energy

$e_j$ = charge of the solid atom, e.s.u., -0.5 for surface oxygen and +1 for silicon.

$r_e$ = equilibrium separation between atoms (sum of van der Waals radius), $1.52\times10^{-10}$ m for oxygen; $2.1\times10^{-9}$ m for silicon

The repulsive energy is fairly short-ranged as indicated by the 12th power in the denominator of equation 2.6.

*(3) Polarization Energy*

The contribution of polarization is given as

$$\Phi_p = -\frac{1}{2} \alpha_i E^2 \tag{2.8}$$

using

$$E - \nabla\left(\sum_{j} \frac{e_j}{r_i - r_j}\right)$$

where

$r_i$ = position vector of a sorbate atom

$r_j$ = position vector of a sorbent atom, generated by Chem-X program

For the calculation of short range interactions, i.e., dispersion, repulsive and polarization energies, a probe ion was positioned over the surface of a unit lattice cell. As can be seen from Figure 2.2, the distance between a probe sorbate ion and surface atoms increases as the pair-wise interaction goes to surface atoms located further away from the lattice immediately adjacent to the sorbate atom. Calculation reveals that short-ranged interactions diminish so quickly that interactions between the probe atom and sorbent atoms farther than 6 lattice cells away are negligible. Dispersion, repulsive and polarization potential energies were calculated accordingly and summed as a total short-ranged potential energy.

The surface of quartz is constructed by oxygen-silicon tetrahedra and is not homogeneous on an atomic scale. Interaction energies will be affected by the location of the sorbate on the surface of the quartz. It is therefore necessary to repeat the calculation with the probe ion systematically positioned all over the surface of the cell. Also the surface of the sorbent is not flat at the atomic scale. The vertical coordinate of the sorbate ion depends on the geometry of the atom arrangement on the surface (Figure

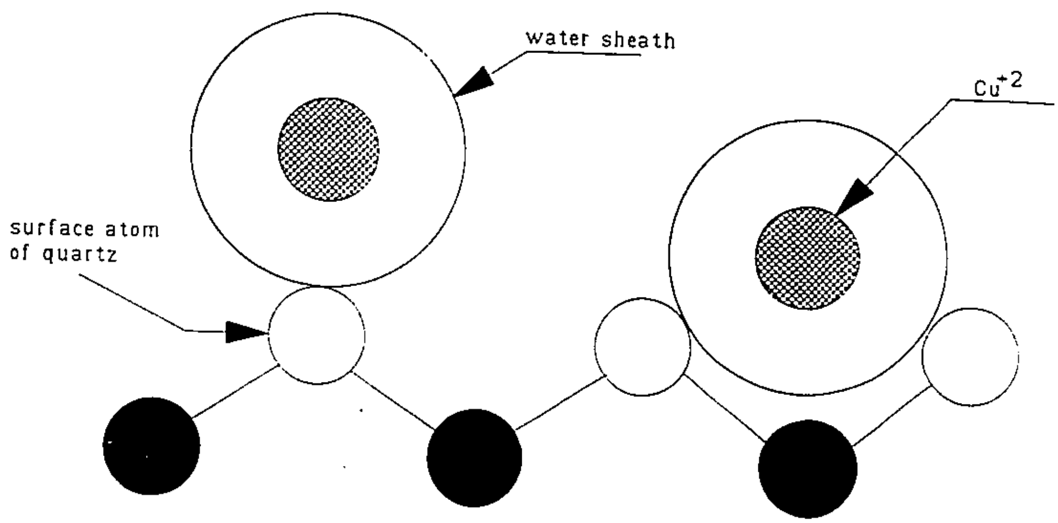


Figure 2.3 schematic of $Cu^{2+}$ adsorption on quartz

2.3). Such calculations resulted in an undulating interaction potential distribution with maxima and minima, as shown schematically in Figure 2.4. The depressed valleys indicate locations of stronger adsorption potential. The minus sign here simply means that the energy is attractive. Since the potential distribution continues over the surface, the adsorbed ions can usually be regarded as mobile [Ross and Olivier 1964]. At low sorbate concentration, the coverage of the surface will be low. One can presume that all adsorbed sorbates will move to depressed potential wells on the surface. In other words, the potential energies of the short-ranged interactions may be represented by the minimum value obtained from the calculation of a unit cell. The outcome of the calculation also depends on how the constants of Equation 2.2 are determined. Each of the equations for the calculation of the constants ( Equations 2.3 to 2.5) gives slightly different results [Table 2.1].

**Table 2.1 Constants for the calculation of dispersion force obtained with Equations 2.3 to 2.5.**

| Interaction Pair | Slater-Kirkwood (cal•cm$^6$/mol) | London (cal•cm$^6$/mol) | Kirkwood-Müller (cal•cm$^6$/mol) |
|---|---|---|---|
| Si--Cu | $1.33\times10^{-42}$ | $1.92\times10^{-42}$ | $1.44\times10^{-43}$ |
| O--Cu | $8.17\times10^{-43}$ | $8.61\times10^{-43}$ | $1.02\times10^{-42}$ |

The potential energy of short-ranged interactions was found to be ca. -2.3 kcal/mol, representing one of the potential wells on the surface. Listed in Table 2.2 is a break down of the energy into its components.

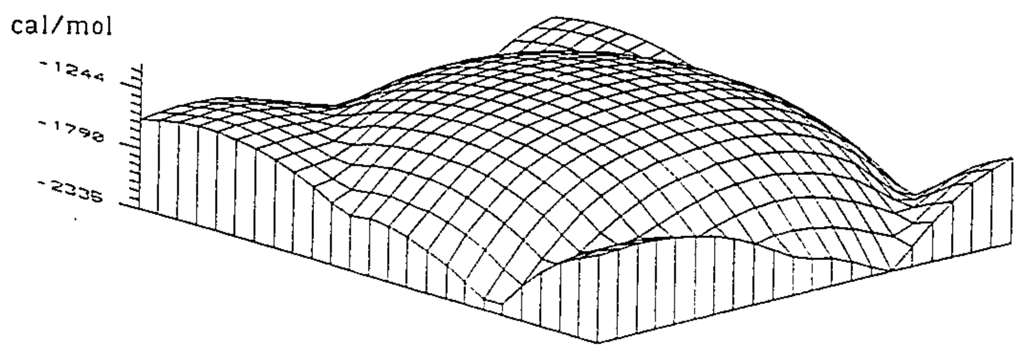


Figure 2.4 potential energy distribution of short-ranged interactions between $Cu^{+2}$ and quartz

**Table 2.2 Maximum short-ranged interactions of Cu on quartz.**

| Interaction Pair | Dispersion (cal/mol) | Repulsive (cal/mol) | Polarization (cal/mol) | Summation (cal/mol) |
|---|---|---|---|---|
| O--Cu | -1762 | 112 | -16 | -1666 |
| Si--Cu | -779 | 102 | -15 | -692 |
| Total | -2541 | 214 | -31 | -2358 |

In contrast, Table 2.3 shows energy data for the location on the surface of the quartz where the

short-ranged interactions are minimum.

**Table 2.3 Minimum short-ranged interactions of Cu on quartz.**

| Interaction Pair | Dispersion (Cal/mol) | Repulsive (Cal/mol) | Polarization (Cal/mol) | Summation (Cal/mol) |
|---|---|---|---|---|
| O--Cu | -746 | 30 | -10 | -726 |
| Si--Cu | -289 | 7 | -10 | -292 |
| Total | -1035 | 37 | -20 | -1018 |

It can be seen that in this particular adsorption system, dispersion energy is predominant among the short-ranged interactions.

James and Healy [1972], rather than making theoretical estimates, adopted the experimental data of Dugger et al. [1964] for the free energy change of non-electrostatic adsorption. Using metal ions to replace the weak acidic silanol (-SiOH) groups of the surface of hydrated silica gel, Dugger et al. tested 17 metal ions for free energies of non-electrostatic adsorption. A value of -2.0 kcal/mol was found for $Cu^{2+}$. It is no surprise that Dugger's value is smaller than these estimates. Conceptually, Dugger's data represent the average free energy change of non-electrostatic adsorption. The theoretical modelling process, however, acknowledges heterogeneity of interaction intensity. The magnitude of interaction energy calculated is therefore surface-location dependent. The 2.3 kCal/mol of Table 2.2 is the maximum interaction energy. For the majority of sites on the surface of quartz, lower interaction energies are expected.

*(4) Solvation Energy*

The free energy required to establish a field in a continuous dielectric medium about a spherically symmetric ion (joule per ion) is given by [Andersen & Bockris 1964]

$$G^{o} = \frac{1}{2} \iiint_{v} \bar{X} \cdot \bar{D} dV \tag{2.9}$$

where

$$\bar{D} = \frac{z\, e}{4\pi \rho^2} \quad \textit{electric displacement vector}$$

in which the electric field vector

$$\bar{X} = \frac{z\, e}{4\pi\ \epsilon_o\ \epsilon_p\ \rho^2}$$

where

$\varepsilon_\rho$ = dielectric permittivity of the medium distance $\rho$ from the ion

$\varepsilon_o$ = electric permittivity of free space, $8.85\times10^{-12}$ coulomb $V^{-1}$ $m^{-1}$ in SI units.

Thus if the ion was removed from the medium of continuous dielectric, $\varepsilon_{\rho,i}$, and placed in another medium of dielectric, $\varepsilon_{\rho,j}$, then the change in free energy is given by [Andersen & Bockris 1964]

$$\Delta G^o = \frac{z^2 e^2}{2(4\pi)^2} \int_{\phi=0}^{2\pi} \int_{\theta=0}^{\pi} \int_{P=\rho}^{\infty} \frac{\sin\theta}{\varepsilon_o P^2} \cdot \left( \frac{1}{\varepsilon_{\rho j}} - \frac{1}{\varepsilon_{\rho i}} \right) d\Phi \; d\Theta \; dP \qquad (2.10)$$

Born (1920) first used this approach to estimate the contribution of secondary solvation energy to the total hydration energy of aqueous ions. The equation of Born was found to be of accurate [Laidler et al. 1956, 1976]. Sacher and Laidler [1964] developed simpler expressions which give similar results to that of Andersen and Bockris [1964]. In this study, Sacher and Laidyler's equation is adopted for the calculation of the secondary solvation energy:

$$\Delta G^o_{solv} = \left( \frac{z^2 e^2 N}{16\pi \varepsilon_o} \right) \left( \frac{1}{r_{ion} + 2r_w} - \frac{r_{ion}}{2(r_{ion} + 2r_w)^2} \right) \left( \frac{1}{\varepsilon_{inter}} - \frac{1}{\varepsilon_{bulk}} \right) + \left( \frac{z^2 e^2 N}{32\pi \varepsilon_o} \right) \left( \frac{1}{r_e + 2r_w} \right) \left( \frac{1}{\varepsilon_{solid}} - \frac{1}{\varepsilon_{inter}} \right) \qquad (2.11)$$

in which

$$\varepsilon_{inter} = \frac{\varepsilon_{bulk} - 6}{1 + 1.2x10^{-17}\left(\frac{d\phi}{dx}\right)^2} + 6$$

N = Avogadro's number

$r_{ion}$ = radius of the adsorbed ion, for $Cu^{2+}$ $6.3\times10^{-11}$ m

$r_w$ = radius of water molecule, $1.38\times10^{-10}$ m

z = charge of the adsorbing ion, -2 for $Cu^{2+}$

$\varepsilon_{bulk}$ = dielectric constant of the bulk water,

$\varepsilon_{inter}$ = dielectric constant of the interfacial water

$\varepsilon_{solid}$ = dielectric constant of the solid

The (secondary) solvation energy is calculated to be 8.7 kcal per mole, using equation 2.11 for the Cu-Quartz system. As discussed earlier, the solvation energy is positive and therefore acts against adsorption.

*(5) Columbic Energy*

At standard condition, the free energy change of adsorption due to the electrostatic interaction, or columbic energy, can be expressed as [James & Healy 1972]:

$$\Delta G^{\circ}_{coul} = F\,\Delta\psi_x \tag{2.12}$$

which is the work to bring a mole of ions with a charge of z from infinity to a plane where the surface potential is $\Psi_x$. Here F is the Faraday constant. In Equation 2.12

$$\Delta\psi_x = 2\frac{RT}{zF}\ln\left(\frac{(P+1) + (P-1)\exp(-\kappa x)}{(P+1) - (P-1)\exp(-\kappa x)}\right) \qquad (2.13)$$

$$P = \exp\left(\frac{zF\psi_o}{2RT}\right) \qquad (2.14)$$

$$\kappa = \left(\frac{e^2\,\Sigma_i\, n_i\, z_i^2}{\epsilon\epsilon_o\, k\, T}\right)^{0.5} \qquad (2.15)$$

where

- e = element charge
- n = number of background electrolyte ions per $cm^3$
- k = Boltzmann constant
- x = distance from the solid surface
- $z_i$ = charge of ions in bulk solution
- $\varepsilon$ = dielectric constant of water
- $\varepsilon_o$ = dielectric constant for vacuum
- $\kappa$ = reciprocal thickness of the double layer
- $\psi_o$ = potential at the surface of the solid

The surface potential $\psi_o$ is estimated by [Healy et al. 1977; McGrail et al. 1986]:

$$\sinh\left(\frac{y_0}{2}\right) = \frac{\gamma\delta\sinh(y_N - y_0)}{[1+\cosh(y_N - y_0)]} \qquad (2.16)$$

Where

$$y_0 = \frac{q\psi_0}{kT}$$

and $y_N$ is the Nernst potential given by

$$y_N = 2.3\left(\frac{RT}{zF}\right)(pH_{pzc} - pH)$$

where

$pH_{pzc}$ = pH of point of zero charge

$\gamma$ = dimensionless constant given by

$$\gamma = \frac{\theta N_s}{4Lc}$$

$\theta$ = Debye screening parameter ($cm^{-1}$), given by

$$\theta = \sqrt{\left(\frac{2\rho L^2 q^2 I}{\epsilon RT}\right)}$$

$\rho$ = density of water ($Kg/m^3$)

I = ionic strngth (mole/kg)

$\varepsilon$ = dielectric constant for water

R = gas constant

$N_s$= number of surface silanol groups ($cm^{-2}$)

L = Avogadro's number

c = electrolyte concentration (mole/cm$^3$)

$\delta$ = constant defined by

$$\delta = 2 \times 10^{\frac{\Delta pk}{2}}$$

$\Delta pK = pK_- - pK_+$

the pKs are effective dissociation constants for the surface silanol groups, given by:

$$K_- = \frac{[SiO^-][H^+]_s}{[SiOH]}$$

$$K_+ = \frac{[SiOH][H^+]_s}{[SiOH_2^+]}$$

As indicated by equation 2.16, the surface potential of a particle is regulated by the pH of the system. The range of the electrostatic interaction, on the other hand, depends upon the ionic strength. Once these two parameters are defined, the interaction energy can be readily obtained with equations 2.12 to 2.16. The result of the calculation is plotted in comparison with the short range forces in Figure 2.5. At the given conditions, as can been seen from the plot, short range forces are less important both in terms of magnitude and distance of interaction. The change in electrostatic free energy at the plane of adsorption is -9.7 kcal per mol. The combination of the two potential energies is also shown in the plot.

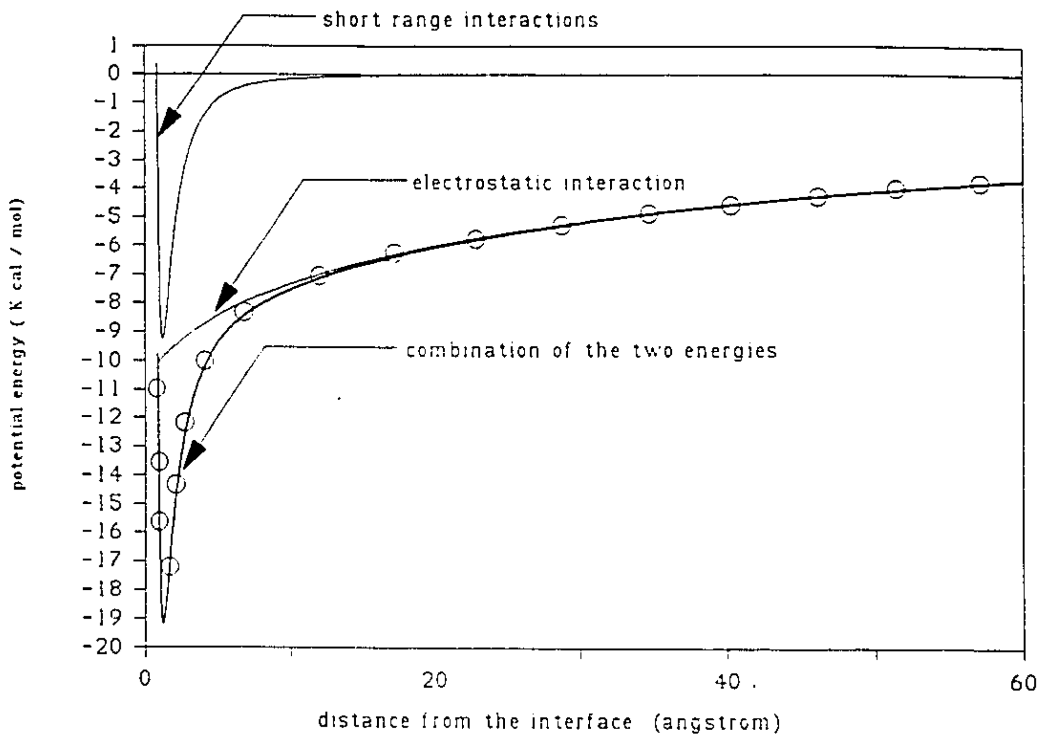


Figure 2.5 comparison and combination of short range and electrostatic interactions (ionic strength $10^{-4}$ mol/l, pH 5)

## 2.4 Development of Double Layer Interaction Theory

### 2.4.1 DLI as Mechanism of Particle Concentration Effect

In the study of adsorption, the affinity of the sorbate to the solid surface is often expressed as a partition coefficient:

$$K_p = \frac{\textit{sorbate concentration on solids}}{\textit{sorbate concentration in solution}} \tag{2.17}$$

At low sorbate concentration, the adsorption will follow a linear pattern:

$$\Gamma = K_p\, C \tag{2.18}$$

where $\Gamma$ is the amount of adsorption per unit sorbent, or concentration of adsorption, and C is the sorbate concentration in solution. Equation 2.18 is a classical expression for adsorption, in which the concentration of sorbent is irrelevant, since sorbent concentration is not furnished in the equation, nor is $K_p$ regarded as a function of it. However the following theoretical reasoning suggests that this is not always true.

Two scenarios can be proposed for high sorbent concentration. First, the interparticle distances will decrease as a result of high particle concentration. Consequently, the frequency of interparticle collision will increase. The effect of interparticle collision will be discussed later in chapter 3. Here the focus will be on the effect of decreased interparticle distance.

As has been discussed in Section 2.2.5, particles in an aquatic system are usually charged, and surrounded by an electric double layer. At low particle concentration, the

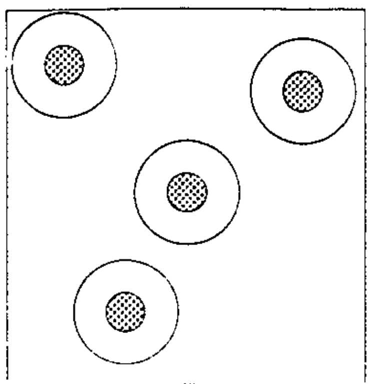

a. low particel concentration

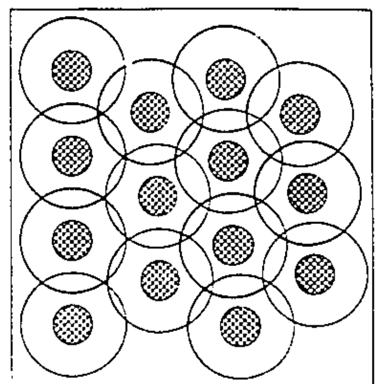

b. high particle concentration

Figure 2.6 significant double layer interaction happens at high particle concentration particles are scattered far apart (Figure 2.6 a) and there is no significant interaction among particles except some occasional interparticle collisions. Increasing particle concentration will reduce interparticle distance, eventually causing overlapping of double layers (Figure 2.6 b.). The overlap of the double layers changes the potential balance of the system, which can be qualitatively analyzed using Figure 2.7. Suppose curve 1 and curve 2 represent the adsorption energy to two different particle surfaces respectively. Note that here only the electrostatic potential is considered. With the existence of long-ranged columbic force, short-ranged forces are much less important in terms of interparticle interaction. In other words, short-ranged forces can barely have any impact on another particle. At low particle concentration, the particles are far away from one another, and potential curve 2 does not overlap with potential curve 1. The potential energy difference between the surface of the particle and the bulk solution for the adsorption of the sorbate is $\Delta G_o$ in Figure 2.7. When the electric double layers of two particles overlap as a result of increased particle concentration, the electrostatic adsorption forces of the two particles overlap. The electrostatic adsorption forces of the two particles on a metal ion will counteract each other. In terms of adsorption potential energy, however, the potential energy will be cumulative, forming potential curve 3 [Verwey and Overbeek 1948]. At high particle concentration, for the bulk metal ions sandwiched between the particles, the free energy change of adsorption, i.e., $\Delta G_2$ is now less than $\Delta G_o$, because the potential difference between adsorbed ions and ions in the solution has been reduced by $\Delta G_1$. The closer the two particles, the smaller $\Delta G_2$ becomes, which means less adsorption.

### 2.4.2 Mathematical Modelling of Double Layer Interaction

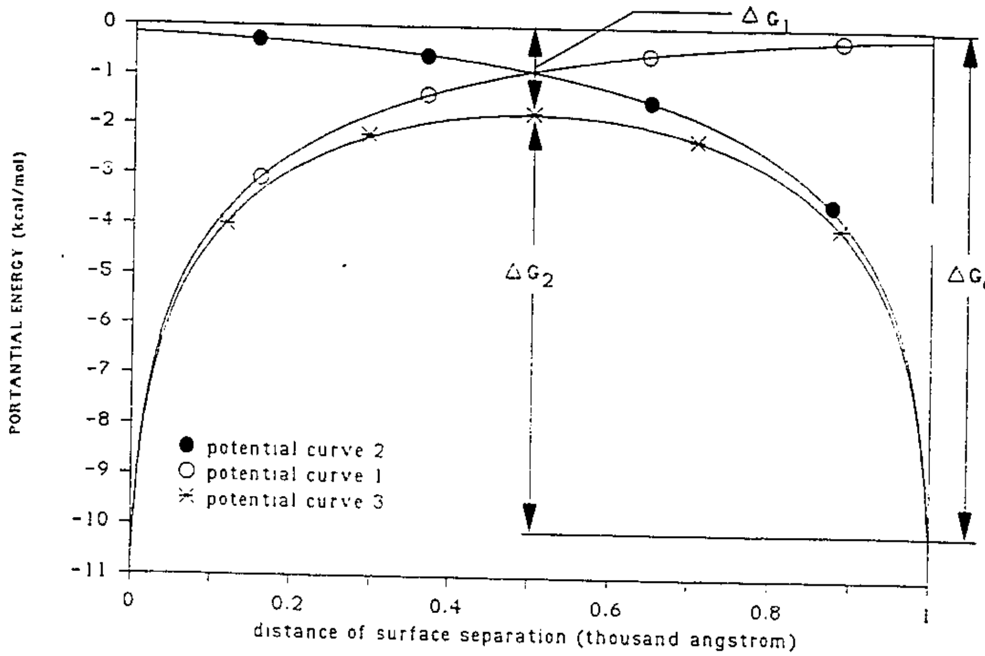


Figure 2.7 DOUBLE LAYER OVERLAP AND REDUCING OF ADSORPTION ENERGY

Quantitative estimation of the change of adsorption upon the impact of particle concentration was attempted in this study. As discussed below, through the theoretical relationship between adsorption energy and adsorption constant, it can be deduced that a small reduction of the adsorption energy can cause significant change in adsorption, regardless of the magnitude of the absolute adsorption potential energy.

At sufficiently low sorbate concentrations, the equilibrium relationship between aqueous phase and adsorbed phase concentrations will be linear. As mentioned before, the adsorbed quantity is thus proportional to the adsorption constant:

$$\Gamma = K_p \cdot C \qquad (2.18)$$

where $K_p$ is the partition coefficient and C the bulk concentration of the sorbate. For standard condition, $K_p$ can be described as [Ross & Olivier 1964; Ruthven 1984]:

$$K_p = A \cdot \exp\left(-\frac{\Delta G^o}{RT}\right) \qquad (2.19)$$

where A is a constant. R and T are gas constant and absolute temperature respectively. $\Delta G^o$ is the standard free energy change for the transfer of one mole of the solute from infinity of the solution onto the surface of the sorbent. When double layers overlap, the adsorption energy will decrease as discussed above. If the adsorbed quantities before and after the overlap are $\Gamma_0$ and $\Gamma_2$ respectively, the ratio of the two quantities may be expressed as:

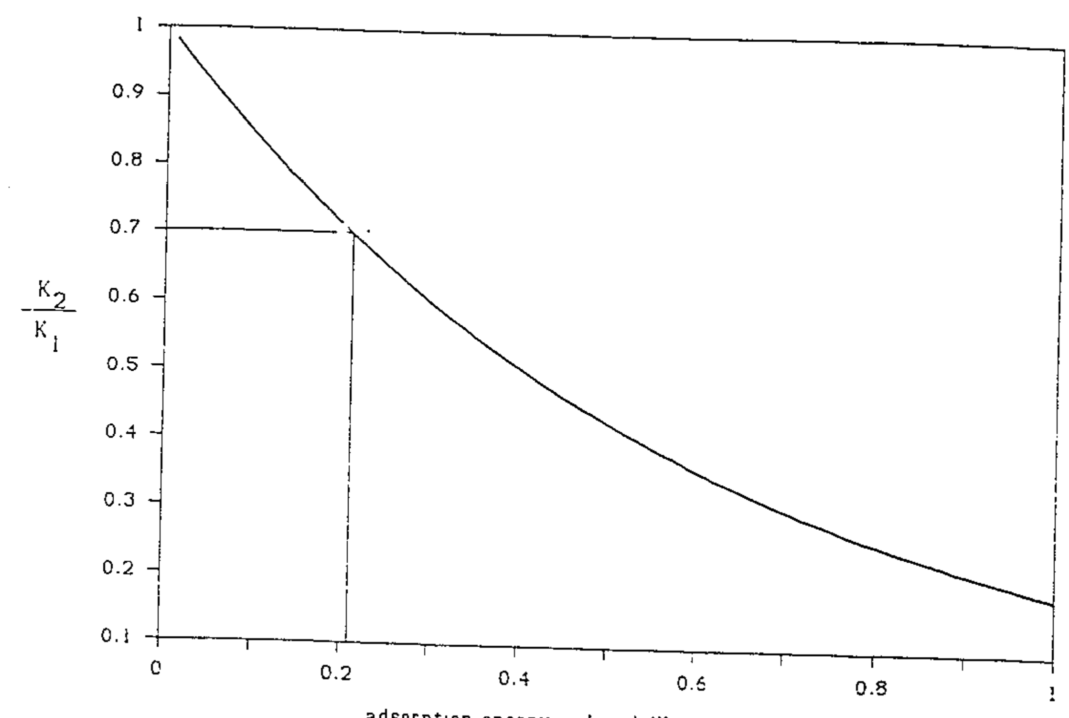


Figure 2.8 effect of reducing adsorption energy on adsorption constant

$$\frac{\Gamma_2}{\Gamma_0} = \frac{K_{p2}}{K_{p0}} = \exp\left(-\frac{\Delta G_2^o - \Delta G_0^o}{RT}\right) \qquad (2.20)$$

Equation 2.20 is used to produce the curve in Figure 2.8. Figure 2.8 shows, for instance, that a decrease of approximately 0.21 kcal/mol in adsorption energy can cause a decline of the adsorption constant by one third, regardless of the magnitude of the absolute adsorption energy. The same fractional decrease in adsorption is expected, at a given sorbate concentration (C in equation 2.18). For the stated system conditions, this energy change corresponds to a double layer interaction induced by a surface separation of 2270 Å.

This calculation, however, is based on a double layer interaction of flat surfaces. For a pair of flat surfaces set in parallel, the overlap of double layer and their interaction is uniform anywhere on the surface. Sorbent particles, however, are not flat surfaces. Not only can the overlap of the double layer be partial, but also the extent of overlap depends upon the geometry of the surface. In order to minimize the uncertainty due to the irregularity of the actual particles, a well defined geometry is needed as a first approximation for the particles. A sphere is chosen, since it is easy to handle mathematically yet somewhat similar to the real particle shape.

The surface of the spheres are divided into many parallel rings in order to calculate the interaction between two spherical particles (Figure 2.9). The surface part of each ring is subject to double layer interaction of different intensity, depending on the separation distance between the rings. Accordingly, each ring on the surface of the sphere bears

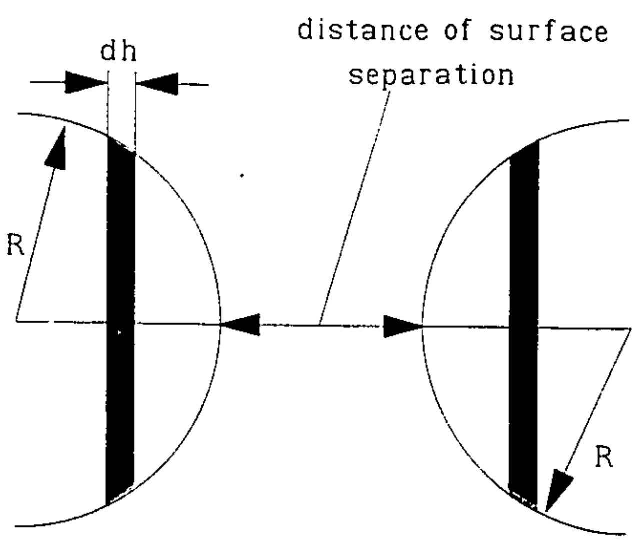


Figure 2.9 Particle spheres can be divided into many parallel rings for the calculation of the interaction energy.

different adsorption energy. The average adsorption energy per unit area of the surface is the integration of the energies of all the rings normalized by the integrated surface area:

$$\Delta G^o = \frac{1}{A} \int_0^R 2\pi R \, \Delta G_i \, dh \qquad (2.21)$$

where A is the area of a half sphere, R the radius of the sphere, $\Delta G_i$ the adsorption energy at the *i*th spot of the sphere and dh the thickness of the ring. Two different approaches may be used for the calculation of $\Delta G_i$ in Equation 2.21. In his study of particle aggregation, Derjaguin [1940] proposed the "ring-pair" protocol for the calculation of repulsive forces between colloidal particles. As illustrated in Figure 2.10, rings of the same radius may be treated as an interaction ring-pair. Take, for instance, ring a1 and b1. Cross interactions between rings of different radii are not considered, however, such as the interactions between ring a1 and b2 (dotted lines). This treatment is simpler mathematically, but is valid only under an assumption that the interparticle distance is much smaller than the size of the particle. For this assumption, the two interacting surfaces resemble two flat parallel sheets, close to each other. Any cross-interaction would be over a much greater distance and therefore negligible.

A general approach, on the other hand, should consider interactions between all possible rings. This calculation was carried out, and Appendix A contains the detailed mathematical treatment. An analytical solution for Equation 2.22 could not be found either manually or with the help of the computing software package, Maple (see Appendix B for details). Thus a numerical integration method was applied to the calculation.

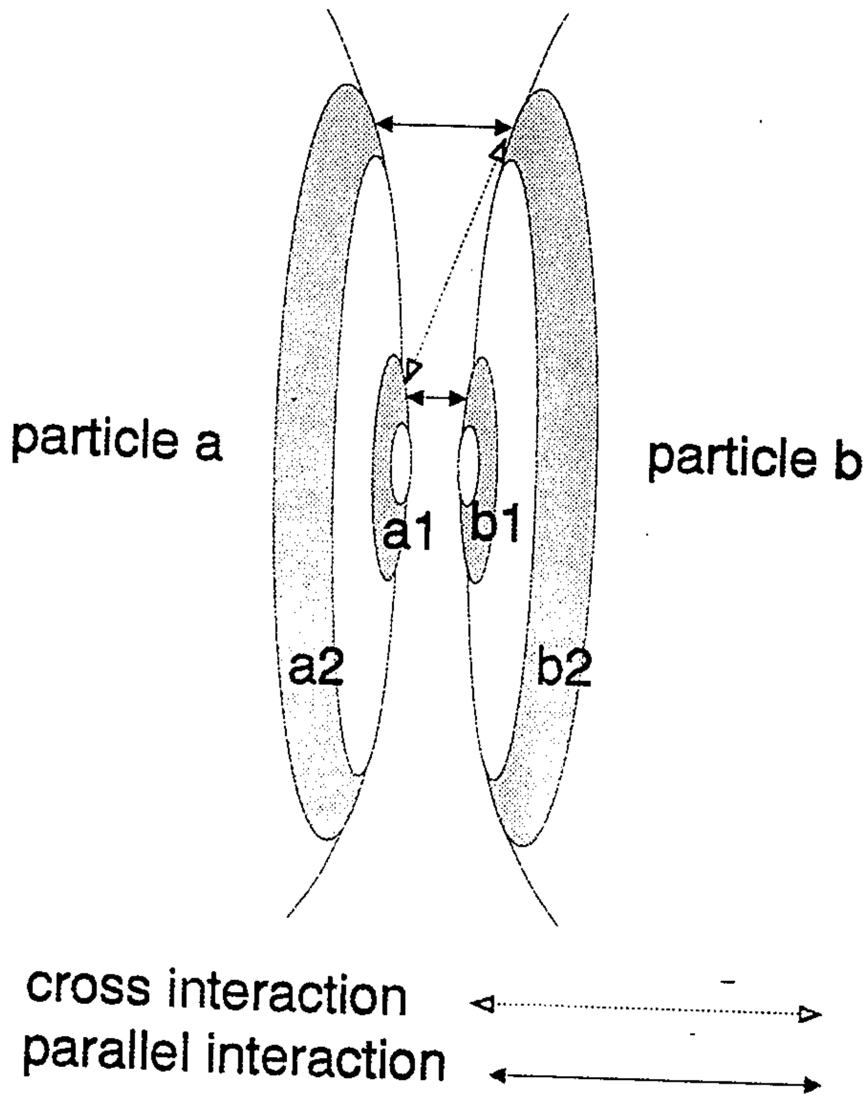


Figure 2.10 ring-pair interaction can be either parallel and cross

The above discussion on interparticle interaction considers only the interaction between two particles. In a colloidal solution, a particle can interact simultaneously with more than one particle. Barclay et al. [1972], using scanning electron micrography on a concentrated dispersed suspension, showed that spherical particles are affected by their neighbours. They tend to pack in a pattern with a coordination of 12 adjacent spheres. Figure 2.11 shows the 12-fold coordination that would be obtained for spheres of similar size in close packing. Since potential energy is additive, the total interaction impact on a sphere would be 12 times that of a single interaction. Contributions from more distant particles would be negligible due to exponential decrease with distance and are not considered.

### 2.4.3 Applicability of the DLI Model

*(1) Generality of the DLI Model*

The derivation of the DLI model was based on an ionized sorbate (metal ion). Nevertheless, the same principles may be applied to the adsorption of organics.

For the adsorption of organics, usually with low or no polarity, the following mechanisms may be involved:

(1) dispersion

(2) repulsive

(3) polarization

(4) hydrophobic

As discussed in section 2.4, adsorption results from the combination of all mechanisms. Variation of any one of the contributors will alter adsorption. Most of the aforementioned

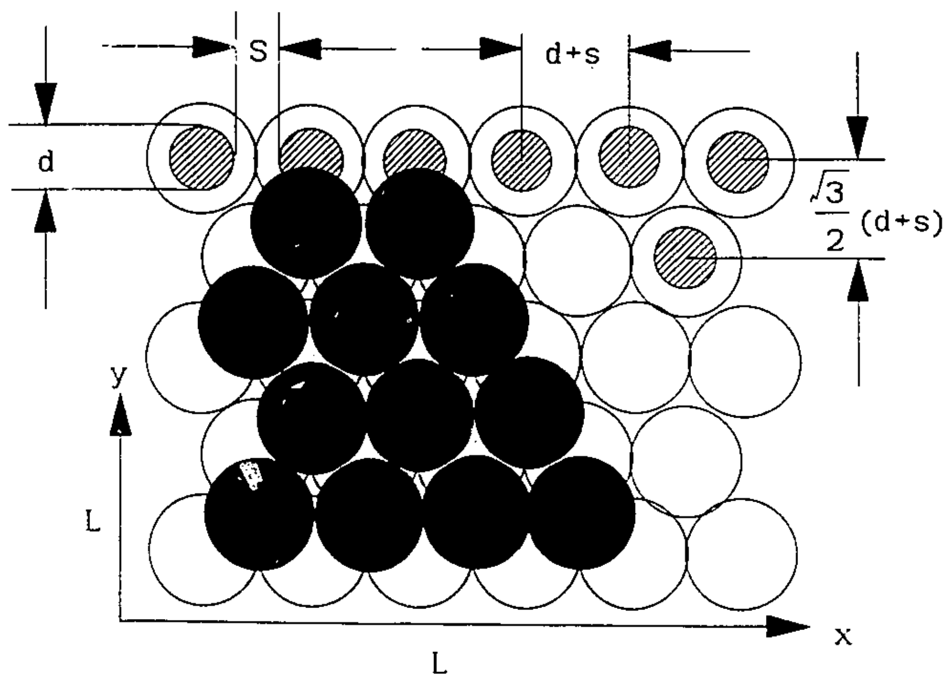


Figure 2.11 closely packed spheres

mechanisms are not affected in double layer interaction, with the exception of polarization. Recall the expression of polarization energy (equation 2.8):

$$\phi_p = -\frac{1}{2}\,\alpha_i\,E^2 \quad (2.8)$$

The energy of polarization is sensitive to change in electric field, E, since it is proportional to the square of E. The overlap of double layers is equivalent to imposing an electric field of reversed sign onto the existing electric field, consequently weakening the existing field. This effect will in turn reduce adsorption. With organics sorbates, the polarizability, $\alpha_i$, can be much larger than that of inorganic sorbates, and the desorption caused by polarization can be significant. An attempt was made to quantify the impact on organic adsorption, which is developed further in later discussions.

*(2) Critical Parameters of DLI Model*

Ionic strength and particle geometry are decisive factors in double layer interaction. Ionic strength dictates the thickness of double layer and consequently the range of electrostatic force. This relationship can be better visualized through a plot (Figure 2.12) generated with Equations 2.12 to 2.15. The plot shows clearly that ionic strength strongly affects the range of the adsorption potential. At high ionic strength, double layers become so thin that no significant interaction and desorption can occur, regardless of other parameters.

At a given double layer thickness, the percentage of overlap is a function of particle size. While small particles can have almost 100% double layer overlap, large ones can only have limited or insignificant interaction (Figure 2.13). This implies that:

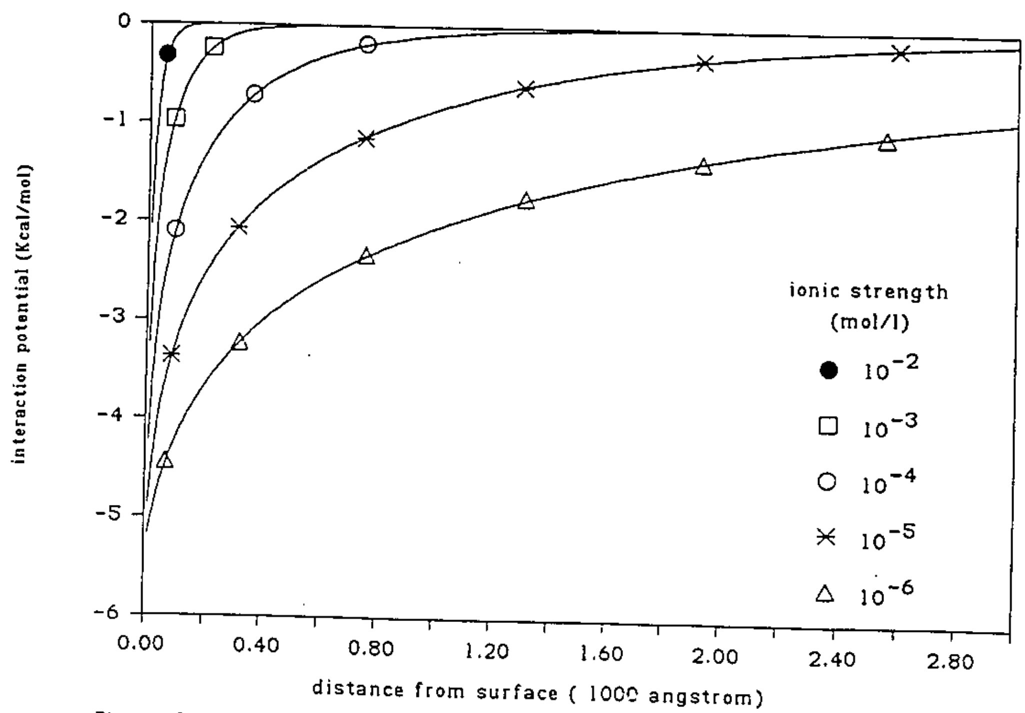


Figure 2.12 interaction potential of electrical double layer at different ionic strength.

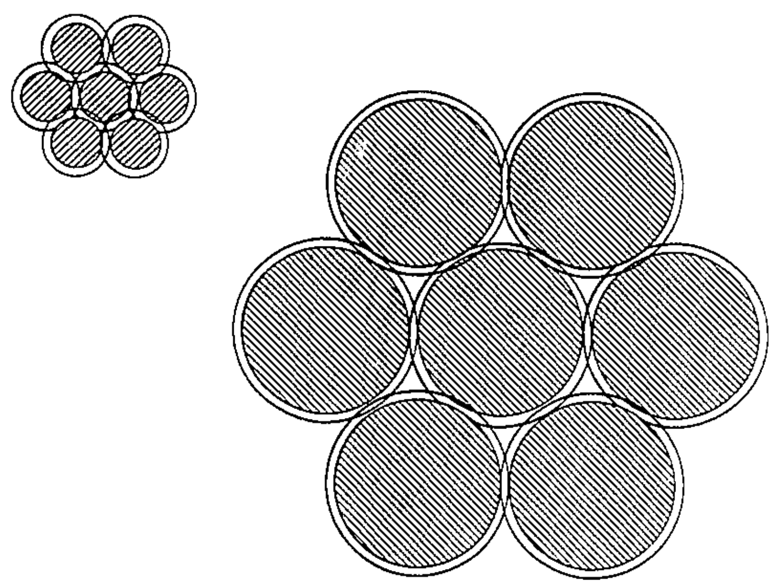

Figure 2.13 Given a double layer thickness, the larger the particle size, the less the percentage of overlap.

(a) When the size of particles exceeds certain limit, no significant double layer interaction can happen, since most of the surfaces will be too far apart from each other.

(b) For porous particles, the majority of the surfaces are internal. Adsorption occurs essentially at inner surfaces. In this case, no significant double layer interaction will be observed from high particle concentration. The change of interparticles concentration will not affect the geometry of the inner space.

(c) The term "particle concentration", (i.e., weight of sorbent per unit volume solution) does not carry sufficient information about the particles with regard to the particle concentration effect, because it fails to characterize some a crucial properties of the particles, i.e., the size and interparticle distances. For a given particle concentration, the particle size is the important detrmining variable for inter-particle interaction. At a given particle weight/per volume, smaller particle size means smaller interparticle distance and stronger double layer interaction. Interparticle distance, therefore, would be a more appropriate term for describing the amount of particle in the system when particle concentration effect is of concern.

# 3. COLLISION HYPOTHESIS: THEORETICAL AND EXPERIMENTAL STUDY

## 3.1 The Necessity of Studying Collision Hypothesis

As introduced in Chapter 1, Mackay and Powers [1987] suggest that inter-particle collisions may play a role in the desorption of loosely adsorbed hydrophobic organics. In this hypothesis, the cause of desorption is also attributed to interparticle interactions, yet the mechanism is believed to be purely mechanical. According to this theory, during an inter-particle collision that happens in the solution, the momentum and kinetic energies of the particles overcomes the adsorption force and dislodge the sorbates from the surface of the particles.

In order to explore the effect of double layer interaction, it is necessary to exclude or minimize the interference of other possible mechanisms. As will be summarized later, by choosing an appropriate experimental adsorption system, all the other proposed mechanisms or factors that may cause the particle concentration effect can be eliminated, with the exception of the collision mechanism. Generally speaking, interparticle collisions always exist in experimental systems, where the need for agitation is essential. In the study of the particle concentration effect, a common practice is to change the concentration of particles by either adding in more particles to the system or altering the volume of the system. Both approaches will inevitably vary the frequency of interparticle collision. If interparticle collision is the cause (or one of the causes) of the particle concentration effect, it will contribute to the phenomenon accordingly.

To assess the validity of the collision theory, one of the challenges is how the collision effect, (if it exists at all), might be distinguished from other interparticle interactions experimentally? When particle concentration is increased, the frequency of interparticle collision changes accordingly, but so do all the other possible interparticle interactions. In such experiments, it is difficult to single out the mechanism that is responsible for the particle concentration effect. In other words, the design of the experiment should be such that the effect of interparticle collision can be isolated from that of other possible mechanisms.

### 3.2 Frequency of Collisions between Particles

Particles in suspension collide with each other as a consequence of at least three mechanisms of particle transport:

(1) Particles move because of their thermal energy (Brownian motion).

(2) Relative motion of particles caused by velocity gradients of the fluid.

(3) Particles of different gravitational settling velocities may collide in settling.

Mechanism 3 is negligible in our case, because particles used in the experiments are usually very fine with minimum settling speed, also the agitation is always strong enough to prevent particles from settling. Thus only the first two mechanisms need to be addressed.

From theories of particle agglomeration [Stumm & Morgan 1980], the time-dependent decrease in the concentration of particles in a monodisperse suspension due to collisions by Brownian motion (perikinetic collision) can be represented by

$$-\frac{dN}{dt} = \alpha_p \frac{4kT}{3\eta} N^2 \qquad (3.1)$$

where

k = Boltzmann's constant

N = number of particles per cubic centimetre

t = time

T = absolute temperature

$\alpha_p$ = fraction of perikinetic collisions leading to permanent agglomeration (effective collision)

$\eta$ = absolute viscosity

The rate of decrease in particles due to agglomeration of particles in a monodisperse suspension under the influence of a mean velocity gradient (orthokinetic collision) can be described by

$$-\frac{dN}{dt} = \frac{2}{3}\alpha_o G d^3 N^2 \qquad (3.2)$$

where

d = particle diameter

G = velocity gradient

$\alpha_o$ = fraction of orthokinetic collisions leading to permanent agglomeration (effective collision)

Since we are interested in the collision frequency only, equations 3.1 and 3.2 can be modified to fit our purpose. If the coefficients of effective collision are removed from the right side of these equations, what is left represents the total number of collisions in unit time, or frequency of collision. Thus the frequency of collision from both orthokinetic and perikinetic collisions can be expressed as

$$\textit{Collision Frequency} = \frac{4kT}{3\eta}N^2 + \frac{4}{3}Gd^3N^2 \tag{3.3}$$

Equation 3.3 may be used to help design the study of collision effect. As can be seen from the equation, there are several parameters that can affect the frequency of collision. At a given temperature T, $\eta$ is fixed. The rest of the parameters, d, N and G, can all be manipulated to alter frequency of collision. As has been discussed in Chapter 2, however, the change of particle size d, or particle concentration N will also have an impact on double layer interactions. The only parameter that will not bring in effects other than collision frequency is velocity gradient G. In equation 3.3, if all the other parameters are fixed, the change of frequency of collision will be proportional to G. By varying G, the effect of collision on adsorption may be evaluated without upsetting other balances or equilibrium. The first term on the right side of equation 3.3 is the Brownian motion term. It will not be affected by the velocity gradient. Also, when the particle size is larger than 1 µm, Brownian motion becomes virtually negligible.

### 3.3 Design of Couette Device

#### 3.3.1 Introduction

It is clear from the above discussion that a good control over the velocity gradient

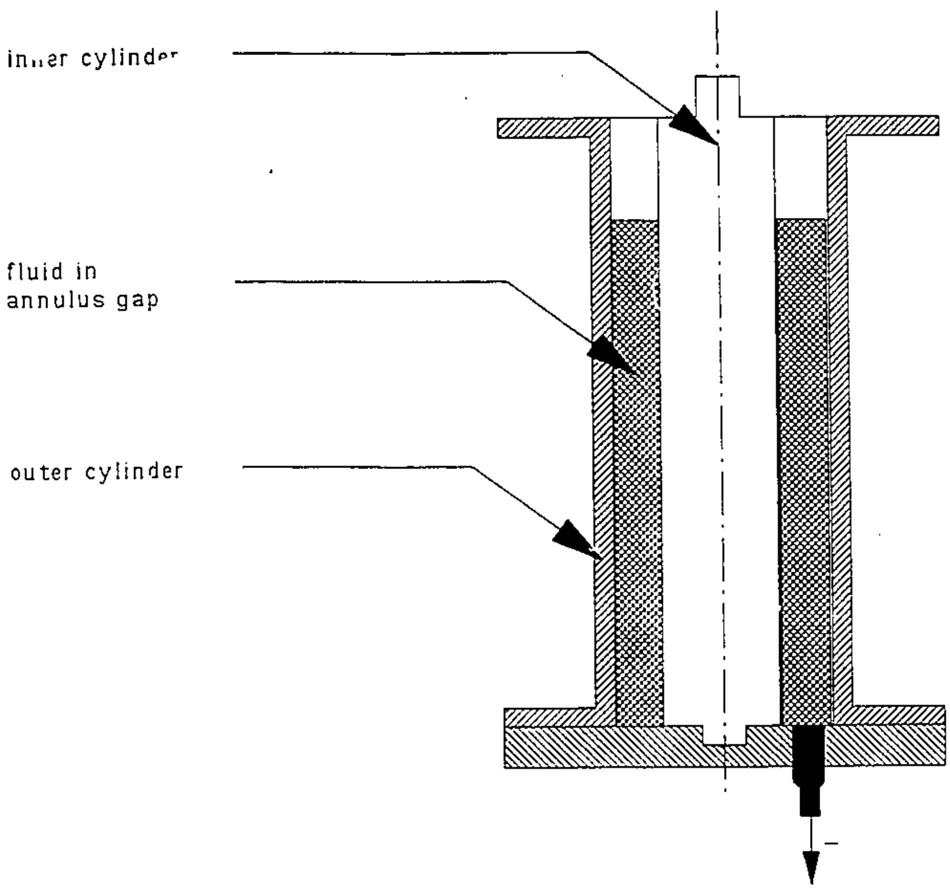


Fig.3.1 Couette device is constructed by two coaxialcylinders with an annulus gap filled with fluid.

of the flow is desirable for studying the effect of collision on adsorption. Unfortunately, a uniform velocity gradient only exists in a perfect laminar flow. Typically, the kind of agitation employed in an adsorption experiment is meant to create turbulent flow, so that maximum mass transfer can be achieved. In order to obtain an uniform velocity gradient and to control it quantitatively, a Couette device was fabricated. The basic structure of a Couette device is two coaxial cylinders with an annulus gap between them (Figure 3.1). One of the cylinders rotates while the other one stays stationary. Since the annulus gap is fairly narrow, the relative motion of the two cylinders will create a laminar flow under certain conditions (Figure 3.2), and the velocity gradient can be calculated accordingly.

Couette in 1890 was the first to investigate the fluid motion in annuli. The principal application of Couette device has been studied extensively since early 20th century [Rayleigh, 1917; Taylor, 1923; 1935; 1936; Chandrasekhar, 1954; Donelly, 1968]. It is better known as "flocculator", since most of its applications are on the study of flocculation of colloid particles. Equations and empirical curves are well documented for the design of the Couette device [Ives & Bhole 1975, 1977]. Yet the design of a Couette device is by no means an easy job. A designer may find himself facing the dilemma of trading off between desired performance characteristics and great difficulties and high costs of manufacturing. Instead of simple duplication, one must also consider the needs and circumstances of the specific research.

### 3.3.2 Review of Typical Designs

Parameters of a Couette device to be individually determined include:

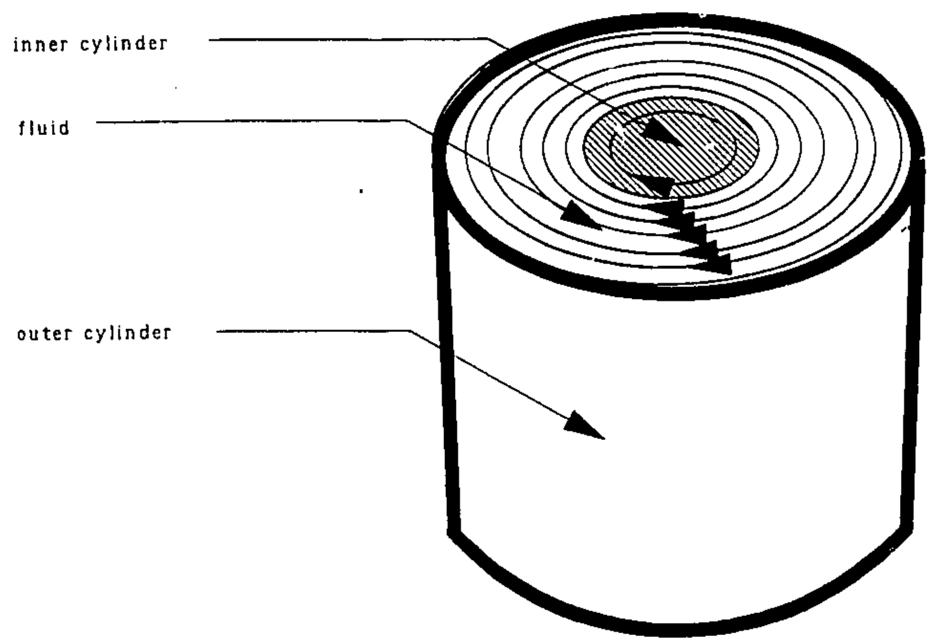


Fig. 3.2 Relative motion of the two cylinders creates a laminar flow pattern.

*(1) Type of Cylinders*

In general, each cylinder is uniform in diameter along the axle, so will be the width of the annular gap. Ives [1975] came up with a tapped inner cylinder for the flocculation of colloids. The width of the annular gap between the inner and outer cylinders varies along the axle in such a way that the gap becomes larger as the feed travels from the inlet to the outlet. This design provides accommodation space for the flocs generated along the path of the flow so that the environment of the experiment can retain consistency through the device.

*(2) Direction of Device Mounting*

Theoretically, the Couette device can be mounted either horizontally or vertically. Flocculators, however, are commonly positioned horizontally. This is because as flocs form during the process, they tend to settle down on the bottom of the flocculator if the flocculator is in a vertical position. In a horizontally mounted flocculator, the rotation of the inner cylinder will eliminate this problem by generating a current of bottom-top circulating. One of the shortcomings of the horizontal arrangement is the end effect. Theoretically, the working part of the device is the annular gap between the inner and outer cylinders and only this part should be in contact with the process liquid. The desired flow pattern can thus be generated which will in turn allow precise calculation. In practice, however, liquid will inevitably contact the end surfaces of the device. The current generated by the end spaces is not laminar flow because the velocity gradient there is not linear. The turbulence tends to perturb the system from the desired hydraulic characteristics when it becomes significant. One way of reducing the influence of the end effect is to use as long as possible cylinders. In doing so, the significance of the end effect becomes negligible, compared to the predominent "ideal" flow pattern generated by the annular gap. Another way of reducing end effect is simply position the device vertically. In this case, an air gap is left on the top end of the device between the liquid and the cap of the device, there will be virtually no end effect on the top end because the friction between the liquid and air is negligible. The strength of the end effect will be cut by half by mounting the device vertically.

*(3) Gap Width*

The annular gap affects the range of velocity gradient and stability of flow. Too wide an annular gap results in a big variation of shear over the width, and turbulence is likely to happen. A narrow annulus, on the contrary, tends to create small variation in shear force over the gap width, but a narrow annulus gap demands greater co-axial machining precision of the cylinders, or the pulsation generated will up set the flow pattern.

*(4) Cylinder Radius and Annulus Width*

The diameter of the cylinders and the width of the annular gap is critical to the characteristics and performance of the device. Figure 3.3 is a design chart for Couette devices. In order to have laminar flow pattern, the diameters of the cylinders have to be in the proper range. A useful empirical index for estimating

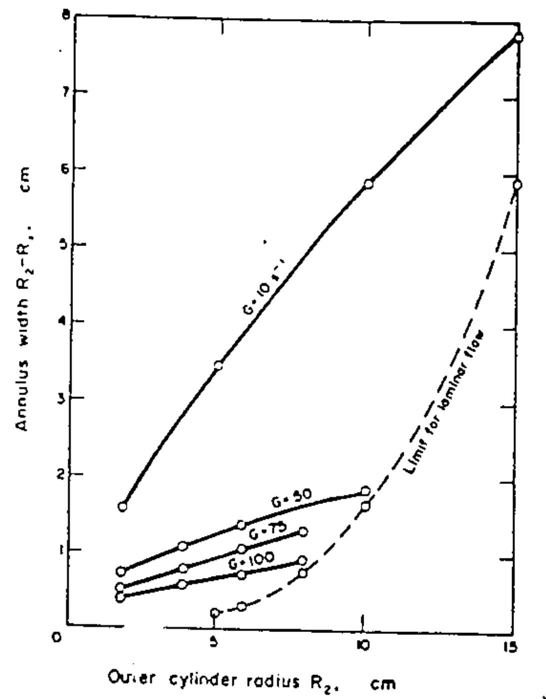


Fig. 3.3 Design chart for Couette flocculators, to keep within laminar flow regime. (from Van Duuren, 1968)

the design is the ratio of the annular gap and the outer cylinder radius. Any ratio below 0.23 is considered a "narrow " gap, or a "safe" design.

*(5) Length of the Cylinders*

In theory, the longer the cylinders, the better the performance, as has been discussed earlier. Yet in practice the maximum length is ultimately limited by constructional difficulties and cost.

*(6) Rotating Cylinder*

Research has found that outer cylinder rotating is a better configuration than inner cylinder rotating because it generates better laminal flow. So in most cases, the former was adopted.

*(7) Rotating Speed*

The design chart also defines the maximum rotation speed of the cylinder before tubulence is generated. To obtain higher velocity gradient, smaller cylinder radius and narrower annulus width are required. When the inner cylinder rotates, the relationship between velocity gradient G and angular velocity of the rotation cylinder is:

$$G=\frac{2\omega_i R_i R_o}{R_o^2-R_i^2} \tag{3.4}$$

where

$\omega_i$ = the angular velocity of the inner cylinder

$R_i$ = inner diameter of inner cylinder

$R_o$ = outer diameter of outer cylinder

Listed in Table 3.1 are some typical flocculator designs.

**Table 3.1 Examples of Flocculator Design**

| Name of Author (Year of Work) | Lick (1971) | Ives (1975) | Ives-2 (1975) |
|---|---|---|---|
| Type of Cylinder | uniform R | uniform R | tapped R |
| Annu. Gap Width (mm) | 2 | 9.95 | 6.94-13 |
| R of Inner Cylinder (mm) | 25 | 57.5 | 57.5 |
| R of Outer Cylinder (mm) | 23 | 47.5 | 44.5-50.5 |
| Gap/(R of Out Cylinder) | 0.08 | 0.17 | 0.12-0.23 |
| Cylinder Length (mm) | 254 | 400 | 400 |
| (Cylinder Length)/Gap | 127 | 40.2 | 57.6-30.8 |
| Maximum Gap Volume (ml) | 76.7 | 1,313 | 3,747 |
| Maximum Rotation (RPM) | 857 | 220 | 220 |

## 3.3 Design of Couette Device for This Study

Being different from flocculation researches, the nature and characteristics of this study call for special considerations in the design of the device:

*(1) Type of Cylinders*

Cylinders of uniform diameter will be used, because no flocculation is expected.

The system is operating as batch mode, the conditions anywhere in the device should be the same.

*(2) Direction of Device Mounting*

In this case, there is more than one reason that the device needs to be mounted vertically:

(a) The amount of glass beads available for the experiment is limited, in order to reach desired high particle concentration, the device may only be partially filled with water. With horizontal mounting, the volume of the system is fixed. Unless the whole space is filled, a laminar flow pattern cannot be achieved. For the case of vertical mounting, on the other hand, the flow pattern will not be affected by the amount of liquid in the device.

(b) Sealing of the driving shaft would be difficult if the device is horizontally placed. With vertical mounting, as can be seen from the assembly diagram, there is no need for the water-tight sealing on the top end. Gravity force will always keep the liquid away from the top cap.

(c) As discussed earlier, another advantage of vertical mounting is reduction of the end effect. End effect may not be noticeable when the cylinders are long enough. In our case, the designed length of the cylinders is considered great enough to avoid significant end effect. Nevertheless, when liquid level in the system is reduced to obtain high particle concentration, the working length of the cylinders becomes small and end effect may gain more importance. By vertically mounting the device, the impact of end effect is reduced by 50%, which is equivalent to double the working length of the cylinders.

As mentioned earlier, the major problem caused by vertical mounting is the gravitational settling of particles. It is therefore necessary to check the settling characteristics of the particles used in the experiment. The rate of settling (m/hr) can be estimated with Stoke's equation:

$$S=\frac{2r^2(\rho_p-\rho_m)g}{9\eta} \tag{3.5}$$

where

S = rate of settling (m/hr)

r = radius of the spherical particle (0.8 μm)

$\rho_m$ = density of medium (1 g/cm$^3$)

$\rho_p$ = density of particle (2.7 g/cm$^3$)

μ = viscosity of medium (3.205 kg/m at 25$^0$C)

The particles employed in the collision experiment are ϕ1.6 μm glass beads. Calculated with equation 3.5, the settling speed is $2.7\text{x}10^{-6}$ m/sec or $9.7\text{x}10^{-3}$ m/hr. So the conclusion is that such a low settling speed will not pose any problem in the system.

*(3) Rotating Cylinder*

From hydraulics point of view, outer-cylinder-rotation is a better configuration, because it allows higher rotating speed without going to turbulent flow. But the construction of the device will be much more complicated. For the present purpose of preliminary experiment, inner cylinder-rotation is sufficient.

*(4) Maximum Rotating Speed*

For this study, two maximum rotating speeds are of concern. The first is the absolute maximum speed that is restricted only by the mechanical capacity of the system. This is important, because for starting the adsorption experiment, the rotor must be able to spin at a sufficient high speed so that a turbulent flow pattern can be created to ensure the adsorption system is homogeneous in terms of sorbents and sorbates distribution. The maximum speed the rotor can reach depends on the capacity of the motor and the mechanical feature of the system. The second maximum rotating speed is the limit over which the flow pattern will turn into turbulent flow from laminar flow. Preferably the system can run at a high speed under laminar flow. This will allow test on frequency of collision over a wide range. At the time of design, this maximum speed may be estimated from empirical calculation, but practically, only experimenting on the system can determine the exact rotating speed boundary between laminar and turbulent flow.

*(5) Material*

For the constuction of flocculators, metal is widely used, especially for mechanical parts such as shaft and bearings. Since trace amount of metal is the object of this study, metals are prohibited from contacting the process fluid. Plastic becomes the choice of the building material for the system. While plastics are suitable for most of the parts, they may not be appropriate for shaft and bearings. Not only is their mechanical strength inferior to that of commonly-used steel, but also they are poor heat conductors. At high rotating speed, the heat generated at the bearing may accumulate and cause premature failure of the system. A water-tight, contamination-free bearing is technically possible but expensive and complex. It was decided to try the simple, inexpensive plastic shaft and bearing first. After all, the conclusion can only be made by the actual experiment.

A couple of designs were originally proposed for the construction of the Couette device in this study. Table 3.2 is a summary of the designs.

**Table 3.2 Proposed Parameters for Couette Device**

| Series No. | No.1 | No.2 | No.3 | No.4 |
|---|---|---|---|---|
| Rotating cylinder | inner | inner | outer | outer |
| Annu. Gap Width (mm) | 5 | 5 | 2 | 5 |
| R of Outer Cylinder (mm) | 50 | 29 | 25 | 50 |
| R of Inner Cylinder (mm) | 45 | 24 | 23 | 45 |
| Gap/(R of Out Cylinder) | 0.10 | 0.17 | 0.08 | 0.1 |
| Cylinder Length (mm) | 400 | 400 | 400 | 400 |
| (Cylinder Length)/Gap | 80 | 80 | 200 | 80 |
| Maximum Gap Volume (ml) | 596 | 333 | 120 | 596 |
| Glass Beads Needed (g) | 0.6 - 6.0 | 0.3 - 3.0 | 0.12 - 1.2 | 0.6 - 6.0 |

After comparing pros and cons, design No.2 was selected for the construction of the Couette device. Figure 3.4 is a assembly drawing of the device. Note that there is an inlet on top of the rotor (inner cylinder) and an outlet on the bottom of the device. Plexiglass is suitable for the construction of the outer cylinder, where transparency is needed for the observation of the experiment. Amongst plastic materials, teflon is a good candidate for bearing and rotor shaft. It is self-lubricant, chemically stable and stands relative high temperature. However because of its high cost, Teflon was only used for the two end pieces. The inner cylinder was made of Delrin.

## 3.4 Experimenting with Couette Device

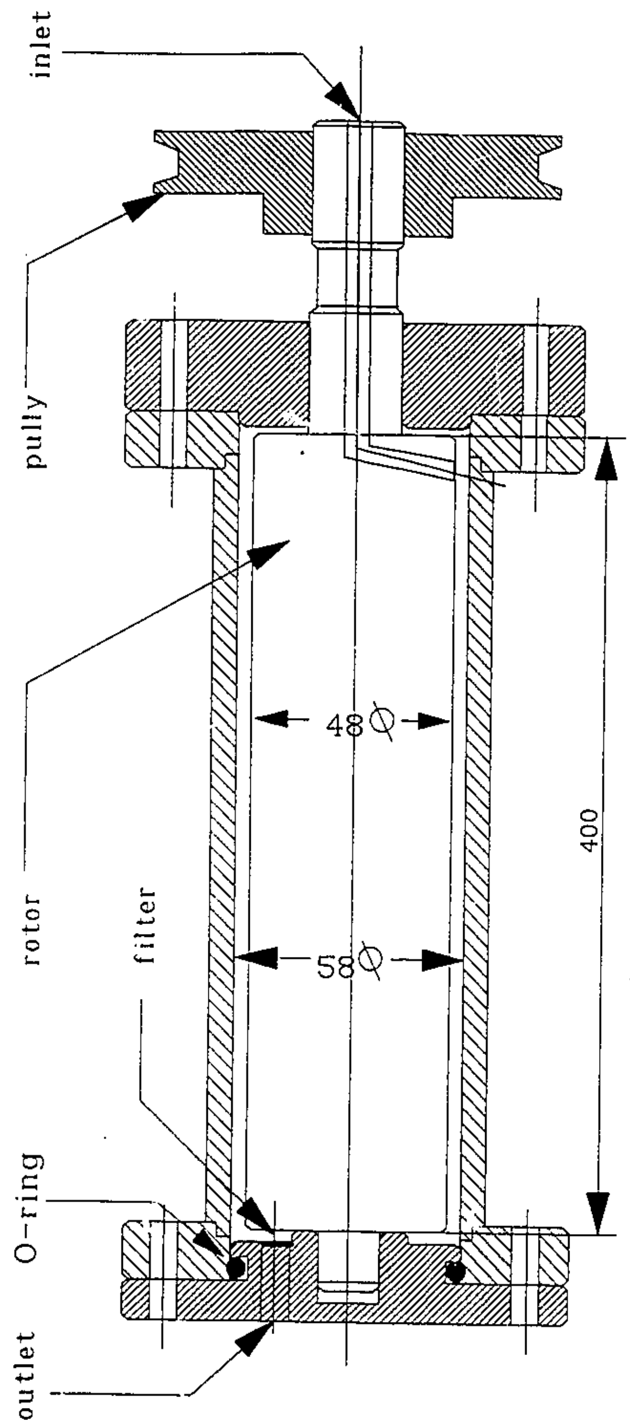


Fig.3.4 Assembly drawing of the Couette device.

### 3.4.1 Preparation and Testing

The Couette device is mounted on a steel frame and driven by an air motor through a belt. The no-load speed of the air motor can reach 560 rpm at 30 psi air pressure. It can drive the rotor at continuously variable speed from 0 to 300 rpm. Liquid and glass beads can be added through the inlet on the top of the rotor. The outlet on the bottom of the device serves as a sampling and volume adjusting pot.

Before an adsorption experiment can be conducted in the Couette device, a dye test is necessary to characterize its hydraulic performance [Taylor, 1935; 1936; Gemmell, 1963; Ives & Bhole, 1975]. The purpose of the test is to identify visually flow patterns at various rotating speeds. After the annular gap was filled with water, a red dye was spiked into the device. As the inner cylinder rotates, some ring-shaped bands appeared, indicating laminar flow pattern (Figure 3.5). The bands begin to deteriorate around 120 rpm, marking the speed limit of the laminar flow region of the device.

### 3.4.2 Adsorption Experiment on the Couette Device

The adsorption system tested on the Couette device is copper adsorption onto 1.6 μm glass beads, using acetic acid/sodium acetate buffer to maintain pH 5.5. The initial copper solution concentration is ca. 1 μmol/l. Particle concentration varies from 1 g/l to 50g/l. The same adsorption system is used in other experiments, detailed system information will be elaborated in Chapter 4.

The glass beads were pre-soaked in the buffer for at least 24 hrs before being transferred into the Couette device. After $Cu^{2+}$ was added, the Couette device was filled with buffer solution to a predetermined volume. The rotor then spun at the maximum

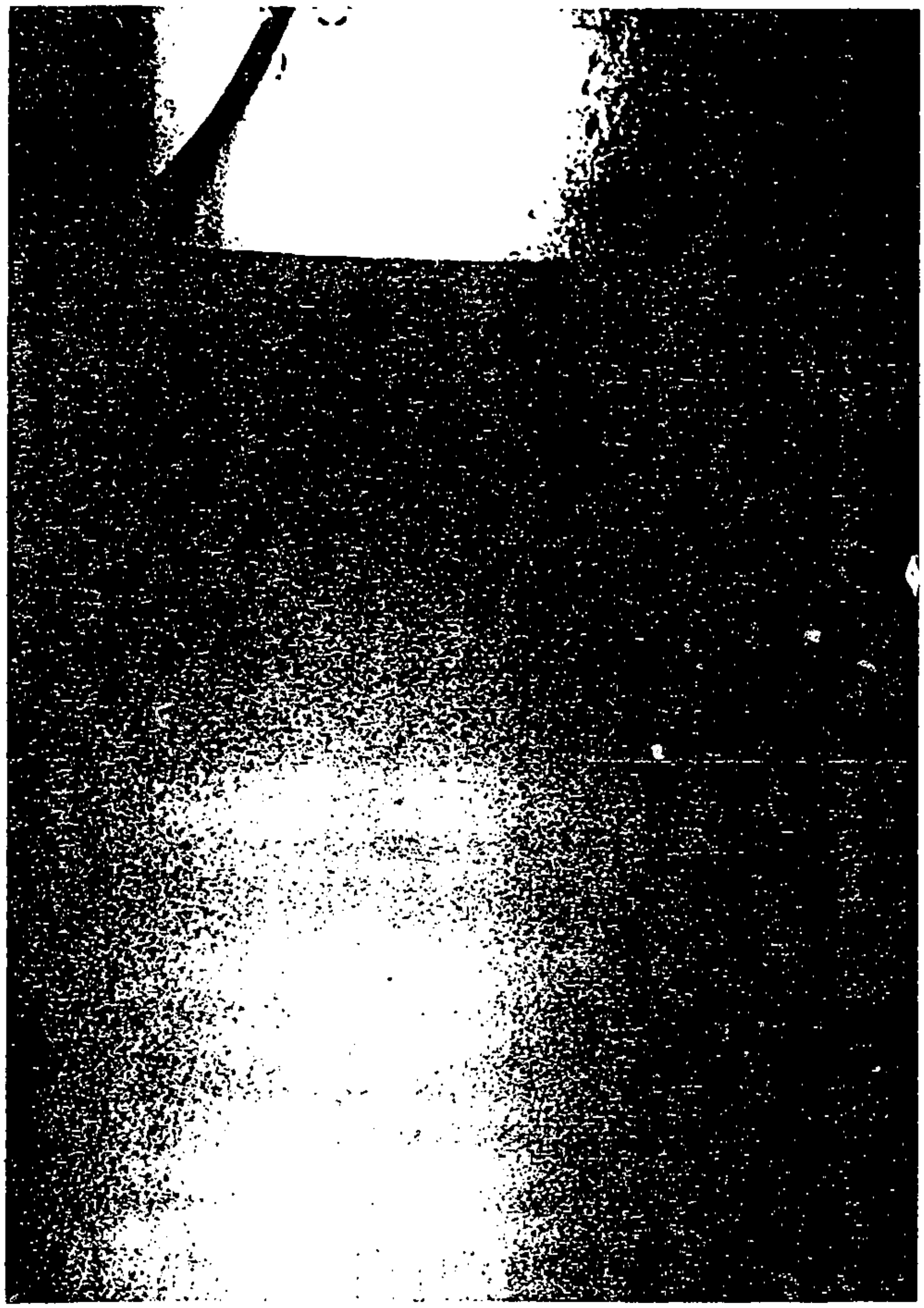

Figure 3.5 As the inner cylinder rotates, some ring-shaped bands appeared, indicating laminar flow pattern.

speed for ca. 10 minutes to mix the adsorption system into an even distribution.

After the initial fast spin, the rotor was set to a series of predetermined speeds, ranging from 30 to 120 rpm. Each speed lasts 40 minutes to allow proper equilibrium time, then a sample was taken from the outlet on the bottom of the device. Nuclearpore filter paper was used at the outlet to prevent glass beads from escaping from the device. The pore size of the filter paper is 0.7 μm. Samples were analyzed with a Perkin-Elmer 2380 Atomic Absorption Spectrophotometer. A graphite furnace was used in the analysis. The adsorbed metal concentration is assumed to be the difference between the initial solution concentration of metal and the equilibrium metal concentration. More information will be introduced on the analytical work in Chapter 4.

The results of the adsorption experiment using the Couette device are all negative. That is, at various rotating speeds, no change in equilibrium concentration of metal was ever discovered.

### 3.5 Theoretical Analysis.

Experimentation is confined by the capacity of the Couette device; it can provide no more information beyond its scope. For instance, the Couette device cannot maintain laminar flow at high rpm. It is therefore very desirable to be able to estimate the effect of interparticle collision theoretically, as a supplement to the experimentation.

A rigorous description of interparticle collision is very complex and involves quantum mechanics. For a semi-quantitative estimation, however, a much simpler mathematical treatment is sufficient. Statistically, the probability of three or more particles bumping into one another simultaneously is much smaller than that of two particles. Thus

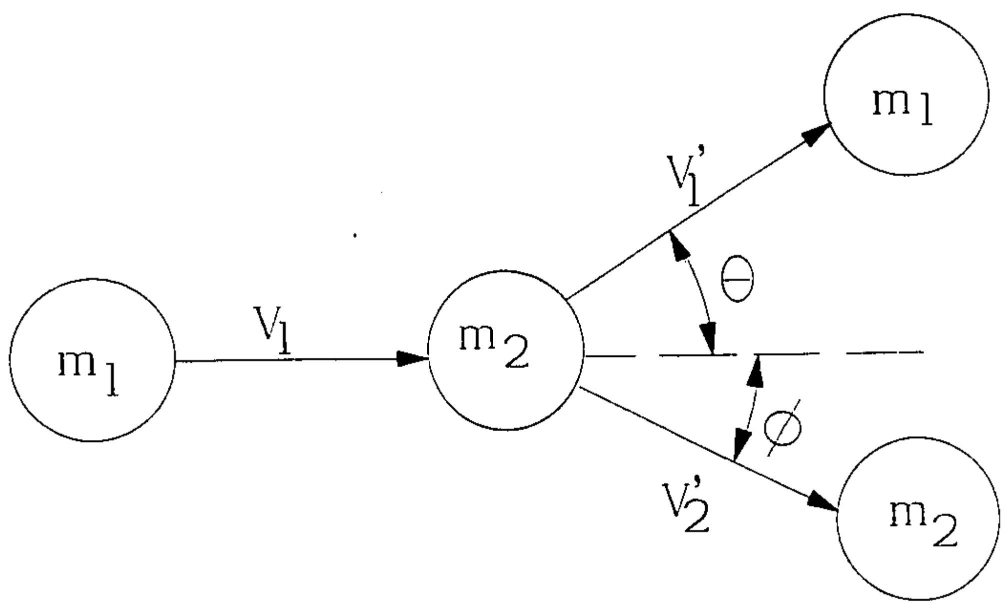


Fig.3.6 collision of two particles

we can discuss the problem on the basis of two-particle collision, which is schematically illustrated in Figure 3.6. In Figure 3.6, particle 1 bumps into particle 2, transferring some of its kinetic energy to the latter. Because it is the relative movement of the two particles that counts, one can assume that particle 2 is stationary while particle 1 is travelling at a speed $V_1$ which equals to the relative travelling speed. Assume the two particles had an elastic collision, both particles may change their travelling speed and direction, but the total momentum and kinetic energy should be constant. Namely, the laws of conservation of momentum and kinetic energy hold:

$$m_1\upsilon_1 = m_1\upsilon_1' + m_2\upsilon_2' \tag{3.6}$$

$$\frac{1}{2}m_1\upsilon_1^2 = \frac{1}{2}m_1\upsilon_1'^2 + \frac{1}{2}m_2\upsilon_1'^2 \tag{3.7}$$

where

$m_1$= mass of particle one

$m_2$= mass of particle two

$\upsilon_1$= velocity of particle one before collision

$\upsilon_1'$=velocity of particle one after collision

$\upsilon_2'$=velocity of particle two after collision

A detailed mathematical manipulation of Equation 3.6 and 3.7 is given in Appendix C. The result indicates that half of the original kinetic energy of particle one will be transferred to particle two, provided the particles are of the same size. Namely:

$$\Delta E = \frac{1}{4} m_1 v_1^2 \tag{3.8}$$

With Equation 3.8 the impact of collision can be estimated if the relative speed of the particles is known. In a Couette device, the fastest speed is obtained on the surface of the rotor. In the following calculation, this maximum speed was used to ensure that collision energy is not underestimated.

The mean velocity gradient can be calculated with

$$G = \frac{2\omega R_1 R_2}{R_2^2 - R_1^2} \tag{3.9}$$

where

$\omega$= angular speed of rotor

$R_1$= radius of inner cylinder

$R_2$= radius of outer cylinder

Table 3.3 shows two examples of theoretical estimation of collision energy. One is with lower rotating speed and particle concentration. The other one is with very high particle concentration and rotor speed.

**Table 3.3 Theoretical Estimation of Collision Energy**

| | | |
|---|---|---|
| Rotating Speed (rpm) | 60 | -- 600 |
| Particle Concentration (g/l) | 4 | 160 |
| Mean Velocity Gradient ($sec^{-1}$) | 42.2 | 421.8 |
| Collision Frequency (unit volume) ($cm^{-3}\cdot sec^{-1}$) | $1.3x10^{8}$ | $2.1x10^{12}$ |
| Collision Frequency (per particle) ($particle^{-1}\cdot sec^{-1}$) | $1.4x10^{-2}$ | 5.6 |
| Relative Velocity of Particles (cm/sec) | 15.7 | 157 |
| Collision Energy (cal/mol) | $8.84x10^{-5}$ | $8.8x10^{-3}$ |

## 3.6 Conclusion on Collision Theory

Both experimental and theoretical work do not support collision theory. With the Couette device, the frequency of interparticle collision can be altered by adjusting rotor speed. Other system parameters were not disturbed. No desorption was observed at various collision frequency. Theoretical estimation also suggests that there is a tremendous gap between adsorption energy and collision energy. It can been seen from Table 3.3 that the collision energy of the system is relatively low. Even at a hypothetical 600 rpm rotor speed, collision energy is less than 0.01 cal/mol. Adsorption energy of metals usually reaches several thousand cal/mol level, which is some six orders of magnitude higher then the estimated collision energy. It is therefore highly unlikely that interparticle collision can cause desorption. In other words, the possibility of interparticle collision effect in the given system has been excluded.

# 4. EXPERIMENTING ON PARTICLE CONCENTRATION EFFECT

## 4.1 Preliminary Experiment

As introduced in chapter 1, the phenomenon of the particle concentration effect has been observed by many research groups. Most of the experiments were conducted with natural material as sorbent, typically, sediment or clay. Natural sorbents are very complicated, many processes can happen simultaneously, including biological ones (resulting in non-equilibrated systems). It is therefore very difficult to pinpoint the mechanism in such experiments. Nevertheless, it is necessary to conduct similar experiments for the simple reason of confirming the phenomenon.

The fact that some research workers failed to produce the particle concentration effect in their experiments suggests that in addition to particle concentration, some other factors may also play roles in the process. Subtle differences in experimental conditions may provide useful clues on the mechanistic study of the phenomenon.

### 4.1.1 Approach

The phenomenon of the particle concentration effect was discovered unexpectedly through a common procedure of adsorption experiment, i.e., by comparison of partition coefficients obtained from experiments with various amount of sorbent. Similar experiments were conducted in this study. The results are displayed in Table 4.1.

**Table 4.1 Variation of the Partition Coefficient Under Different Sorbent Concentrations ***

| Particle Conc. (g/l) | Initial Sorbate Conc. (ppb) | Equilibrium Sorbate Conc. (ppb) | Partition Coefficient (l/kg) |
|---|---|---|---|
| 0.1 | 64 | $55^{+3.7}_{-2.0}$ | 1636 |
| 0.5 | 64 | $41^{+4.2}_{-3.1}$ | 1092 |
| 5.0 | 159 | $52^{+4.5}_{-5.2}$ | 415 |
| 10.0 | 159 | $42^{+1.9}_{-3.3}$ | 282 |

* Conditions: sorbent: Kaolinite; sorbate: $Cu^{2+}$; ionic strength: $10^{-3}$; Buffer: NaAc/HAc pH= 4.5.
* Definition of Partition coefficient as stated in Chapter 1 (Equation 1.1).

The data in Table 4.1 clearly show that partition coefficient drops drastically as particle concentration increases.

While this type of experiment originally uncovered the phenomenon of particle concentration effect, it does not provide a proper approach to tackle the problem. This is because when different amounts of solid particles are used in the experiments (for instance, a high concentration versus a low concentration), the process is susceptible to some interferences. As a matter of fact, some research workers believe that the particle concentration effect is actually misinterpreted artifacts caused by such interferences, as described in Chapter 1. When comparing two adsorption experiments of different particle concentrations, potential interferences include:

*(1) Kinetic Effect*

When high particle concentration is used in an adsorption experiment, the diffusion of sorbate towards the surface of the particles becomes slower. Depending on the adsorption system, substantially longer time may be needed to reach equilibrium or steady state. If diffusion becomes the controlling step, the apparent partition coefficient will decrease, unless sufficient agitation and reaction time is provided.

*(2) Aggregation Effect*

At high particle concentration, interparticle collision becomes more frequent. Particles are more likely to form aggregates. Aggregation brings particles together, leaving limited passage for mass exchange with the exterior environment. When sorbates are large organic molecules, they may not be able to access interior surfaces of the aggregates. Even when small sorbates are small such as metal ions, the diffusion speed will be also reduced. Aggregation also reduces surface area available for adsorption. The combination of the two effects, namely reduction of surface area and restricted access to the surface, will lessen adsorption.

*(3) Third Phase Adsorption*

As described in Chapter 1, tiny colloidal particles or ligands existing in natural systems are difficult to remove during solid-liquid separation. The concentration of the "third phase" is proportional to the amount of particles added into the system. When more solids are used to obtain higher particle concentration, the colloid concentration will also increase accordingly. If solid-liquid separation is performed for the purpose of taking a solution sample, the colloid concentration in the sample will be high too, as compared to a sample obtained from a low particle concentration system. Analytically, because sorbates on solids can not be measured directly, adsorption on solids is estimated by measuring sorbate concentration in the equilibrated solution. When the sample is analyzed for sorbate concentration, the portion that adsorbed onto the colloids will be calculated as the solution concentration, since the colloids can not be separated effectively from the sample. Thus a false increase of solution concentration of the sorbate will be recorded, resulting misleadingly in a lower amount of adsorption on the solids. To summarize the above discussion, because of the various mechanisms might involved in the experimental approach of the simple "low-high" particle concentrations as described in Section 4.11, no clear and certain mechanistic interpretation can be drawn from the data obtained.

As stated in Chapter 1, the purpose of the present study is to identify if there is an "intrinsic" mechanism behind the phenomenon. This can only be done after the afore mentioned artifacts and other mechanismes are excluded.

A better way of conducting an adsorption experiment on particle concentration effect is, instead of changing the quantity of solids, to alter the particle concentration by changing the volume of the system. The experiment starts at a given condition. After the adsorption has reached equilibrium, a sample is taken for measuring the equilibrated sorbate concentration in the solution. In the second stage of the experiment, while all the other parameters remain constant, the volume of the system is changed to adjust particle concentration. Apparently, this can be accomplished by either increasing or decreasing the volume, i.e., dilute or concentrate the adsorption system.

To concentrate the adsorption system is a better approach than to dilute it. Because to dilute the adsorption system may be more susceptible to artifacts. For instance, by starting an experiment at a high particle concentration, the above discussed kinetic and aggregation effects may already exist. When the system is later diluted, there is more than one reason to expect the apparent adsorption partition coefficient to increase because:

*(1) Kinetic Effect*

At lower particle concentration, diffusion and transportation of sorbate is improved. If the adsorption system was at equilibrium before the dilution, the adsorption will not be affected. On the other hand, adsorption is likely to increase if kinetic effect was restricting the adsorption before the dilution. In this case, the increase of the apparent partition coefficient is a result of kinetic effect, on top of the possible interparticle interaction. The dilution of the adsorption system can thus cause "false" particle concentration effect.

*(2) Aggregation Effect*

The dilution of the system will ease aggregation (if there was any), the solids then become less compact or loose, providing more surface area and easier access to inner surfaces. Again, the apparent partition coefficient of adsorption may increase as the result of reduced aggregation, namely, another artifact.

*(3) Third Phase Adsorption*

The third-phase adsorption effect may also manifest itself if the adsorption system is diluted. At the first equilibrium with high particle concentration, the colloid concentration will be high in a solution sample after solid-liquid separation. After dilution, the concentration of the colloids is also diluted as are all the other constituents in the system. Thus a solution sample taken after the dilutution will have lower colloid concentration, leading to the false impression of a higher apparent partition coefficient.

Based on the above discussion, a conclusion can be drawn that diluting an adsorption system may create artifacts in the study of the particle concentration effect.

In contrast to the case of system diluting, to concentrate an adsorption system is basically immune from those potential problems. In a concentrating experiment, the adsorption experiment starts at low particle concentration. After the first equilibrium and taking a sample, the system volume is reduced by removing part of the solution. Although the particle concentration becomes higher, the above-mentioned mechanisms can not interfere with the process:

*(1) Kinetic Effect*

When the adsorption system is concentrated, mass transfer process becomes sluggish. But this will not affect the amount of adsorption kinetically. If the system was at equilibrium before volume adjustment, the slow down of diffusion will not have any impact on the equilibrium, because both adsorption and desorption are affected to the same extent. If the system was not equilibrated before the concentrating, the increase of the particle concentration will not result in desorption kinetically.

*(2) Aggregation Effect*

Concentrating the system may cause aggregation. Aggregation can compact the solids and restrict access to the inside surfaces. Yet there will be no change in equilibrium. Instead, the aggregation simply "preserves" the adsorbed equilibrium. The adsorbed portion of the sorbates is trapped or embedded inside the aggregates. Therefore no change of apparent adsorption partition coefficient should happen because of aggregation.

*(3) Third Adsorption Phase*

During the process of concentrating the system, two techniques were used: filtration and centrifugation. The proper selection of operating parameters for both processes is crucial. The pore size of the filter and the speed of the centrifugation should be such that the concentration of the colloids in the system should not change after the concentrating process. If samples are taken before and after the volume reduction, no difference in sorbate concentration in the solution will be detected, since colloids concentration, as well as sorbate concentration in the true solution phase, stay constant. Unless, of course, certain interparticle interaction causes desorption.

There is, however, one precondition for the above argument. That is, the total amount of colloids in the system should be constant. Unfortunately, this may not always be true, particularly in the case of using clay as sorbent. It is believed that the concentration of colloids in the solution is at equilibrium with the solids. The equilibrium is sustained by two opposite processes in the system: peptization and aggregation [Morel and Gschwend 1987]. The two processes always exist simultaneously. Given other system parameters, the equilibrium will be a function of particle concentration. When particle concentration varies, the equilibrium concentration of the colloids also changes correspondingly. Apparently, when this happens, the experiment of volume reduction can no longer be immune to the third phase adsorption effect.

As will be discussed later, the problem of a third adsorption phase can be ultimately eliminated by using a dimensionally well defined sorbent. For the purpose of the preliminary study where clay is used as sorbent, the volume-reduction approach is still the best experimental design available for minimizing artifacts.

Solid-liquid separation is a key step in the experiment. Basically two approaches are applicable: centrifugation and filtration. Centrifugation is the most popular method in such studies. This is because sediments, the most common object of adsorption study, are usually difficult to separate with filtration which is susceptible to fouling. The drawback of filtration is membrane's proneness to fouling. When applied on natural sediments, a filter will usually be plugged before the filtration is completed. Compared with centrifugation, filtration has rather limited applicability. With centrifugation, solid-liquid separation process can be controlled by applying proper rotating speed. The higher the rotating speed, the smaller the particles that can be removed from the liquid column. Centrifugation technique, however, may create a problem in the study of particle concentration effect. During the separation process with centrifugation, particles are densely packed or even compressed on the bottom of the centrifugal vessel. If any interparticle interaction plays a role in the particle concentration effect, such as double layer interaction, the compacted packing may have changed the intensity of interaction that exists in a particle suspension. In the suspension, the particles are separated and moving independently, whereas in the centrifugation process, the particles are closely packed against one another. Any information extracted from the supernatant of centrifugation may actually not represent the suspension system in terms of interparticle interactions. Instead, it reflects the adsorption status when solids are closely packed. With filtration technique, this problem can be avoided. By properly designing the apparatus, when taking a sample through filtration, the adsorption system will not be disturbed. In this study, therefore, filtration was selected in most experiments as solid-liquid separation technique. The problem of membrane fouling can be overcome by selecting proper solids.

#### 4.1.2 Selection of Sorbent

For the preliminary stage of the study, montmorillonite was originally selected as the sorbent. montmorillonite is a common clay found in sediments. But it was soon found to foul the Milipore 0.45 μm membrane very quickly. As discussed earlier, the experimental approach calls for substantial system volume reduction. Up to 300 ml liquid has to be removed through filtration in each experiment. It is therefore difficult to work with montmorillonite. A second clay, kaolinite, was then tried as the sorbent. It turned out that kaolinite has a much better filterability and meets the experimental requirement.

Quartz was also tested as a sorbent in the preliminary experiment. Fine quartz powder was obtained by crashing large crystals. A 200 mesh sieve was used to remove coarse particles.

#### 4.1.3 Selection of Sorbate

Particle concentration effect has been observed with both metal and organic sorbates by other researchers. As explained in Chapter 2, the modelling of double layer interaction involves calculations that require detailed information such as the location of the sorbate on the surface and the geometry of the sorbate, etc. Assumptions were made to accomplish the calculation. It would be very difficult to carry out such calculations based on molecules of organic sorbates. So metal was chosen as sorbate to minimize the uncertainty of the modelling.

For most of the study, copper was used for the simple reason that it is sensitive and reliable to be analyzed by atomic absorption. The stock solution is prepared from Cupric Nitrate (made by BDH). The $Cu^{2+}$ concentration of the stock solution is $10^{-2}$ mol/l.

### 4.1.4 Experimental Set Up

Figure 4.1 outlines the experiment set up for the preliminary stage of the study. A 250 ml Nalgene filter unit serves as the adsorption reactor, containing the mixture of particles and solution. The mixture is constantly agitated by a motor-driven plastic propeller so that the mixture is maintained as a suspension. On the bottom of the reactor is a Millipore membrane of 0.45 μm pore size. While the membrane keeps the particles in the reactor, the solution permeates through the membrane continuously. The permeate of the filter is collected in the sample bottle and returned to the adsorption system when sampling is not needed. Because the permeate in the sample bottle is constantly collected and recycled, it represents the solution concentration in the reactor, when the system is at equilibrium.

Sorbate concentration in the experiments will be low so that the adsorption falls into the "Henry's Law" range, i.e., linear relationship holds between amount of adsorption and sorbent concentration in the solution. This arrangement greatly reduces the complexity of modelling. The inconvenience of low concentration is the possibility of contamination from various sources and poorer accuracy of analysis. Also sorbate concentration may change due to adsorption onto the walls of experiment apparatus. Tests must be carried out to assess the impact of those effects.

A test was conducted to check if there is any contamination from the experimental set up. In the test, the system was filled with deionized water and agitated for a few days.

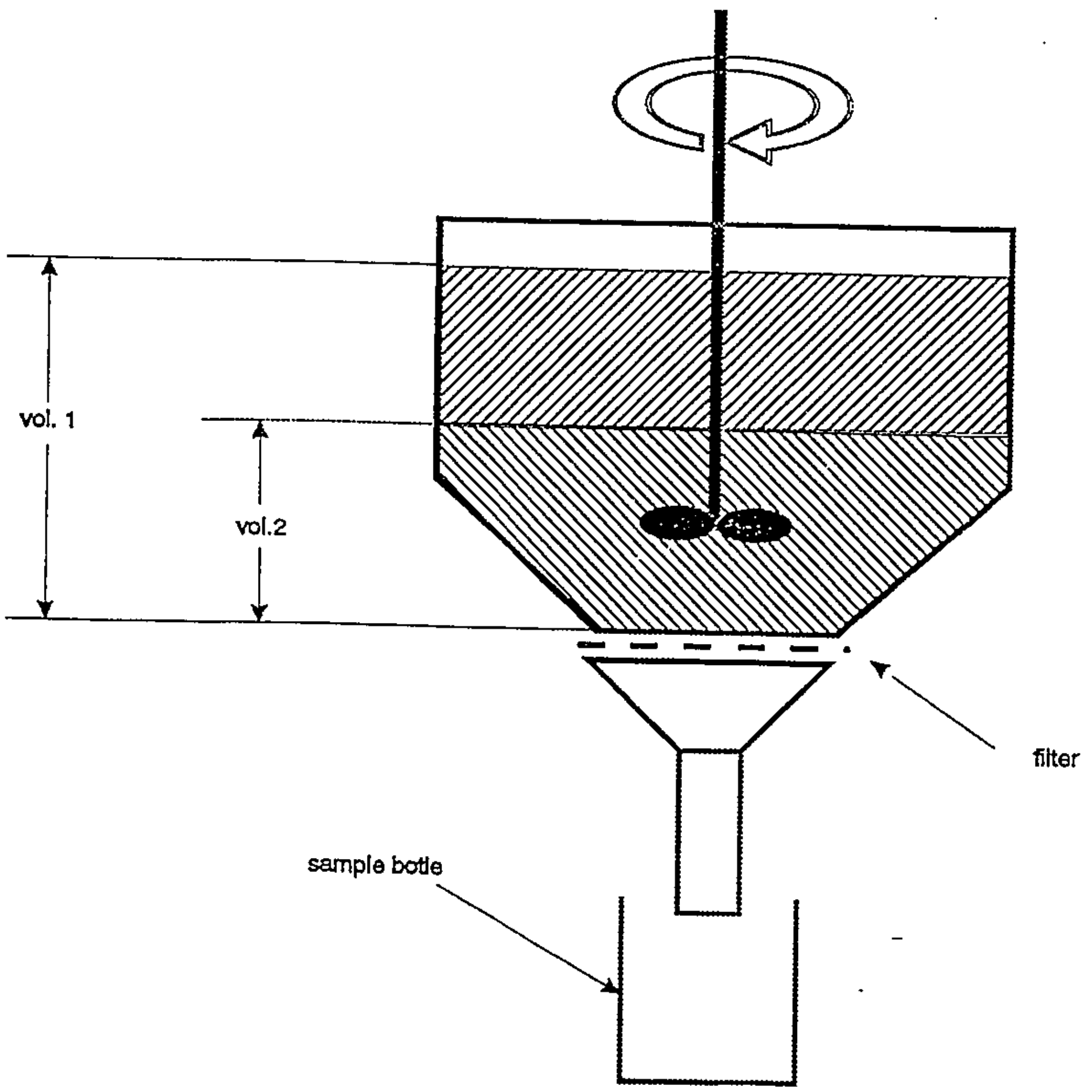


Figure 4.1 Set up for preliminary experiments

Samples were taken daily and analyzed with an atomic adsorption spectrophotometer. No contamination was detected.

A second test on the system is to examine the adsorption of Cu to the wall of the system. A Cu solution of 63.5 ppb was left in the system for 6 days and sampled every day. No detectable change was found during that period.

Since the results of the above tests were all negative, this system is proved to be adequate for the planned experiments.

### 4.1.5 Preparation of Buffer

A constant pH is essential for adsorption experiment. By conducting an isotherm adsorption experiment, it was found that pH 5 is appropriate for the adsorption of Cu onto kaolinite. With a pK of 4.74, acetic acid can provide a buffer at that pH. The buffer is composed of acetic acid and sodium acetate. The chemicals are made by BDH. The following equation was used for the calculation of the concentration of the components.

$$pH = -\log K - \log \frac{[HC_2H_3O_2]}{[C_2H_3O_2^-]} \tag{4.1}$$

Given the buffer system, it is necessary to examine the speciation of the solution. For the purpose of this study, it is very desirable to eliminate or minimize precipitation and excessive complexation in the solution. The estimation of solution speciation was carried out with the computer program MINEQL. Compiled by J.C. Westall et al [ Department of

Civil Engineering, MIT], it is one of the most popular computer packages programmed for the calculation of solution speciation at equilibrium. By inputting total composition of a solution, the program outputs detailed information on the speciation of each component in the system. For the experiments on Cu adsorption, system speciation was checked at three different buffer concentrations that were applied in the experiment. The results are attached in Appendix D. It can be seen from the results that precipitation does not exist and complexation of Cu by acetate is insignificant. The total concentration of Cu used in the calculation is 1 μmol/l. This concentration is higher than any equilibrium concentration actually used in experimental work. Therefore it is safe to say that in the experiments on particle concentration effect, the complications from precipitation and complexation is insignificant.

### 4.1.6 Analytical Method

The analysis of metal concentration was performed with a Perkin-Elmer 2380 Atomic Absorption Spectrophotometer with coated graphite furnace. The analytical procedure is programmed as follows:

| Step | Temperature (°C) | Ramp Time (sec) | Hold Time (sec) |
|---|---|---|---|
| 1 | 50 | 1 | 10 |
| 2 | 120 | 5 | 10 |
| 3 | 1000 | 5 | 20 |
| 5 | 2300 | 0 | 5 |
| 6 | 2600 | 1 | 6 |
| 7 | 20 | 1 | 10 |

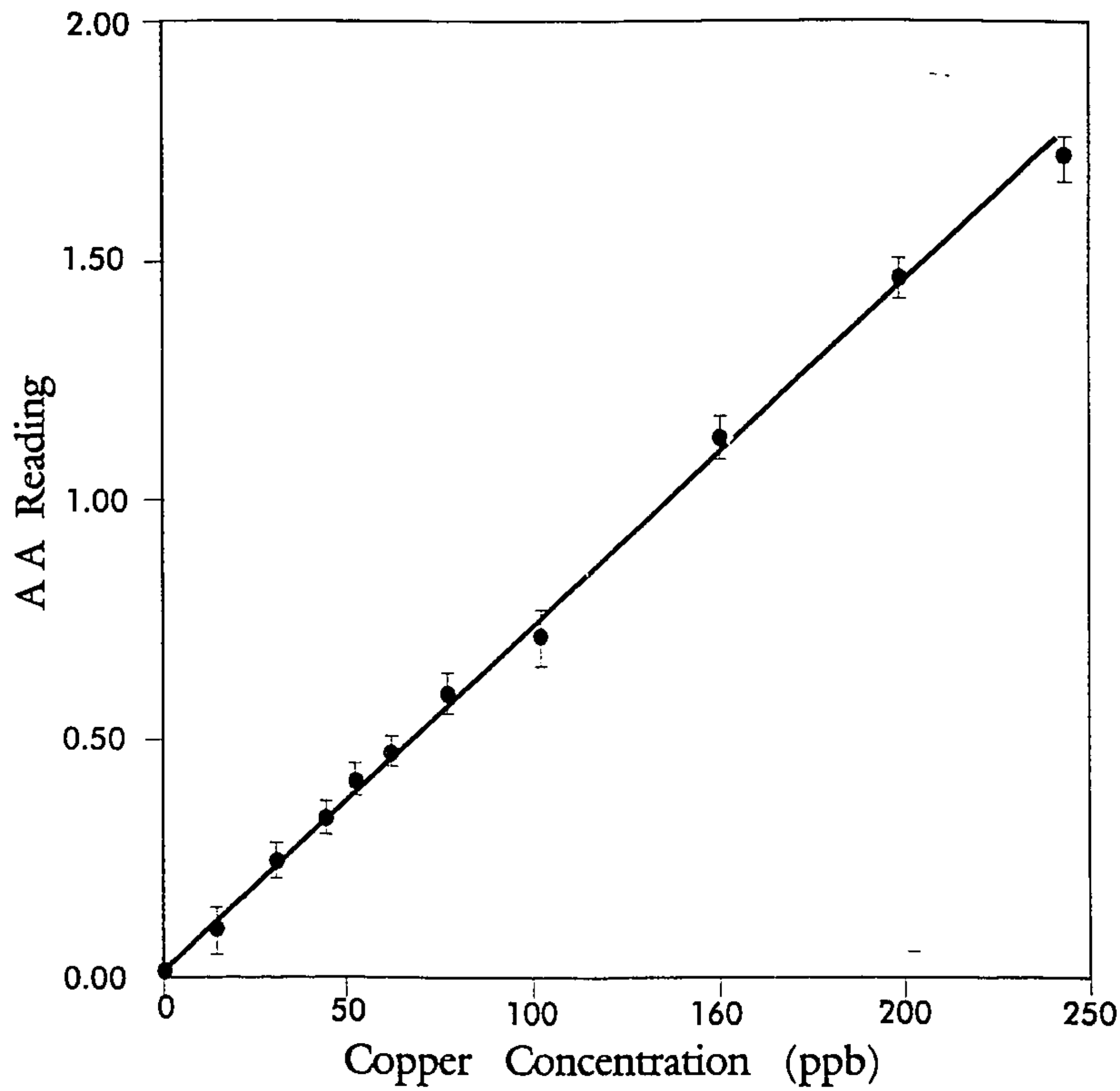


Figure 4.2 LINEARITY OF ATOMIC ABSORPTION ANALYSIS

The sensitivity and linearity of the analysis was examined by running a group of standard samples. The results were shown in Figure 4.2. The results indicate that there is good linear responses within the range in which the adsorption experiments will be.

### 4.1.7 Kinetic Consideration on Preliminary Experiments

Much has been said earlier about the kinetic effect in adsorption. It is therefore imperative to check adsorption speed to ensure that enough adsorption time is allowed to reach adsorption equilibrium or steady state. Kinetic experiments were conducted for this purpose. Using the same set up, copper nitrate was spiked into the adsorption reactor. A very high particle concentration of 20 g/l was chosen for the kinetic experiment. The intention was that it exceeds any particle concentration that will be used in later experiments to ensure that kinetic effect was eliminated. The change of the sorbate concentration in the solution was monitored by taking samples intermittently through filtration. Figure 4.3 plots the change of sorbate concentration in solution versus time. The result suggests that the adsorption of copper onto kaolinite reaches equilibrium or steady state within minutes. A similar test was done on quartz (Figure 4.4) and fast kinetics were also found.

### 4.1.8 Results of Preliminary Experiments

Preliminary experiments were conducted according to the " concentrating" protocol described earlier (Section 4.1.1). Adsorption experiments were always started at lower particle concentration. The particles were presoaked for over 24 hours before being used. After the first equilibrium was established, a solution sample was taken for analysis. The

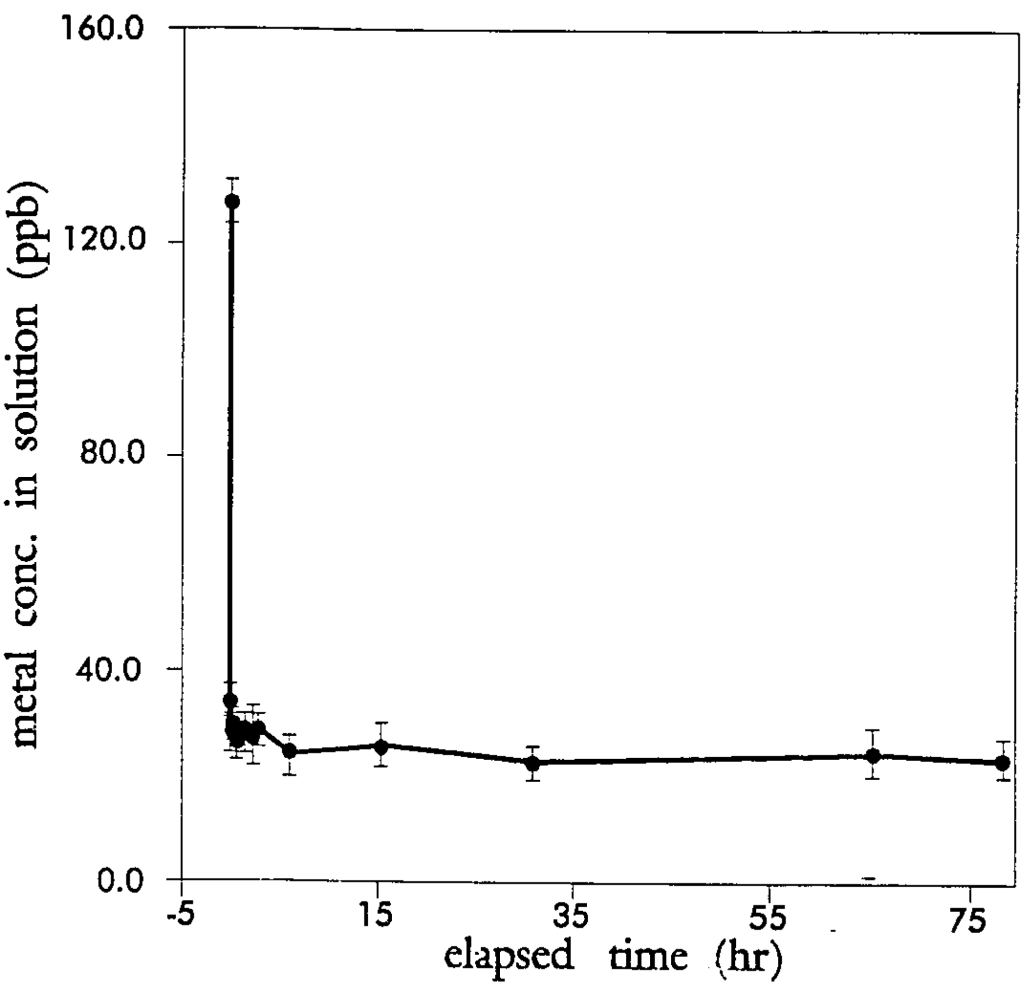


Figure 4. 3 KINETIC EXPERIMENT: COPPER ADSORPTION ON KAOLINITE
(Hac/Ac buffer pH 5; particle concentration 20g/l)

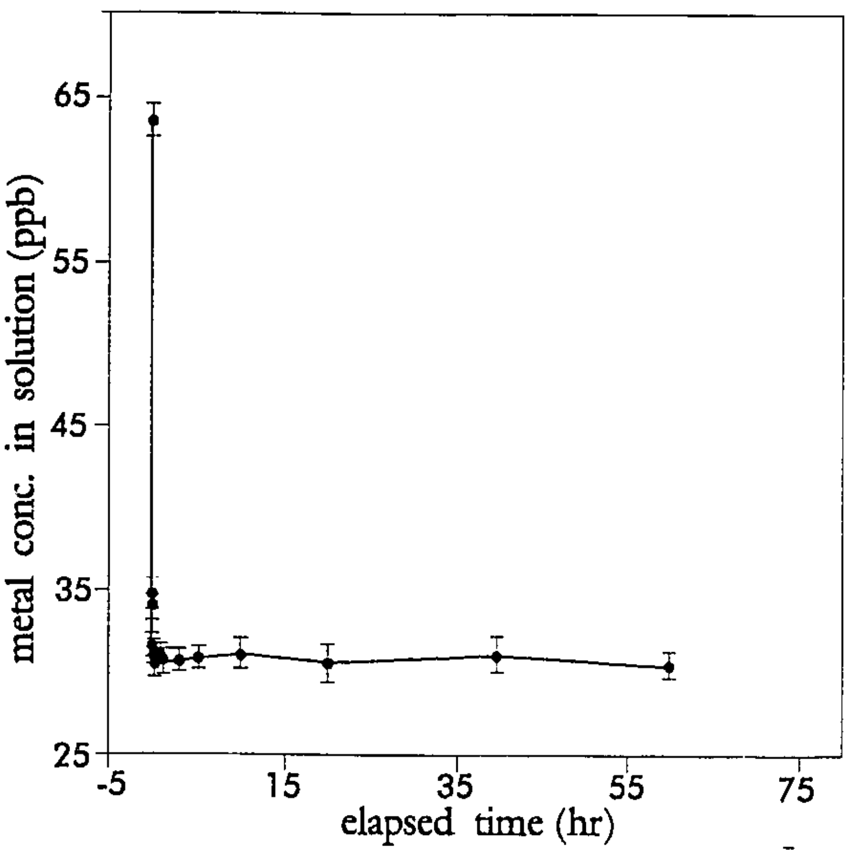


Figure 4.4 KINETIC EXPERIMENT: COPPER ADSORPTION ON QUARTZ (HAc/Ac buffer pH 6; particle concentration 50g/l)

second stage of the experiment was to increase particle concentration while holding other system parameters constant. The particle concentration was increased by draining a portion of the solution through the filter located on the bottom of the reactor, while continuing agitation. After this volume adjustment, a second adsorption equilibrium of the system was in turn reached and another sample was taken under the second equilibrium.

Table 4.2 contains data on Cu adsorption on kaolinite. The difference between the two equilibrium concentrations is remarkable. The last row of data in the table shows the ratio of the two equilibrium concentrations. It can be seen that the solution concentration of the sorbate increased around 20% after the second equilibrium.

**Table 4.2 Particle Concentration Effect: Adsorption of Cu onto Kaolinite ***

| | | | | |
|---|---|---|---|---|
| Initial Particle Concentration (g/l) | 0.1 | 0.5 | 5.0 | 10.0 |
| 1st Equilibrium Cu Concentration in Solution (ppb) | $15.2^{+1.2}_{-0.9}$ | $25.9^{+1.3}_{-1.2}$ | $14.0^{+2.0}_{-1.4}$ | $11.8^{+0.7}_{-0.9}$ |
| Concentrated Particle Concentration (g/l) | 0.2 | 1.0 | 10.0 | 20.0 |
| 2nd Equilibrium Cu Concentration in Solution (ppb) | $18.4^{+1.9}_{-1.3}$ | $33.9^{+1.2}_{-1.0}$ | $17.3^{+1.1}_{-1.6}$ | $15.3^{+1.5}_{-1.4}$ |
| Ratio of the Two Equilibrium Conc. | 1.21 | 1.31 | 1.23 | 1.3 |

* Ionic strength: $10^{-3}$ mol/l; Buffer: NaAc/HAc pH = 4.9.

A similar experiment was conducted using quartz as sorbent. Again, the particle concentration effect was noticeable (Table 4.3).

**Table 4.3 Particle Concentration Effect: Cu Adsorption Onto Quartz**

| | | |
|---|---|---|
| Initial Particle Concentration (g/l) | 1.0 | 10.0 |
| 1st Equilibrium Cu Concentration in solution (ppb) | $76.0^{+5.7}_{-4.2}$ | $145.0^{+4.7}_{-4.1}$ |
| Concentrated Particle Concentration (g/l) | 2.0 | 20.0 |
| 2nd Equilibrium Cu Concentration in Solution (ppb) | $96.0^{+4.1}_{-5.4}$ | $163.0^{+5.2}_{-6.0}$ |
| Ratio of the two equilibrium conc. | 1.3 | 1.1 |

* Ionic strength: $10^{-3}$ mol/l; Buffer: NaAc/HAc pH = 4.5.

Table 4.4 was composed for estimating the influence of ionic strength and particle concentration range.

**Table 4.4 Effect of Ionic Strength and Particle Concentration Range on the Ratio of Sorbate Equilibrium Concentrations ***

| Particle Conc. Change (g/l) | Ionic Strength $10^{-2}$ mol/l | Ionic Strength $10^{-3}$ mol/l | Ionic Strength $10^{-4}$ mol/l |
|---|---|---|---|
| 0.1 ⇒ 0.2 | 1.12 | 1.21 | 1.10 |
| 0.5 ⇒ 1.0 | 1.03 | 1.31 | L30 |
| 5.0 ⇒ 10 | 1.15 | 1.23 | 1.44 |
| 10 ⇒ 20 | 1.03 | 1.30 | 1.34 |

* Sorbent: Kaolinite; Sorbate: Cu; Buffer: NaAc/HAc pH = 4.9.

From Table 4.4, it can be seen that the ratio of the two equilibrium concentrations is always equal or greater to 1. Nevertheless variations seem relatively too pronounced to determine the influence of ionic strength and concentration range. A statistical analysis is therefore necessary. The statistic package MINITAB was used for the test.

**Table 4.5 Statistic Analysis of the Variance of the Concentration Ratio**

| Variance Source | | S.S. | M.S. | S. Ratio |
|---|---|---|---|---|
| Particle Conc. | 3 | 0.026 | 0.009 | 0.87 |
| Ionic Strength | 2 | 0.105 | 0.052 | 5.76 |
| Error | 6 | 0.054 | 0.009 | - |
| Total | 11 | 0.185 | - | - |

It is generally believed that there is a threshold of particle concentration, below which no particle concentration effect can be observed. The threshold is system specific. It is therefore desirable to have the experiments done with the particle concentration range above the threshold. Results of the statistical analysis (Table 4.5) indicate that particle concentration ranges chosen (0.1-0.2, 0.5-1.0, 5-10, 10-20 g/l) are all above the threshold, because not much difference has been found among the particle concentration ranges as a factor (S Ratio 0.87<< F 4.76). On the other hand, however, it shows statistic significant evidence (S Ratio 5.76 > F 5.14), that ionic strength has caused variation in the equilibrium concentration ratio and is therefore an important factor.

The effect of ionic strength observed is worth noting. It is well known that high ionic strength can cause coagulation and consequently reduce surface area of the particles. Should coagulation be the cause of the particle concentration effect in these experiments, the equilibrium concentration ratio ought to increase when ionic strength is raised. Yet the opposite happened. The particle concentration effect are more pronounced as ionic strength decreased. This observation is consistent with that of Di Toro [1986]. It is easy to explain this behaviour of adsorption with double layer interaction theory. The interaction range of double layer is inversely proportional to ionic strength.

At high ionic strength, double layer is suppressed and interparticle interaction is weakened or diminished. Some research workers, such as McKinley and Jenne [1989], failed to see the particle concentration effect in their carefully designed and controlled experiments, probably simply because they were using relatively high ionic strength (0.1 mol/l in the case of McKinley and Jenne).

### 4.1.9 Application of DLI Model on Preliminary Experiments

As a mathematical model, the ultimate purpose of the DLI (Double Layer Interaction) model is to describe the adsorptive behaviour of particulate substances in natural waters. The difficulty of such applications, however, lays in the fact that multiple mechanisms are usually involved in the process, as discussed in Section 4.1.1. In addition, particles vary in composition, size, geometry, physical and chemical properties, adding complicity to modelling process. Not to mention that many data are simply not available. Nevertheless, it is possible to apply the DLI model to the preliminary experiment, provided that any insufficient information is covered by reasonable assumptions.

As has been discussed in Chapter 2, the geometry and size distribution of the particles are essential for the modelling of the double layer interaction. More detailed discussion on microstructure and grain size of sediment can be found late in Chapter 5. In the case of this preliminary experiment, however, the size distribution of the clay particles is not available. For the purpose of demonstration, similar modelling information found in literature was used. Pusch [1970] presented a histogram (Figure 4.5) of size distribution in his study of clay particles. The median value is 0.029 μm and the quartiles

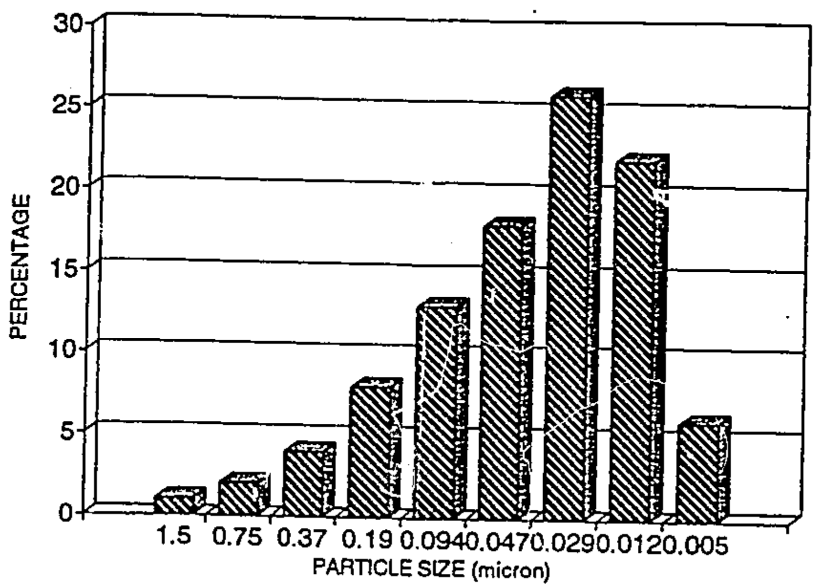


Fig.4.5 histogram of clay particle size distribution (Pusch 1970)

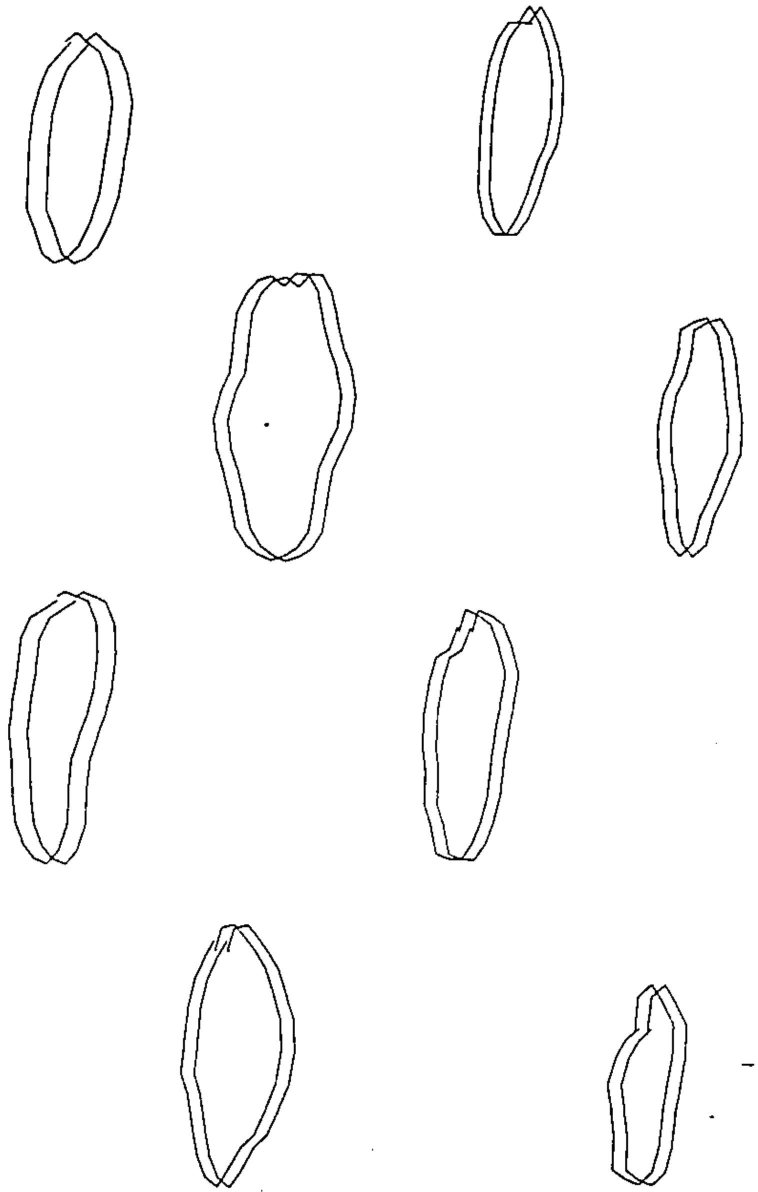

Figure 4.6 In a stable colloidal suspension, clay particles are distributed evenly throughout the volume of the system.

0.015 and 0.082 $\mu m$ respectively. Inputting this set of data into the DLI model, together with other parameters from the preliminary experiments, the results are encouraging.

Assuming that the colloidal system is at stable condition, i.e., repulsive force between the clay particles is dominating and the particles are distributed evenly throughout the volume of the system, every single particle should be allocated at such an equilibrium position that the distances to all its neighbours are uniform (Figure 4.6). Based on the particle concentration used in the preliminary experiment, the average interparticle distance can therefore be readily estimated (Table 4.6).

**Table 4.6 Average Interparticle Distance in Preliminary Experiments**

| Particle Concentration (g/l) | 0.1 | 0.2 | 0.5 | 1.0 | 5.0 | 10 | 20 |
|---|---|---|---|---|---|---|---|
| Interparticle Distance (Å) | 643 | 511 | 376 | 299 | 175 | 139 | 110 |

A calculation with the DLI model shows that except where a high ionic strength combines with a low particle concentration, the average interparticle distances are such that particles are within one another's interacting range. According to these interparticle distances, the change of adsorption energy, caused by the interaction of the double layers, can be calculated, based on the experimental parameters used in the preliminary experiments (the approach of calculation is described in Appendix F). In table 4.7, the calculated energies are compared with experimentally extrapolated energies, at each ionic strength and particle concentration used in the preliminary experiments on clay suspension.

**Table 4.7 Comparison between theoretically predicted and experimentally extrapolated adsorption energy change (cal/mol)**

| Ionic Strength (mol/l) | $10^{-2}$ | | $10^{-3}$ | | $10^{-4}$ | |
|---|---|---|---|---|---|---|
| Particle Conc. Change (g/l) | DLI Model Prediction | Experimental Extrapolation | DLI Model Prediction | Experimental Extrapolation | DLI MOdel Prediction | Experimental Extrapolation |
| 0.1⇒0.2 | 1 | 18 | 109 | 234 | 189 | 131 |
| 0.5⇒1.0 | 16 | 45 | 223 | 194 | 271 | 219 |
| 5.0⇒10.0 | 143 | 119 | 288 | 205 | 324 | 275 |
| 10.0⇒20.0 | 193 | 24 | 282 | 173 | 391 | 212 |

It can be seen from Table 4.7 that the two set of data are mostly within the same order of magnitude yet do not match very well. Noticeably at high ionic strength ($10^{-2}$), the match of the data is the poorest. The poor match of the data is not surprising considering, first of all, the particle sizes employed in the calculation might be very different from the actual ones.

What is more important is that more than one mechanism is contributing to the process, as has been elaborated in Section 4.1.

## 4.2 The Second Stage of Experiments

### 4.2.1 Using Glass Beads as Sorbent

Having confirmed the phenomenon of the particle concentration effect in the first phase of experiments, the next step of the research calls for an unambiguous experimental approach to verify the theoretical model. So far clay has been used as sorbent and the linkage between the theoretical model and the experiments may have been potentially interfered by two factors. Firstly, there is peptization effect as discussed in Section 4.1.1. Apparently, when this effect looms in the background, any quantitative result derived from experimental data is questionable. Secondly, the wide size distribution and irregularity of the sorbent create great uncertainty to mathematical treatment. The focus of the next stage of experimental work is therefore to gain quantitative information, while further confirming the particle concentration effect.

The key point of experimenting on the particle concentration effect is to be able to single out one factor or mechanism to be examined and to eliminate or minimize other factors or mechanisms. The design of preliminary experiments tried to follow the same principle. There is, however, insufficiency in the experimental system used in preliminary experiments, primarily the sorbent. As discussed earlier, uncertainty was introduced when the solid/liquid separation process failed to completely remove colloidal particles generated from kaolinite. Also, the calibration of the mathematical model calls for well defined sorbent particles in terms of size and geometry.

Glass beads seem to be a good material for this purpose. The merits of glass beads include:

1. Glass beads are physicochemically stable and resistant, they do not release ligands and colloids.
2. Glass beads are relatively well defined spheres facilitating close-to-ideal surface geometry for mathematical modelling.
3. The narrow size distribution of glass beads makes it easy to estimate the total number of them and their average separation distance, based on the weight of the glass beads. These calculations are essential for mathematical modelling.
4. With glass beads, two factors eliminate the problem of surface area reduction when aggregation, if there is any, occurs. Firstly, contact between spherical surfaces can only be a "point", the affected area is rather small compared to

the total surface area of the spheres. Secondly, the size of the glass beads is relatively well defined and is huge compared to hydrated metal ions. Even when the beads are closely packed, the metal ions should be able to move around the surfaces freely. In other words, the aggregation of beads, if there is any, will not affect surface area of adsorption significantly.

Given these advantages, most of the suspected mechanisms other than double layer interaction can be eliminated. In other words, if particle concentration effect is observed during an experiment, double layer interaction should be exclusively responsible.

Two sizes of glass beads are employed in the present research. The diameters of the beads are 1.6 and 50 micron respectively. The use of 2 kinds of particles enables examination of the mechanism of particle concentration effect from a different angle. By comparing the experimental results of the two kinds of particles, the effect of particle size can be extracted. Listed in Appendix E is the information provided by the manufacturer of the glass beads. Also Appendix F contains microscopic pictures of the glass beads.

### 4.2.2 Preparative Experiments on Glass Beads

The adsorption pH of Cu on the glass beads was found to be higher than that of kaolinite (Figure 4.7) The same buffer was utilized for the adsorption of Cu except the pH is a half unit higher, at pH 5.5. In the later stage of the experiments, Ni and Cd were also used as sorbates. Their adsorption on glass beads under different pH is shown in Figure 4.8 and 4.9 respectively. For the purpose of model calculation, the pH

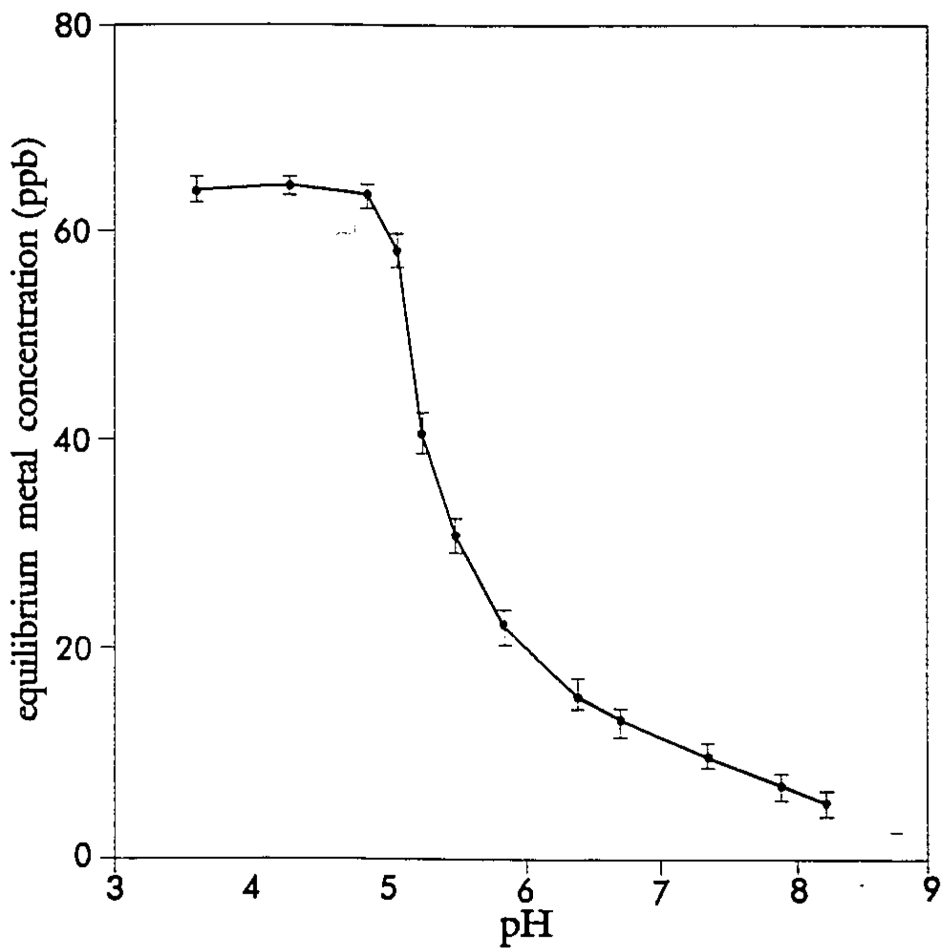


Figure 4. 7 pH EFFECT ON COPPER ADSORPTION ONTO GLASS BEADS
( 1.6 micron beads at $10^{-3}$ micron mol/l ionic strength)

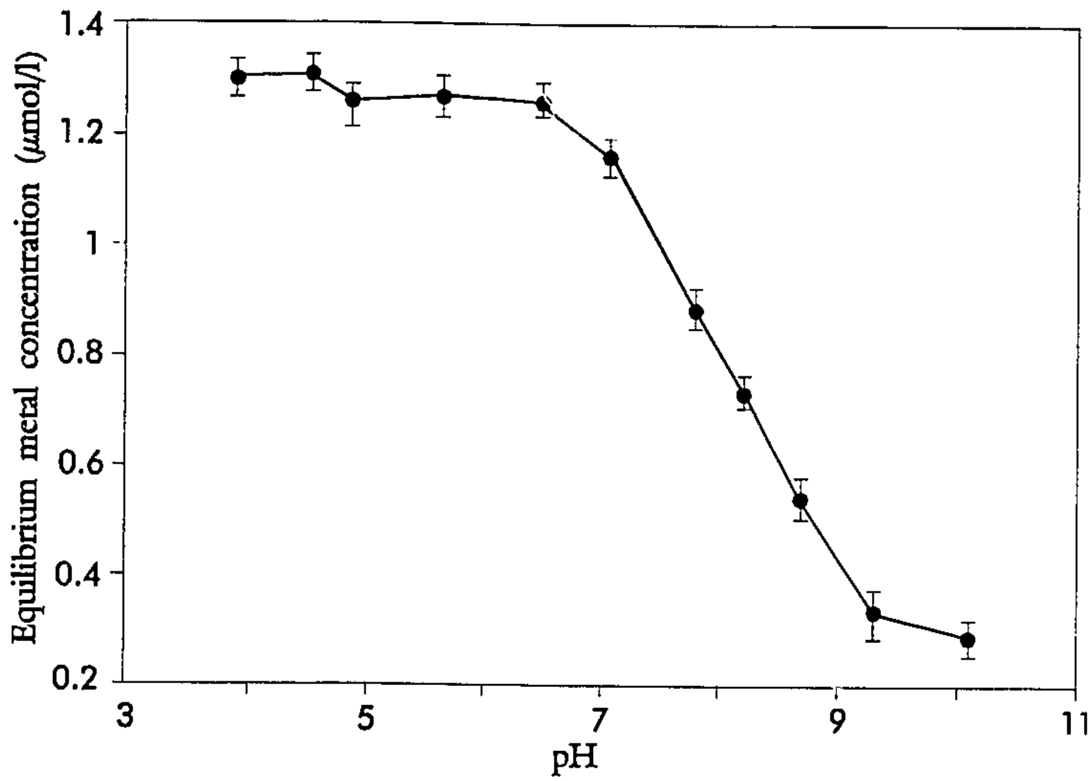


Figure 4.8 EFFECT OF pH ON Cd ADSORPTION ONTO GLASS BEADS

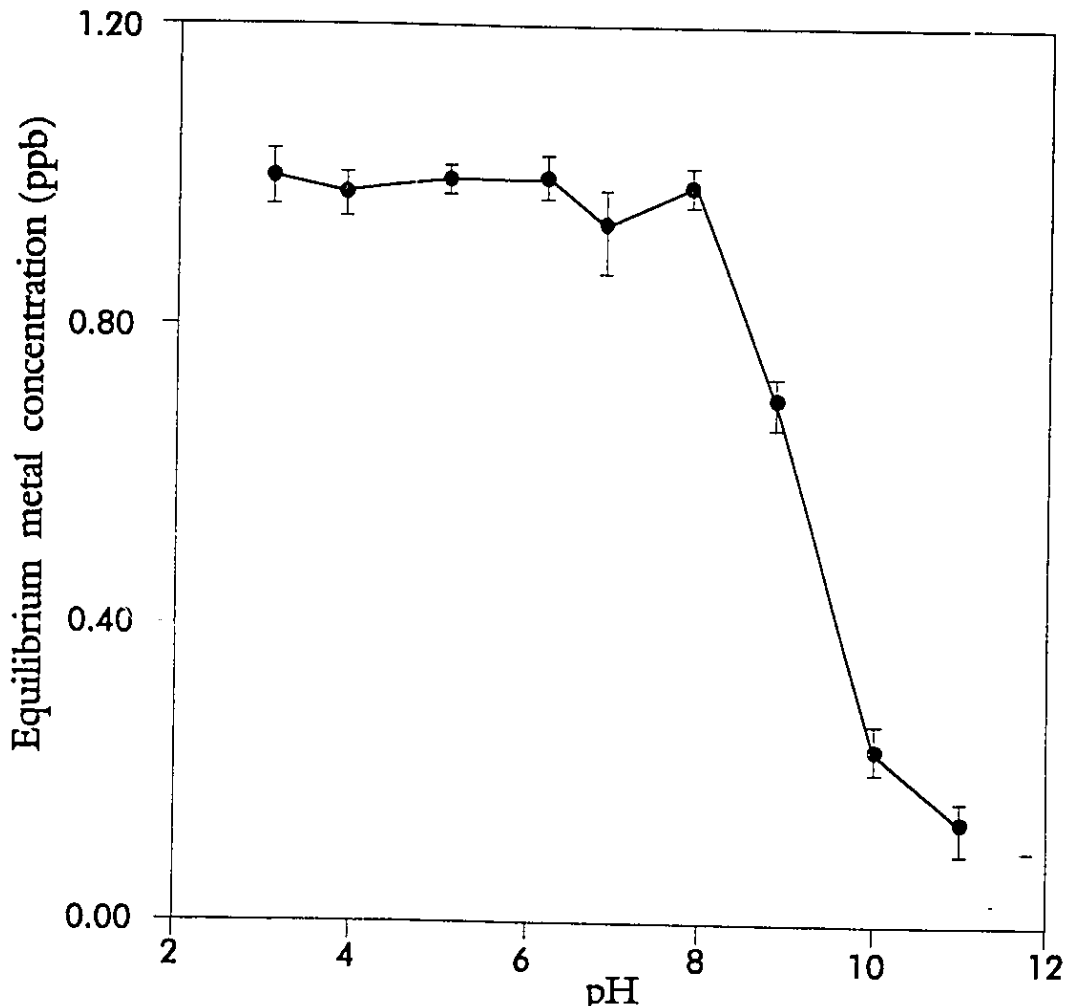


Figure 4.9 EFFECT OF pH ON THE ADSORPTION OF Ni ONTO GLASS BEADS

of zero point of charge of the glass beads needs to be determined (see Equation 2.16). A common method is pH titration [Stumm & Morgan 1981]. In the process, the suspension of glass beads was titrated with either acid or base under a certain ionic strength. A few titrating curves have been generated through this method, each under a different ionic strength (Figure 4.10). The shape of the curves varies from one another because of the effect of different ionic strength. At the $pH_{zpc}$, i.e., pH of zero point of charge, ionic strength exerts no impact on the process. Consequently, all the curves should pass a common point where the $pH_{zpc}$ is. Unfortunately, as indicated by the curves in Figure 4.10, the $pH_{zpc}$ of glass beads falls into the lower range of the pH scale, and is impossible to determine with titration. This is because ionic strength increases overwhelmingly as more acid is added into the system to further decrease the pH. The curves soon become overlapped and indistinguishable as their ionic strength approaches the same value. Alternatively, another method was adopted for the measuring of the $pH_{pzc}$, i.e., to use a Coulter 440 Electrophoresis unit. The work was done by Dr. Pelton's group (Department of Chemical Engineering, McMaster University), and the $pH_{pzc}$ was determined as 2.0.

Also checked is the pH reading with the electrode in the suspension and in the filtrate. According to Donan effect theory [van Olphen 1977], suspended particles can affect pH reading when an electrode is in contact with the suspension. No difference was found within the particle concentration range that was used in the experiments. Probably because the particle concentration is too low (considering the size of the glass beads) to generate the Donan effect.

#### 4.2.3 Experimenting on System Volume Reduction

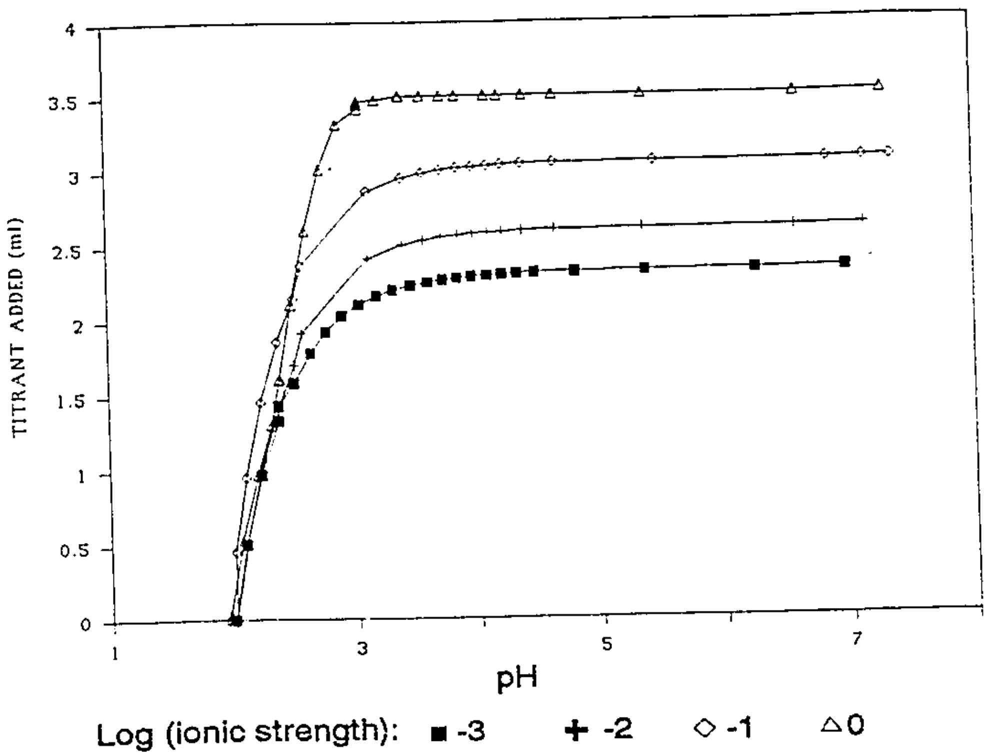


Figure 4.10 titration of glass beads: determination of pH of point of zero charge

Di Toro has done some experiments with glass beads [Di Toro 1986]. The sizes of the beads used were $\phi 2$ and $\phi 8$ μm respectively. Particle concentration effect has been observed in both cases. Checking Di Toro's experimental system with the DLI model, It was found that even with the $\phi 2$ μm glass beads, the double layer interaction ought to be insignificant. As discussed in Chapter 2, at a given particle weight, the distance of separation between particles is reversely proportional to the cubic power of the particle size. On the scale of colloidal particles, 2 μm is fairly large. The DLI model predicts that with Di Toro's system parameters, it will take particle concentration of two orders of magnitude higher to be able to generate detectable particle concentration effect.

The considerable discrepancy between Di Toro's data and the prediction of the DLI model raised the question of whether the DLI model was fundamentally wrong. The answer to the question can only be found through experimentation. A series of experiments were conducted on glass beads, both $\phi 50$ μm and $\phi 1.6$ μm. The experiments covered a wider range of particle concentration than that of Di Toro's. Also various ionic strengths have been tried in an effort to create the particle concentration effect. Yet the particle concentration effect was never observed in any of these experiments. The results of the experiments seem to agree with the DLI model. The DLI model is predicting that if the size of the glass beads is much smaller, volume reduction experiments would generate the same phenomenon of particle concentration effect as those observed in the preliminary experiments. With the given sizes and concentration of the glass beads, however, double layer interaction will not generate detectable particle concentration effect. It would take a much higher particle concentration to do that. The reason that Di Toro observed particle concentration effect is probably because centrifugation was used for liquid-particle separation. This will be explained in detail later in the next section.

### 4.2.4 Double Layer Interaction of Glass Beads

A volume reduction experiment always starts with a low particle concentration suspension and followed by a high particle concentration suspension after volume reduction. The particle concentration effect is examined by comparing the adsorption in each case. As has been discussed in the last section, with a diameter of 1.6 μm, the DLI model predicts that particle concentration effect is insignificant unless the glass beads are very close to one another. In other words, a suspension of very high particle concentration is needed to generate the particle concentration effect. Because of the high cost of micro glass beads, the amount of the beads available are insufficient for making a suspension of such high particle concentration.

A novel design of the experiment was developed to overcome this dilemma and demonstrate the particle concentration effect with small amount of 1.6 μm glass beads. The experiment is based on the following principle. If the low particle concentration suspension is centrifuged, the glass beads are closely packed on the bottom of the centrifugation vessel. Under the centrifugal force, the glass beads are in contact with each other, the separation distance between the cambered surfaces of the glass beads is minimized and the geometry of the surface separation can be readily calculated. Consequently, a solution sample taken from the supernatant of the centrifugation will reflect the adsorption equilibrium at the maximum double layer interaction. Using both centrifugation and filtration in the same experiment, there are two samples for comparison: one is the sample from the suspension of low particle concentration (minimum double layer interaction), the other is the sample from the supernatant of centrifugation (maximum double layer interaction). If double layer interaction does not have any impact on adsorption, the sorbent concentration in the two samples should be alike, i.e., no desorption happens because of double layer interaction. If the opposite is true, the sample taken from the supernatant of the centrifugation should contain higher sorbate concentration, since the adsorption equilibrium moves to desorption.

Figure 4.11 illustrates schematically the experimental scheme. Except a few modifications, the set up is similar to the previous one for the preliminary experiments, . The 0.45 μm pore-size filter membrane was replaced by the Nuclearpore filter membrane of 0.4 μm pore size. The Nuclearpore membrane distinguishes itself from the other filters by the fact that its pores are generated by radioactive particles and are therefore uniform in geometry. The combination of the Nuclearpore membrane and glass beads ensures the effectiveness of filtration. No particle can penetrate the membrane and the solution sample will be free of particle. The most important modification is the addition of the centrifugation process. The experiment procedure is as follows:

(1) Prepare particle suspension with pre-soaked glass beads and buffer solution in the adsorption reactor.

(2) Spike in sorbate and agitate properly until equilibrium is reached.

(3) Collect a sample of equilibrated solution through the filter on the bottom of the

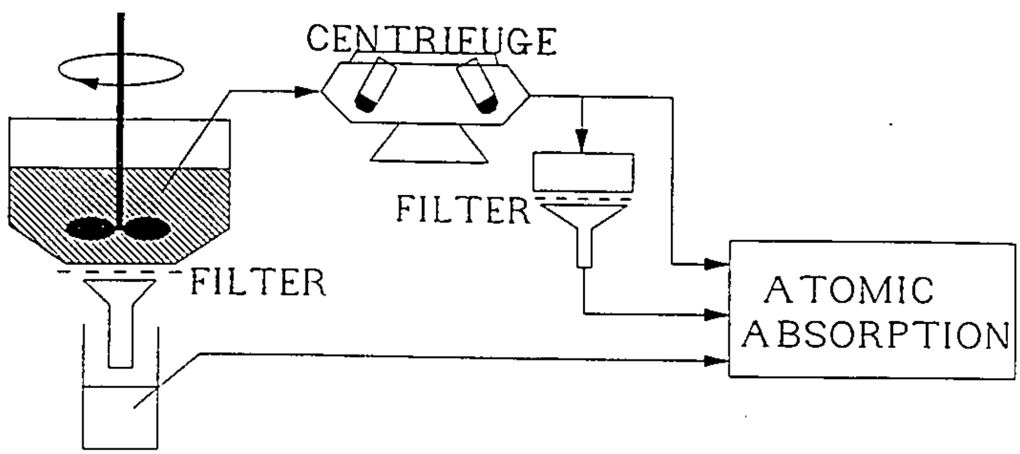


Figure 4.11 experiment set up for comparison between centrifugation and filtration

reactor.

(4) Immediately transfer the suspension in the reactor into a centrifugation vessel.

(5) Separate glass beads and solution through centrifugation process. The strength and duration of the centrifugation ensures a new equilibrium of sorbate partition between glass beads and the solution. Calculation of the centrifugal force has confirmed a rapid and complete separation of glass beads from the solution.

(6) Sample the supernatant of the centrifuged sample.

(7) Analyze the two samples (from filtration and centrifugation respectively) for sorbate concentration and compare the results.

(8) Part of the supernatant of the centrifugation is also filtered (Fig.4.11) with the 0.4 μm Nuclearpore membrane before being analyzed by the atomic absorption spectrometer. The comparison between the analytical results from atomic absorbtion with that of the unfiltered supernatant shows no difference in Cu concentration, indicating that the separation of the glass beads from the solution with centrifugation is complete.

The experimental results with Cu as sorbate are shown in Table 4.8. In the table, equilibrium concentration of filtered samples is compared with that of centrifuged samples. Both $\phi$1.6 and $\phi$50 μm glass beads were tested. Instead of using the weight of the beads as measurement of their quantity, total surface area was used for the purpose of comparison between the two sizes of glass beads. The amount of glass beads used was such that the total surface area of the two types of glass beads was identical. In this way, the results of adsorption experiments can be readily compared.

With the $\phi$1.6 μm beads, the results (Table 4.8) all show an increase in the concentration of the solution phase after centrifugation process. Since the centrifugation was conducted immediately after a filtration sample was taken from the adsorption system, sorbate concentration in both samples should be identical if the particle concentration effect is not involved. As has been discussed earlier, in this process all the mechanisms that can otherwise induce particle concentration effect have been excluded except double layer interaction. It is conceivable that desorption caused by double layer interaction is the only logical explanation.

The last column in Table 4.8 is the prediction of the DLI model on the equilibrium solution concentration when centrifugation is used. It predicts significant increase of sorbate concentration in solution phase for all the experiments utilizing $\phi$1.6 μm beads. For $\phi$50 μm beads, the effect is negligible because of the surface geometry.

**Table 4.8 Cu Adsorption Onto Glass Beads: Comparison Between Experimental Data and DLI Model Prediction**

| Size of Beads (μm) | Ionic Strength (mol/l) | Filtered Eq. Conc. (μmol/l) | Centrifuge Eq. Conc. (μmol/l) | DLI Model Prediction (μmol/l) |
|---|---|---|---|---|
| 1.6 | $0.9 \times 10^{-4}$ | $0.14^{+0.031}_{-0.027}$ | $0.24^{+0.032}_{-0.026}$ | 0.23 |
| 1.6 | $1.7 \times 10^{-3}$ | $0.31^{+0.032}_{-0.035}$ | $0.46^{+0.033}_{-0.031}$ | 0.45 |
| 1.6 | $1.9 \times 10^{-2}$ | $0.43^{+0.041}_{-0.44}$ | $0.57^{+0.043}_{-0.034}$ | 0.60 |
| 50 | $1.5 \times 10^{-3}$ | $0.76^{+0.046}_{-0.043}$ | $0.80^{+0.050}_{-0.047}$ | 0.78 |

To better visualize the change in adsorption, Figure 4.12 has been created using the data in Table 4.8. The black portion of the bars represents the equilibrium

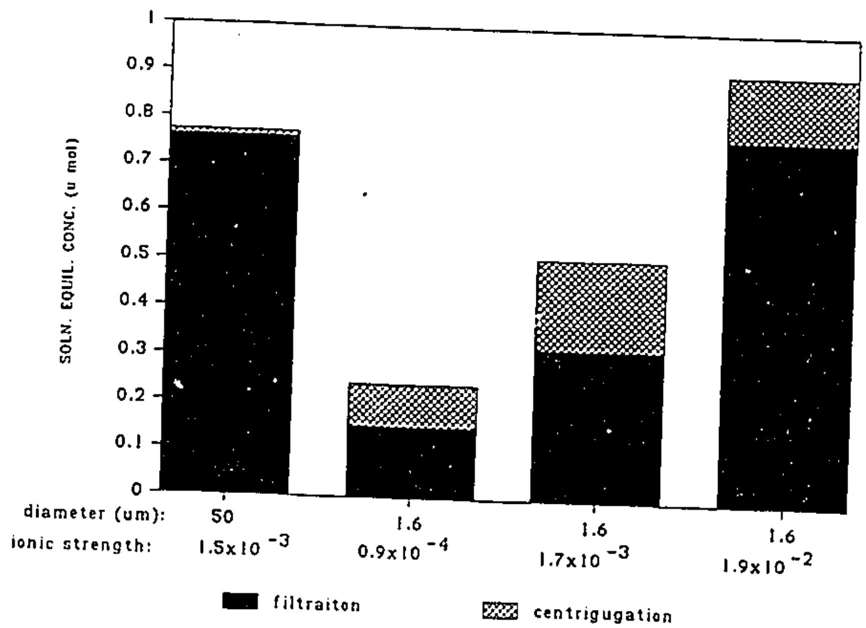


Figure 4.12 Cu adsorption onto glass beads: comparison between filtration and centrifugation

concentrations of Cu in the solution obtained with filtration. The textured portion of the bars designate the desorption of Cu from the glass beads after centrifugation process. For the purpose of comparing clearly between different sizes of beads and ionic strength, the unit of the Y-axis is transformed into percentage in Figure 4.13. Here the black portion of the bars, which is the metal equilibrium concentration in the solution obtained with filtration, is used as 100%. The textured portion shows how much the solution metal concentration has increased after centrifugation, in terms of percentage.

The modified bar chart made it easier to see effects of particle size and ionic strength. It is clear that the $\phi$1.6 $\mu$m glass beads always responded with desorption under centrifugation while the $\phi$ 50 $\mu$m glass beads appear indifferent. This observation agrees well with the DLI theory. Also supporting the DLI model is the observation that the particle concentration effect becomes more pronounced as ionic strength decreases. At an ionic strength of $1.9\times10^{-2}$ mol/l, the particle concentration effect is much less significant than at $1.7\times10^{-3}$ mol/l. Yet the strength of the particle concentration effect hardly increased in magnitude when the ionic strength reduced from $1.7\times10^{-3}$ to $0.9\times10^{-4}$. This is probably because of the pH instability of the system. The pH of the suspension made with glass beads tends to increase over time. At very low ionic strength, the buffer is too weak to hold the pH constant against the drift. In Figure 4.14, the effect of double layer interaction is plotted in the form of reduced adsorption energy. Comparisons are made between DLI predictions and experimental observations in energy terms. The black bars are DLI model predicted reduction of desorption energy when glass beads are closely packed by centrifugation process. The dotted bars represent experimental observation. Basically experimental observations are consistent with theoretical predictions. The relationship

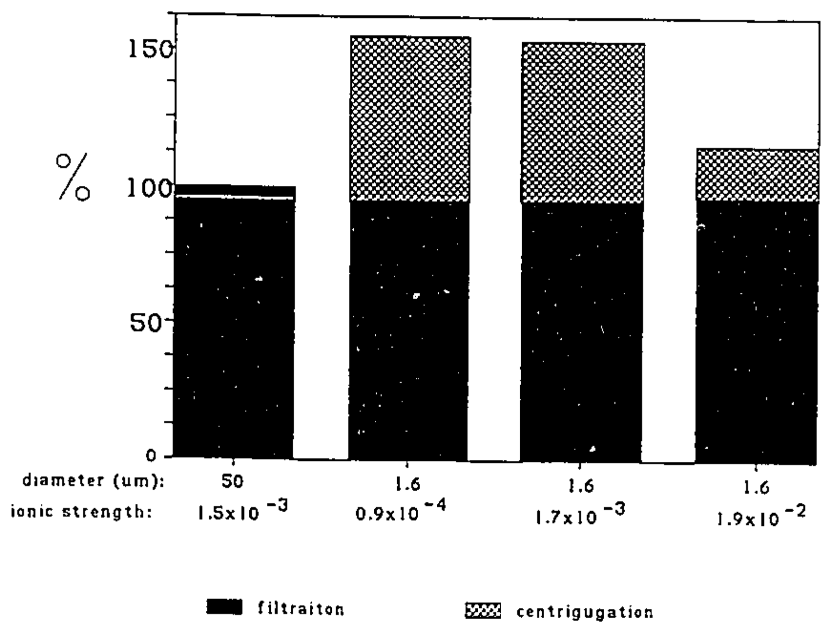


Figure 4.13 Cu adsorption onto glass beads: effect of double layer interaction

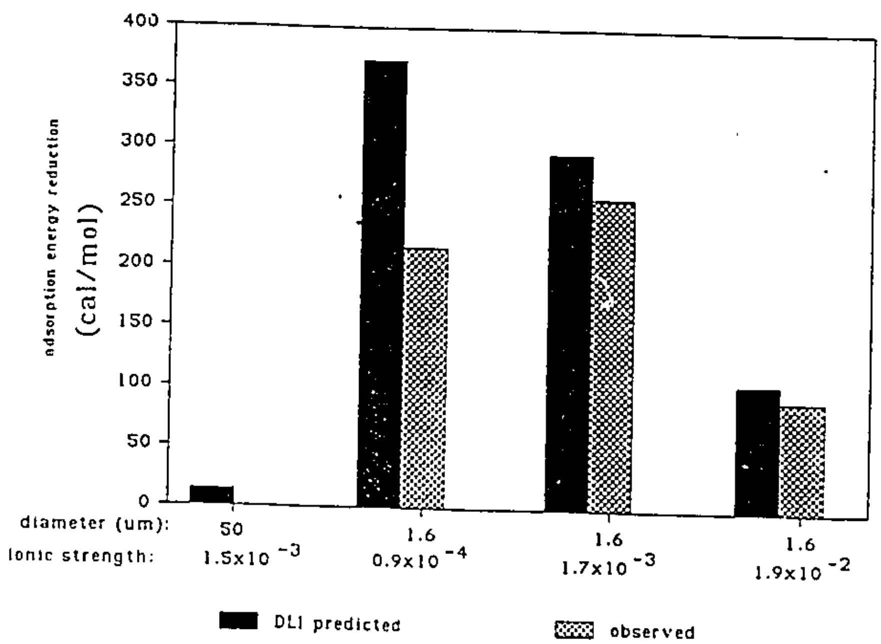


Figure 4.14 Cu adsorption onto glass beads: comparison of reduced adsorption energies

between the amount of adsorption and adsorption energy is not linear (Equation 2.20), nevertheless, the inclinations are similar. An eye-catching discrepancy in Figure 4.13 is the case of $0.9\times10^{-4}$ ionic strength, where the reduction of adsorption energy according to experimental observation falls far short compared to theoretical prediction. Again, this is probably due to the effect of pH drifting. The cause of the pH drifting was scrutinised for the following aspects:

(1) Insufficient soaking time for the glass beads

At the early stage of experiment, the glass beads were soaked at least 24 hrs. before being used in the experiments. Later, suspecting insufficient soaking time to allow equilibrium to establish on their surfaces, the glass beads were always kept in soaking. After each experiment, the glass beads were first washed with deionized water and diluted nitric acid, than rinsed repeatedly with deionized water. Finally, the glass beads were

soaked in the buffer that is identical to the one used in the experiment. This, however, has not been able to eliminate the drift of pH at low ionic strength.

(2) Atmospheric contamination

To avoid this problem, Ar or $N_2$ were gently blown onto the surface of the suspension during the experiment to protect the surface of the system from interaction with the atmosphere.

(3) Contamination from the pH electrode

At low ionic strength, pH electrode may not perform well and also trace amounts of electrolyte may leak into the system, consequently increasing the ionic strength. Tests were done with deionized water and buffer of $10^{-4}$ mole/l without glass beads, it was found that pH readings are relatively stable over time in both cases. This leads to the conclusion that the drift of the pH is not caused by the electrode and the electrode works well at ionic strength as low as $10^{-4}$ mol/l.

(4) De-gas of the solution

In the preliminary experiments, vacuum was utilized to assist filtration when samples were taken. The vacuum may also extract some dissolved gas such as $CO_2$ and contribute to the pH change. Specially designed tests have confirmed the speculation. This is particularly true in systems with glass beads and Nuclearpore filter membrane, because of less fouling of the membrane, the resistance to vacuum is smaller and therefore the pressure drop across the filter membrane is less. The vacuum thus renders stronger de-gas effect to the liquid above the membrane. To eliminate this effect, in all experiments with glass beads, no vacuum was applied for collecting sample. Even without vacuum, solution in the adsorption reactor permeates the membrane and drips into sample bottle constantly. This "leakage" could be stopped by applying a small $N_2$ pressure on the bottom of the adsorption reactor when samples are not being taken. This tactic was nevertheless not adopted. A constant drip to the sample bottle is actually desirable because it ensures the passage from the adsorption reactor to the sample bottle is in constant contact with the solution in the reactor (Figure 4.1). Any accumulation in the sample bottle is recycled to the reactor manually. Sample can be collected at any time after equilibrium. Because of the constant recycle of the filter permeate, the sample solution is always identical to that in the reactor at any given moment, and is free from contamination or dilution problem..

The results shown in Table 4.8 also reveal that all the theoretical predicted reductions of adsorption energy are greater than experimental observations. The possible reasons for this are as follows:

(1) Imperfection of the DLI model

(2) Non-ideal geometry of the glass beads

As can be seen from the microscopic photograph (Appendix F), the glass beads are not exactly the same size and much less than perfectly spherical. The pattern of packing after centrifugation may not be as compact as the ideal situation (Figure 2.11). These non-ideal factors will reduce the extent of double layer interaction and consequently lessen the particle concentration effect.

(3) Insufficient Convection

During the centrifugation, two processes happen simultaneously. The glass beads are settling down onto the bottom of the centrifugation vessel while equal volume of solution is expelled from the bottom of the vessel and goes up, forming a convective current. Most desorption happens only when the glass beads are closely packed, since the double layer interaction comes into play only after this point. In the mean time, convection diminishes to nearly zero. This may create a situation that the sorbate concentration in the immediate area of the glass beads is much higher than in the main body of the supernatant. Although the concentration gradient across the system facilitates diffusion of the sorbate from the sediment of the glass beads to the supernatant, the release will be too slow on the time scale of centrifugation. When a sample is taken from the supernatant, the concentration of the sorbate will be lower than it would be if the solution is well mixed.

Similar experiments were conducted on glass beads with Ni and Cd as sorbates. The approach and set up is exactly identical to those used in the experiments of copper adsorption. As can be seen from Figure 4.9, the appropriate pH for the adsorption of Ni is around 8. That pH, however, poses a problem because of precipitation of $Ni(OH)_2$ under the metal concentration utilized in the experiments (Appendix D). At equilibrium a large portion of the metal is in the form of $Ni(OH)_2$. Nevertheless the experiments proceeded as designed. As can be seen from Table 4.9, under such conditions, the effect of double layer interaction can still be observed. Again, ionic strength plays a decisive role. In the case of high ionic strength, $10^{-1}$, no significant difference can be found between centrifuged and filtered samples. Whereas in the lower ionic strength, $10^{-3}$, solution metal concentration was increased by 20% after centrifugation, indicating significant amount of desorption.

**Table 4.9 Ni Adsorption onto Glass Beads: Comparison Between Filtered and Centrifuged samples**

| | | |
|---|---|---|
| Size of Beads (μm) | 1.6 | 1.6 |
| Ionic Strength (μmol/l) | $1 \times 10^{-1}$ | $1 \times 10^{-3}$ |
| Filtered Ni Conc. (μmol/l) | $0.97^{+0.055}_{-0.047}$ | $1.9^{+0.057}_{-0.059}$ |
| Centrifuged Ni Conc.(μmol/l) | $0.99^{+0.045}_{-0.049}$ | $1.6^{+0.053}_{-0.055}$ |
| Solution Ni Increase (%) | 2* | 20 |

* Statistically insignificant.

The appropriate adsorption pH of Cd is also around 8 (Figure 4.8). Cadmium, however, does not precipitate until pH reaches as high as 10. The results of Cd adsorption are similar to that of Cu: particle concentration effect was observed with $\phi$1.6

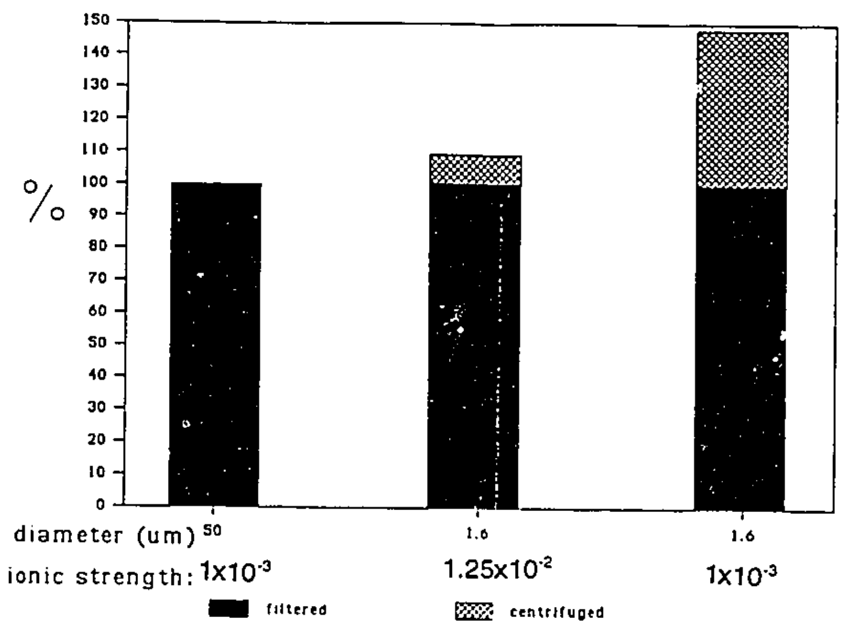


Figure 4.15 Cd adsorption onto glass beads: effect of double layer interaction

μm beads, and no desorption happened on ϕ50 μm beads. The effect of double layer interaction is more significant at lower ionic strength. This can be better visualized in Figure 4.15, which is plotted with the data in Table 4.10. In the plot, the equilibrium concentrations of filtered samples are used as 100%.

**Table 4.10 Cd Adsorption onto Glass Beads: Comparison Between Filtered and Centrifuged samples**

| Size of Beads (μm) | 50 | 1.6 | 1.6 |
|---|---|---|---|
| Ionic Strength (mol/l) | $1x10^{-3}$ | $1.25x10^{-2}$ | $1x10^{-3}$ |
| Filtered Ni Conc. (μmol/l) | $1.4^{+0.031}_{-0.035}$ | $0.53^{+0.030}_{-0.028}$ | $0.33^{+0.027}_{-0.025}$ |
| Centrifuged Ni Conc.(μmol/l) | $1.4^{+0.032}_{-0.030}$ | $0.58^{+0.024}_{-0.024}$ | $0.49^{+0.029}_{-0.025}$ |
| Solution Ni Increase (%) | 0 | 9 | 48 |

In Table 4.11, comparison was made between experimental data and DLI model prediction. Again, the observed interaction is always lower than predicted value, probably for the same reasons discussed in the case of Cu.

**Table 4.11 Cd Adsorption Onto Glass Beads: Comparison Between Experimental Data and DLI Model Prediction**

| Size of Beads (μm) | Ionic Strength (mol/l) | Filtered Eq. Conc. (μmol/l) | Centrifuge Eq. Conc. (μmol/l) | DLI Model Prediction (μmol/l) |
|---|---|---|---|---|
| 50 | $1x10^{-3}$ | 1.4 | 1.4 | 1.4 |
| 1.6 | $1.25x10^{-2}$ | 0.53 | 0.58 | 0.59 |
| 1.6 | $1x10^{-3}$ | 0.43 | 0.49 | 0.53 |

In Figure 4.16, reduced adsorption energies of Cd adsorption onto glass beads were plotted for comparison. Corresponding to the decreased adsorption, the adsorption energy also decrease according to Equation 2.20. Again, predicted energy reductions are

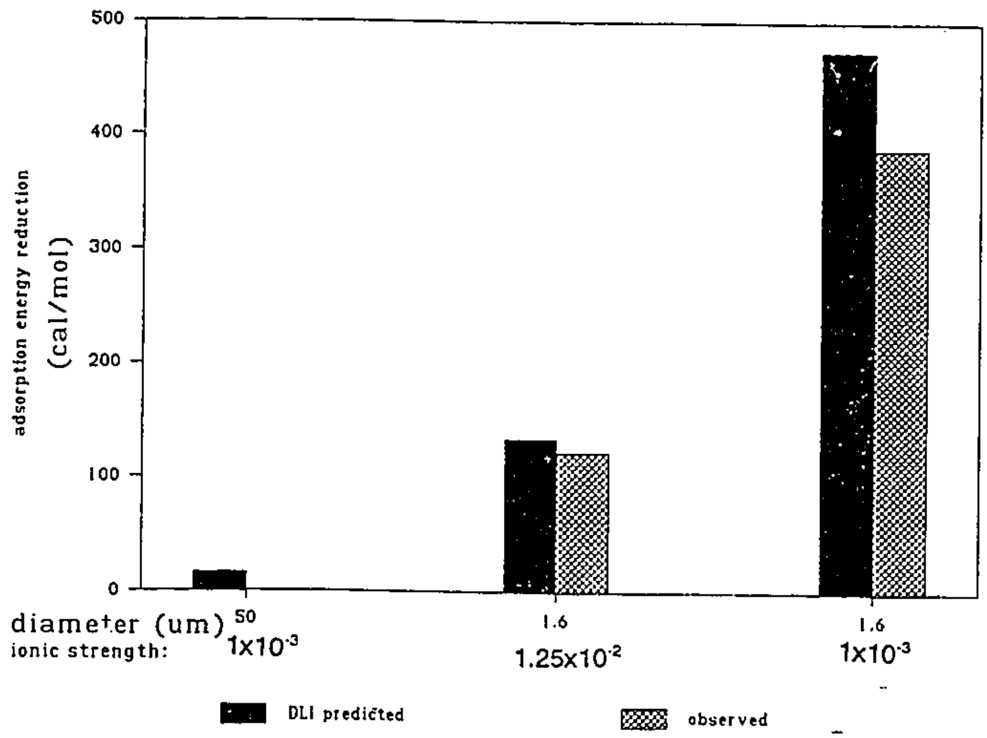


Figure 4.16 Cd adsorption onto glass beads: comparison of reduced adsorption energies

generally greater than observed ones.

# 5. ENVIRONMENTAL IMPLICATIONS OF THE PARTICLE CONCENTRATION EFFECT

## 5.1 Introduction

Environmental implications consider the desorption and cycling of (contaminant) chemicals due to particle concentrations. Particles in natural systems are heterogeneous and are of varying particle size. They are found in suspension in lakes and rivers, are deposited, and are resuspended. During these processes, different desorption processes are ongoing. This section considers the different particles, their sizes, morphologies and changes during the sedimentation-resuspension processes. The DLI theory is then applied at different ionic strengths representative of freshwater systems to estimate the degree of desorption due to particle concentrations.

## 5.2 Behaviour of Particles in Natural Waters

Sedimentation of particles is of great importance in the transport and distribution of matter in natural waters. Millions of tons of solids are brought into aquatic system by run-off water every year as a natural process. The solid particles can be involved in various dynamic processes, as depicted in Figure 5.1 [Mehta et al. 1989]. A suspension in horizontal transport is a mobile suspension. Whether particles will settle depends on their density, size, and the water movement. The suspension may become high density over time and possess a vertical velocity component. Particles deposited from a suspension first form a soft deposit which is referred to as consolidating deposit. As the deposit firms up, it becomes a settled consolidated bed. Entrainment of a stationary

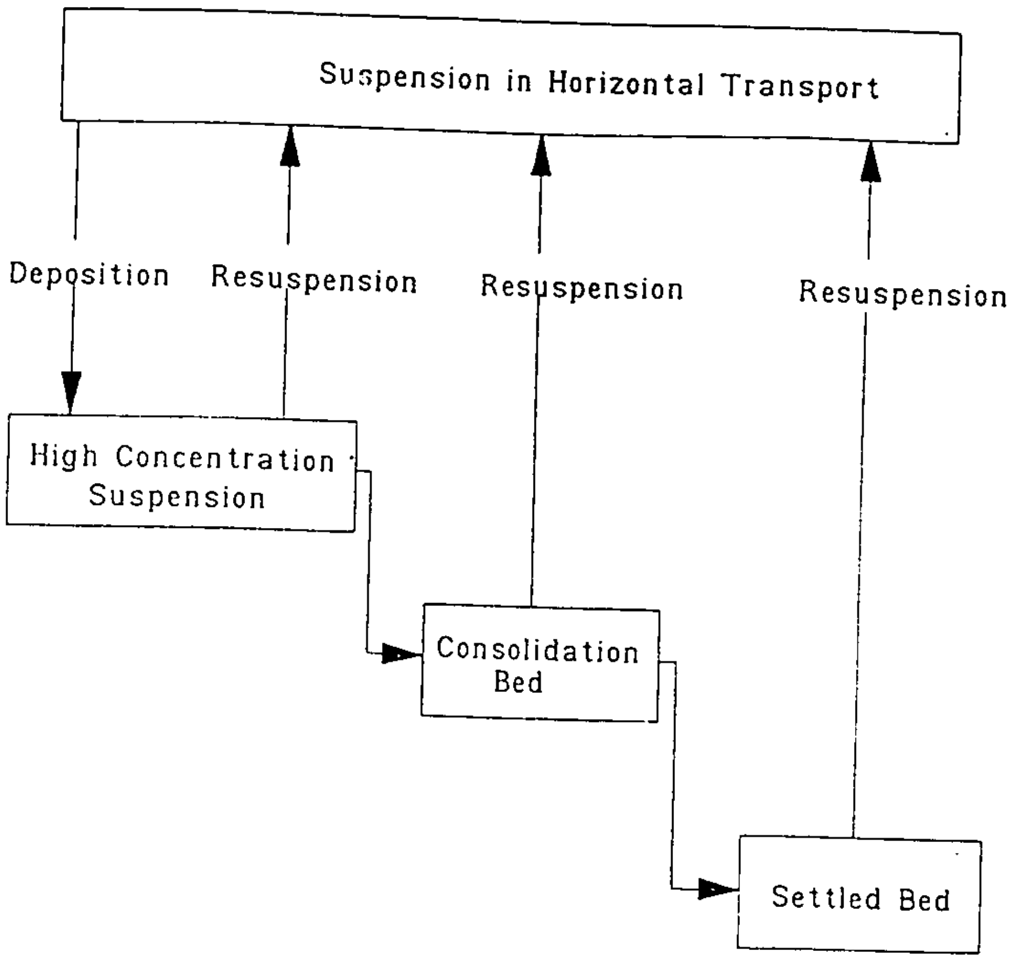


Figure 5.1 physical states and processes governing cohesive sediment transportation.
(after Mehta, 1982)

suspension, which typically could occur shortly after current reversal following slack water, has been referred to as resuspension or re-entrainment [Parker and Kirby 1977]. Entrainment from a consolidating or a settled bed is referred to as erosion or ften than not, the deposition of particles is predominating. It is estimated that all the rivers on the earth bring ca. 183 x $10^{14}$ g of sediment into the oceans per year [Lal 1977]. Much of the dispersed matter of rivers, however, settles before reaching the sea. The sedimentation of the particles on their way to the ocean is causing large scale silting-up of rivers, lakes, harbours, estuaries and navigation channels. All suspended clay particles become cohesive when the salinity exceeds 2 to 3 ppt [Migniot, 1968]. The boundary between cohesive and cohesionless sediment is, unfortunately, not clearly defined and generally varies with the type of material. However,

dominance of interparticle cohesion over gravitational force increases with decreasing particle size. Thus the effect of cohesion on the behaviour of clays (grain size < 2 μm) is much more pronounced than on silts (2 to 60 μm). In fact, cohesion in clayey mud is primarily due to the presence of clay-sized sediment.

### 5.3 Size Distribution of Clay Particles

As discussed in Chapter 2, the size of the particles is a crucial parameter for the estimation of desorption effect caused by double layer interaction. The desorption effect will be significant only when the size of the particles is below a certain level. Based on both theoretical and experimental studies shown in Chapters 2 and 4, it is conceivable that with grain size less than 2 μm, clay particles may interact with one another, leading to the desorption of adsorbed pollutants. Double layer interaction will not have such a effect on particles of larger size, simply because the geometry of larger particles does not allow pronounced overlap of double layers. Naturally, the grain sizes of sediment usually have a wide distribution. Taking, for instance, the analytical results of Bennett et al. [1991], the size of the particles is classified into three categories: coarse (5 to 2 μm), medium (2 to 0.2 μm) and fine (<0.2 μm). The percentage of the fine fraction varies from 30% to 46%. The medium size account for 10% to 14%. The rest, accounting for approximately 40% to 60%, are the coarse fraction. The major clay minerals identified in the sediments are illite, kaolinite, chlorite and smectite.

### 5.4 Sedimentation Velocity of Suspended Particles

The sedimentation process is similar to the centrifugation experiment described in Chapter 4, only at a slower rate. In the centrifugation experiment, the centrifugal force applied to the glass beads in the centrifugation vessel drives the beads down to the bottom of the vessel in a matter of seconds. Settling is a much slower process in natural waters. For particles in natural waters, settling is defined as the component of particle motion affected by gravitational forces. The estimation of the settling velocity is more complicated than simply applying Stokes's law. This is because of the non-ideal shape and behaviour of the particles. Clay particles tend to aggregate during the process of sedimentation. Table 5.1 shows some examples of settling velocities of particles derived from the studies of Migniot [1986] and Chase [1979] in settling tubes. For primary (dispersed) particle diameters of 20, 2 and 0.2 μm, the corresponding Stokes settling velocity of primary particles, aggregate settling velocity, and aggregate diameter are given.

**Table. 5.1 Primary Particle and Aggregate Diameters and Setting Velocities**

| Primary Particle diameter (μm) | Stokes settling velocity (mm/s) | Aggregate settling velocity (mm/s) | Aggregate diameter (μm) | Aggregate velocity divided by Stokes velocity |
|---|---|---|---|---|
| $2 \times 10^{1}$ | $2.4 \times 10^{-1}$ | $2.7 \times 10^{-1}$ | $8.8 \times 10^{1}$ | $1.1 \times 10^{0}$ |
| $2 \times 10^{0}$ | $2.4 \times 10^{-3}$ | $1.7 \times 10^{-1}$ | $5.6 \times 10^{1}$ | $7.1 \times 10^{1}$ |
| $2 \times 10^{-1}$ | $2.4 \times 10^{-5}$ | $1.1 \times 10^{-1}$ | $3.4 \times 10^{1}$ | $4.6 \times 10^{3}$ |

It can be seen from Table 5.1, the ratio of aggregate to Stokes velocity given in the last column ranges from 1.1 at a primary particle diameter of 20 μm to $4.6 \times 10^3$ at 0.2 μm.

The velocity of settling in natural environments is also affected by many factors such as particle density and shear strength in the water body. The whole process, i.e., from suspension to consolidation of sediment, takes place rather slowly. As Mehta [1989] found in his flume experiments, the consolidation of the sediment takes days to stabilize.

## 5.5 Morphological Change of Clay Particles During Sedimentation Process

The density and size of the particles also change during the settling [Partheniades 1965]. In a turbulent flow sediment grains collide to form continuously growing flocs. The flocs may in turn join together to floc aggregates while the latter combine into aggregate networks (Figure 5.2 A). The settling networks come eventually to their loosest equilibrium position determined by the overburden pressure and the bonding forces at the contact points. The freshly deposited bed has a honeycombed structure with large porosity. The basic unit of this structure is the floc, i.e., small clusters of clay particles packed relatively densely with respect to the over-

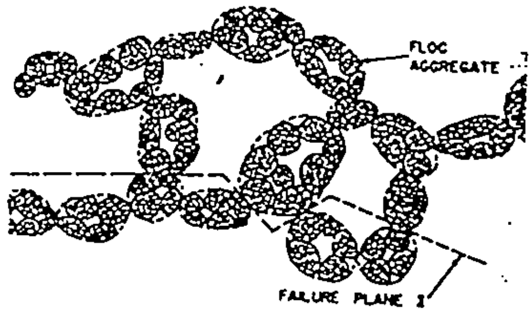


A. at its loosest state

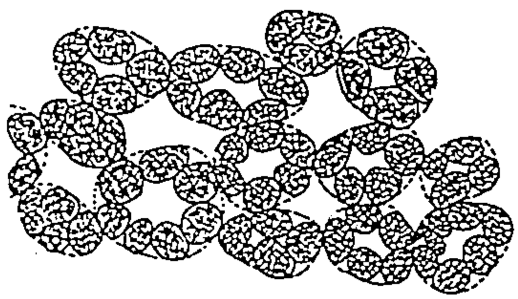

B. at "quasi-homogeneous" state

C. decreasing of average interparticle space

Figure 5.2 schematic structure of flocculated bed

(from Partheniades 1965)

all clay density. As sedimentation continues, the increase of the overburden pressure on the lower deposits will break the bonds between the flocs, thus forcing the flocs closer to each other. The flocs will have more contact points per unit volume of soil and the soil density will increase. Upon further increase of the over burden pressure, the flocs will start deforming while maintaining their original interparticle distance. A "quasi-homogeneous" state will eventually be reached with an average interparticle distance equal to that within the original flocs (Figure 5.2 B). From then on, any further increase of the pressure will deform the flocs, the inter-floc voids will disappear and the entire clay mass will reach a density equal to the original average floc density. Any further increase of load would result from then on in a decrease of the average interparticle space (Figure 5.2 C). This will happen when the sediment begins to consolidate. A new approach for sediment fabric study is the computerized image analyses on scanning and transmission electron micrographs of sediments. In such a study, Bennett et al [1989] found that the pore profiles of the unconsolidated sediments can be described as having pores of aspect ratios (length-to-width ratios) close to 1.0, while that of consolidated sediments approach infinity.

This finding confirms that sediment becomes denser and denser under pressure over time.

A flow chart may be created (Figure 5.3) to summarize the dimensional changes that particles undergo through the process from suspension to consolidated sediment. For convenience of description, the blocks in the flow chart are numbered. Among other changes that might happen during the sedimentation process, from double layer interaction point of view, the variation of the average interparticle distance

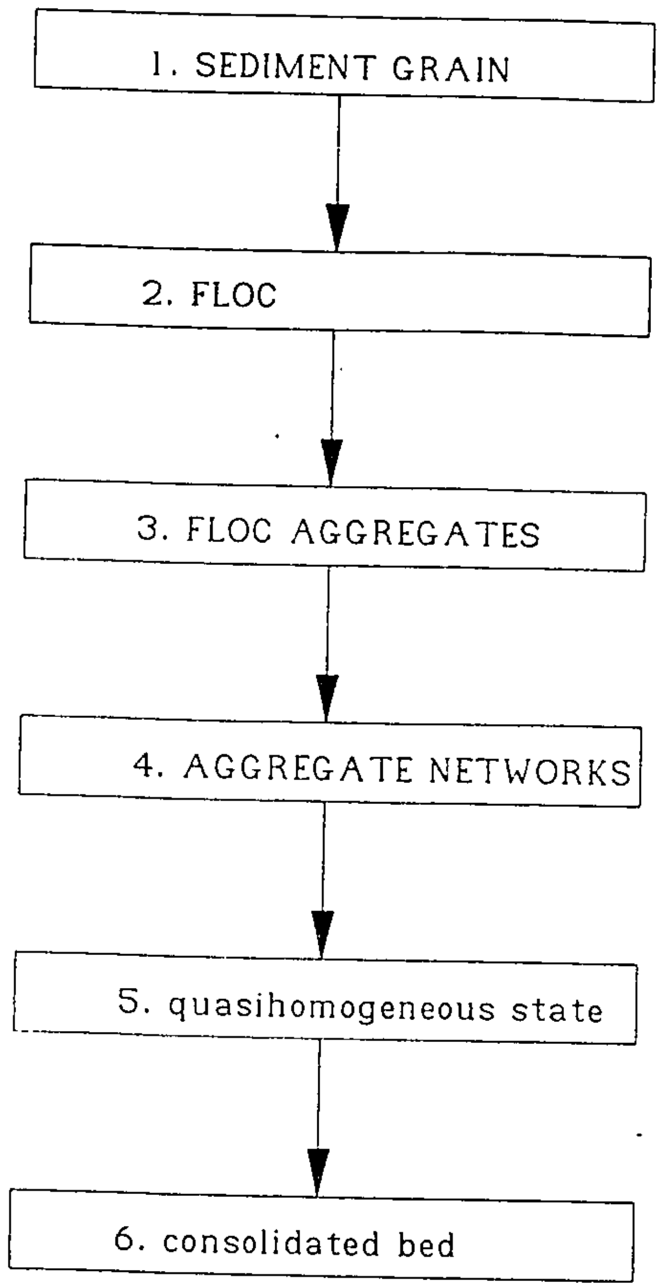


Figure 5.3 sedimentation process of suspended clay particles

is of major concern. According to the aforementioned process of sedimentation, the average interparticle distance is reduced from block 1 to block 2, when suspended particles form flocs. From block 2 to block 5, the average interparticle distance remains relatively steady since the processes involve only the grouping and arranging of flocs without impacting on particles that form the flocs. From block 2 to 5, the density of the system is smaller than or equal to that of the original flocs. From block 5 to 6, however, the sediment goes through consolidation process and the average interparticle distance starts to decline further. The density of the system becomes larger than that of the original flocs and approaches the density of the individual particles. In other words, the flocs are crushed under the pressure and the individual particles will eventually be very close to one another, depending on the pressure applied.

## 5.6 Modelling of Desorption Induced by Sedimentation

### 5.6.1 Objective of Modelling

From the perspective of double layer interaction, only two segments of the process in Figure 5.3, i.e., from block 1 to 2 and 5 to 6, may bring about desorption of originally adsorbed pollutants. Because these two segments are the only ones that involve the change of interparticle distance. The change from block 1 to 2 is only intermediary, the magnitude of the change is relatively small, the system is unstable and subject to further variations. From block 5 to 6, the system undergoes a slow and steady change and approaches the final state of the sedimentation process. To calculate the desorption effect induced by interparticle interaction, it is only necessary

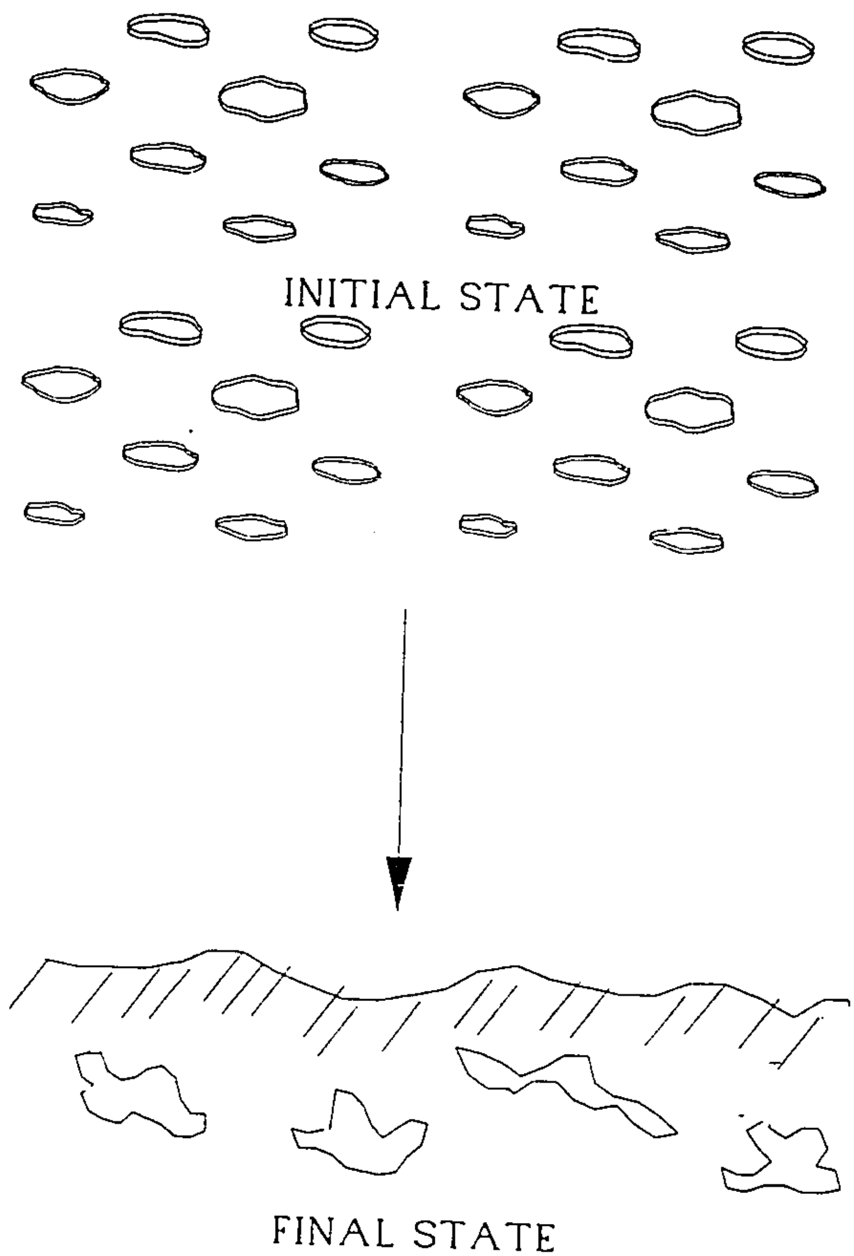


Figure 5.4 initial and final states of sedimentation process

to know the initial and final status of the particles (Figure 5.4). This is because while other parameters hold constant, it is the interparticle distance that dictates the intensity of the interaction. At the initial state, in a suspension of clay particles, the solids in the suspension can be considered as uniformly distributed in the system. The average interparticle distance is so great, compared with the consolidated sediment, that the interparticle interaction is too weak to be significant. On the other hand, particles in the consolidated sediment are tightly packed and consequently endure substantial interparticle interaction. However, unlike in a suspension, the distribution of clay particles in a sediment is not uniform and this poses a challenge to the calculation of the interparticle interaction. A close look at the micro structure of clay becomes necessary.

### 5.6.2 Micro Structure of Clay Sediments

As discussed earlier, in order to evaluate the desorption effect caused by interparticle interaction, it is essential to be able to estimate the average interparticle distances of a sediment. Unfortunately, the studies of the microstructure of fine-grained sediments to date do not provide a straight forward answer to this question. In an effort to quantify fabric parameter and provide a statistical basis for fabric descriptions, a lot of research has been devoted to the fabric of clay sediments. Here fabric refers to the spacial distributions, orientations, associations and shapes of the solid particles. The purpose of studying microstructure in sedimentology is to estimate porosity and permeability of the sediment.

The clay particles have a thin needle or a thin plate shape with one or two of their dimensions much larger than the other. The particle surfaces also have small irregularities of the order of a few Angstrom. In a sediment, the contacts between the clay particles can be face-to-face, edge-to-edge or face-to-edge. The fabric of the sediment is never homogeneous, because of the randomness of the arrangements. Yet fabrics of different sediments manifest characteristic patterns, some develop a greater degree of so called "preferred particle orientation" than others. A preferred particle orientation is a direction that makes the structure of the fabric follow a rather regular pattern. Figure 5.5 [Bennett et al. 1991] shows some examples of fabric patterns of consolidated bentonite and kaolinite. It is obvious that even with kaolinite, which develops "the greatest degree of preferred particle orientation", it is difficult to generate a rigorous mathematical description of the fabric. Some kind of simplified modelling is therefore necessary before calculation of double layer interaction can be conducted on sediments.

In their effort to correlate permeability and fabric microstructure, sedimentologists have been using porosity and void ratio as measurements of the volume of the pore space potentially available for fluid passage. Porosity is the ratio of the volume of the pore space to the total sediment volume and is often expressed as a percentage. Void ratio is the ratio of the pore volume to the volume of the solids. The relationship between porosity and void ratio can be written as:

$$n = \frac{e}{1+e} \tag{5.1}$$

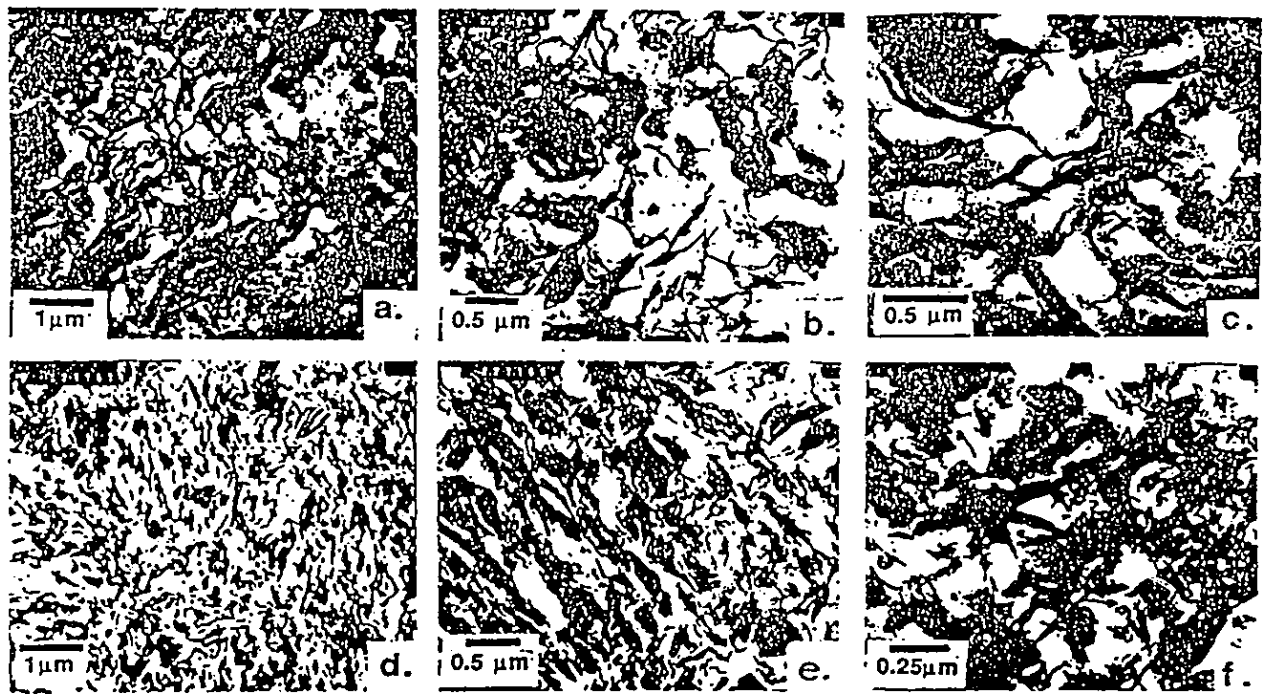


Figure 5.5 TEM photomicrographs of laboratory prepared clays a-c. Bentonite. d-f Kaolinite. Note the significant difference in the fabric between the two sediment types: kaolinite develops the greatest degree of preferred particle orientation.

(Bennett et al. 1991)

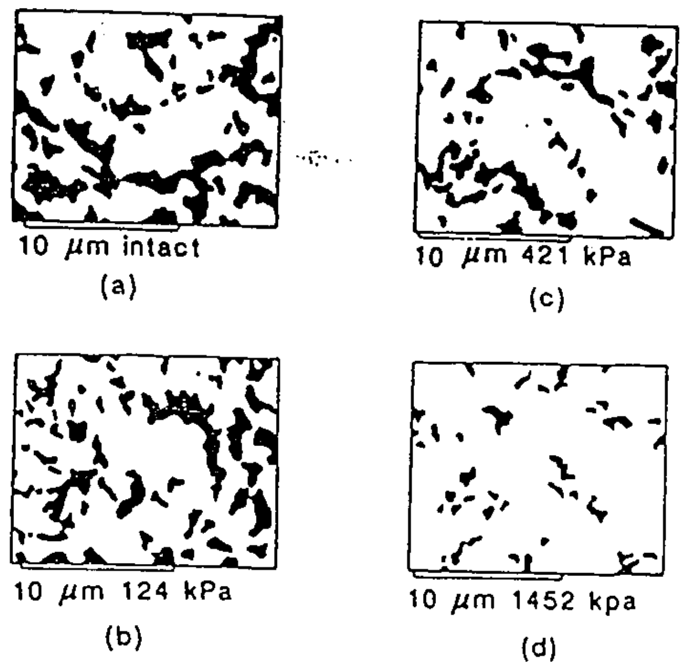


Figure 5.6 Graphic representation of porosity at different stress levels on a vertical plane. Pores are black and particles are white.
(from Delage & Lefebvre 1984)

where n is porosity and e is the void ratio.

Figure 5.6 is a graphic representation of the cross section of a sediment, from which can be seen nothing but solid and void portions. The ratio between solid and void varies depending on the extent of consolidation under different pressure.

### 5.6.3 Approach of Modelling

From the perspective of double layer interaction, two assumptions may be made to furnish an easier approach to the problem:

1. The particles in the solid portion are so closely packed, they are physically contacting one other.
2. For the particles that construct the internal surfaces of the pores, the interactions of their double layers are negligible compared to the solid portion.

Based on the first assumption, it becomes possible to estimate the desorption effect on the solid portion, since the particles are contacting one another, the average interparticle distance may be roughly estimated. As discussed earlier, because clay particles are rather irregularly shaped and arranged, questions remaining are:

1. What percentage of particles are arranged at the "preferred orientation"?
2. Among the contacts between particles, how many are face-to-face, edge-to-face and edge-to-edge respectively?
3. How close can surfaces of particles get until surface irregularity obstructs?

Answers to these questions are highly specific depending on the type of particles and other conditions. It would be much easier to calculate a "maximum interaction" based on "complete and perfect" surface-to-surface contact. It can serve as a limiting condition for the desorption effect. Thus this limiting condition represents the maximum amount of desorption that can occur. The actual desorption effect will be always smaller than that, because, collectively, such "complete and perfect" surface-to-surface contact does not generally exist. Instead, surfaces are always separated to some extent because of surface irregularity or non-preferred orientation, etc.

### 5.6.4 Estimation of Internal Surface Area

The second assumption in Section 5.6.3 addresses the portion of particles that do not contribute to desorption effect because they happen to be on the internal surface of the voids. When calculating the desorption effect, this portion of particles has to be subtracted from the total amount of particles in the sediment. The question then focuses on how to estimate the internal surface area of a given weight of sediment, which is a function of the porosity. The higher the porosity, the larger the internal surface and consequently, the less the extent of desorption.

The porosity of a sediment varies substantially depending on the characteristics of soil-water system and sedimentation conditions, particularly, the pressure of compression. Figure 5.7 [Lambe & Asce, 1958] depicts a typical relationship between pressure and void ratio, i.e., the higher the pressure, the lower the porosity. Listed in Table 5.2 [Bennett et al. 1989] are some examples of clay and carbonate sediments with porosity information. Porosity data alone, however, are insufficient for the calculation of internal surfaces, for the simple reason that a given volume can be millions of tiny pores or a dozen large pores. The internal surface area of the latter is

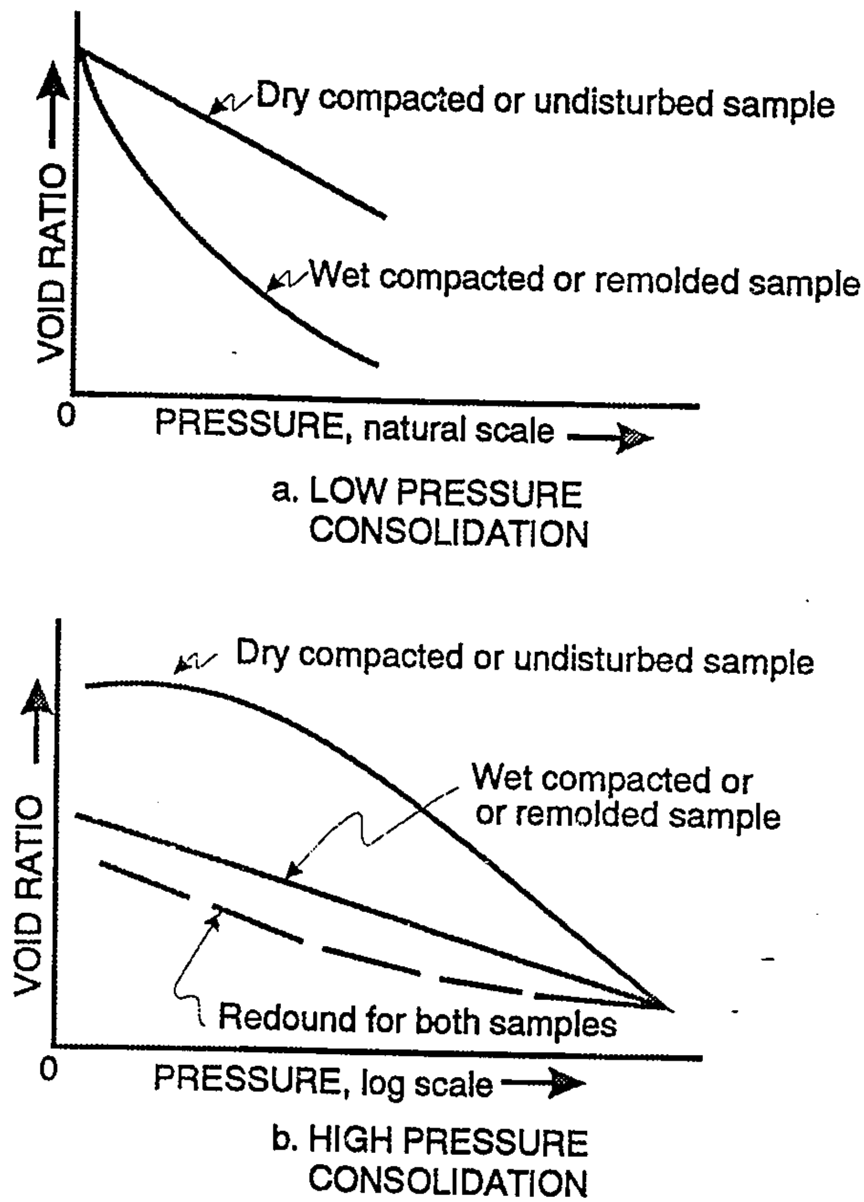


Figure 5.7 effect of one dimensional compression on clay structure (from Lambe and Asce, 1958)

## Table 5.2 Porosity, Permeability and Grain-Size Data for Clay and Carbonate Sediments (from Bennett et al. 1989)

Porosity, permeability and grain-size data for clay and carbonate sediments

| Location (sediment type) | Site and coordinates | Water depth (m) | Sample designation | Depth in core (cm) | Porosity, $n$ (%) | Permeability coefficient, $k$ (cm/s) | Grain size (%): Sand (2000–62.5 μm) | Silt (62.5–2 μm) | Clay (< 2μm) |
|---|---|---|---|---|---|---|---|---|---|
| Mississippi Birdfoot Delta (clay) | 1 (28°49'N, 89°22'W) | 70 | B-1 | 140 | 71 | $10^{-7}$–$10^{-6}$ | 1–2[c] | ~30 | ~69 |
| | | | | 120 (13 kPa)[d] | 70 | $3 \times 10^{-7}$[***] | | | |
| | | | | 120 (400 kPa)[d] | | $8 \times 10^{-8}$[***] | | | |
| | | | | 120 (3200 kPa)[d] | | $7 \times 10^{-10}$[***] | | | |
| | | | | 300 | 69 | $2 \times 10^{-7}$ | | Silty clay | |
| | | | | 1200 | 65 | $2 \times 10^{-8}$ | | Silty clay | |
| | | | | 12100 | 49 | $6 \times 10^{-9}$ | | Silty clay | |
| Laboratory-prepared sample[a] | – | – | Kaolinite | (68.9 × $10^3$ kPa)[d] | 52[**] | $10^{-6}$ | | | |
| | | | | | 25[***] | $10^{-8}$[***] | Approximately 100% < 4 μm | | |
| | – | – | Bentonite | (68.9 × $10^3$ kPa)[d] | 50[**] | $7 \times 10^{-10}$ | | | |
| | | | | | 27[***] | $10^{-11}$[***] | Approximat 100% < 4 μm | | |
| Andros Platform, | 1 (25°15.8'N, 78°50.5'W) | 5 | A1b | 182–187 | 48[b] | $4.23 \times 10^{-3}$[b] | 94 | 1 | 3 |
| | | | | | 46 | $3.85 \times 10^{-3}$ | | | |
| Great Bahama Bank (oolitic carbonate) | 3 (25°22.2'N, 78°56.4'W) | 4.7 | A3b | 24–29 | 61[b] | $5.55 \times 10^{-3}$ | 57 | 29 | 13 |
| | | | | | 54 | | | | |
| | | | | 116–121 | 53[b] | $5.89 \times 10^{-4}$ | 72 | 16 | 11 |
| | | | | 207–212 | 49[b] | $6.05 \times 10^{-7}$[b] | 75 | 14 | 9 |
| | | | | | 50 | $1.97 \times 10^{-3}$ | | | |
| Little Bahama Bank (aragonite needle matrix) | 8 (27°36.6'N, 78°13.3'W) | 970 | LBB-10 | 17 | 59 | $4.14 \times 10^{-3}$ | 4 | 64 | 32 |
| Exuma Sound (coccolith ooze) | 4 (23°50.2'N, 75°34.2'W) | 1920 | 4P3 | 225 | 67 | $3.15 \times 10^{-6}$ | 9 | 11 | 80 |
| | | | 4P4 | 355 | 68 | $2.53 \times 10^{-6}$ | 14 | 16 | 70 |
| | 5 (23°49.8'N, 75°31.2'W) | 1957 | 5P3 | 260 | 55 | $9.08 \times 10^{-6}$ | 6 | 54 | 40 |
| | | | 5P4 | 360 | 54 | $3.15 \times 10^{-6}$ | 9 | 78 | 13 |
| | 6 (23°51.6'N, 75°26.8'W) | 1980 | 6P4 | 403 | 59 | $6.64 \times 10^{-6}$ | 6 | 18 | 77 |
| | 7 (23°48.3'N, 75°22.7'W) | 1815 | 7P2 | 187 | 57 | $7.66 \times 10^{-3}$ | 16 | 60 | 24 |
| | | | 7P5 | 437 | 60 | $2.18 \times 10^{-6}$ | 18 | 61 | 21 |

[a]Enderby and Thompson (1981); [b]in situ (Bennett et al., submitted); [c]percent sand varies between 2 and 3% between 6 and 21 m.
[d]consolidation pressures in laboratory: 13 kPa equivalent to 2 m, 400 kPa equivalent to 80 m, 3200 kPa equivalent to 444 m, 68.9 × $10^3$ kPa equivalent to 5520 m;
[**]initial, before consolidation; [***]at consolidation load

much smaller than that of the former. It is therefore necessary to know the pore size distribution of a particular sediment.

There are several methods available for the measurement of the distribution of pore sizes in a given porous material. The two main classic methods either invoke the concept of capillary condensation in the pores , or depend upon the simpler concept of forced intrusion of a non-wetting liquid into the pore under pressure. The latest development in this field is computerized graphics analysis of clay section photos.

Presented below are data derived from mercury porosimetry measurements on a kaolinite clay [Sridharan et al 1971]. The general procedure for mercury porosimetry was first suggested by Washburn [1921]. The Washburn equation derives the pore size distribution in terms of a model of cylindrical capillaries, which is hardly appropriate to the true pore geometry of the soil clay system. Furthermore, only those pores are intruded which are open to the outside of the sample, also only at the pressure corresponding to their largest continuous opening. As a consequence, the measured pore-size distributions are not exact descriptions of the volume of pores present at each size range. Rather, they are approximations of this, and they may, in fact, be relatively poor approximations if the pore structure is very complex and tortuous. Nevertheless, the range in sizes of pores covered (five orders of magnitude) is so great that limited discrepancies in the measurement ascribed to a specific size class are simply not too important.

The two curves shown in Figure 5.8 are pore-size distributions of artificially-sedimented kaolinite samples. The upper curve is from critical-region dried clay and the lower one is from a sample that was oven-dried at 105°C in the conventional

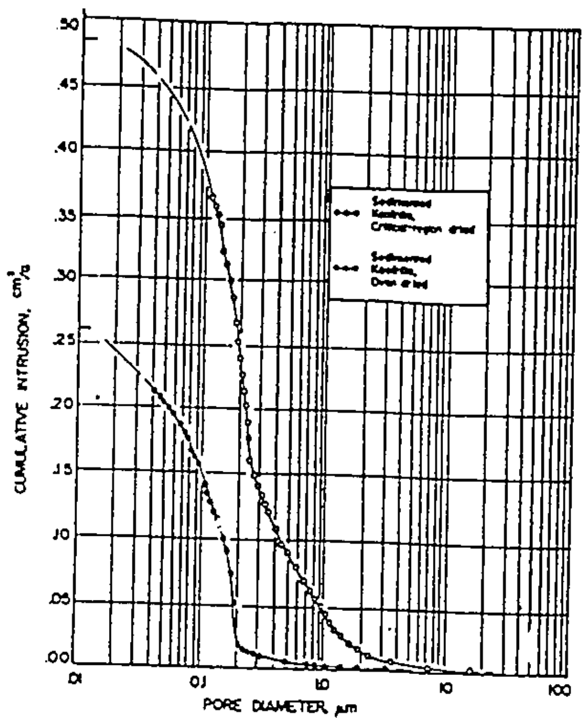


Figure 5.8 Pore-size distributions of artificially-sedimented kaolinite samples; upper line: critical-region dried; lower line: air-and-oven-dried.
( from Sridharan et al. 1971 )

manner. It is believed that close to half of the total pore space was lost in the conventional drying process, all of it in sizes above about 0.2 μm. The distribution of pores finer than this size is essentially the same. In other words, the critical-region dried curve is more realistic. The following discussion will all be referring to this curve.

A brief examination of the curve indicates that:

1. The total pore space is close to 0.5 $cm^3$ per gram of clay. The specific gravity of this clay is 2.62, corresponding to 0.38 $cm^3$ per gram. So over 50% of the sample volume is void space.
2. There are no gross pores. Essentially all of the pore spaces are of diameters commensurate with the size of the clay particles (Figure 5.9).

From Figure 5.8, the total pore volume may be broken down into a few different pore sizes respectively (Table 5.3).

**Table 5.3 A Rough Breakdown of Pore Size Distribution Based on Figure 5.7**

| Pore Size (μm) | 5 | 1 | 0.5 | 0.1 | 0.05 | 0.01 |
|---|---|---|---|---|---|---|
| Cumulative ($cm^3/g$) | 0.006 | 0.042 | 0.086 | 0.38 | 0.44 | 0.48 |
| Breakdown ($cm^3/g$) | 0.006 | 0.036 | 0.0435 | 0.294 | 0.064 | 0.038 |

Calculation based on this set of data has found that in this particular kaolinite roughly 37% of the clay grains are involved in the construction of the pores. As discussed earlier, the majority surfaces of this portion of clay particles will not contribute to

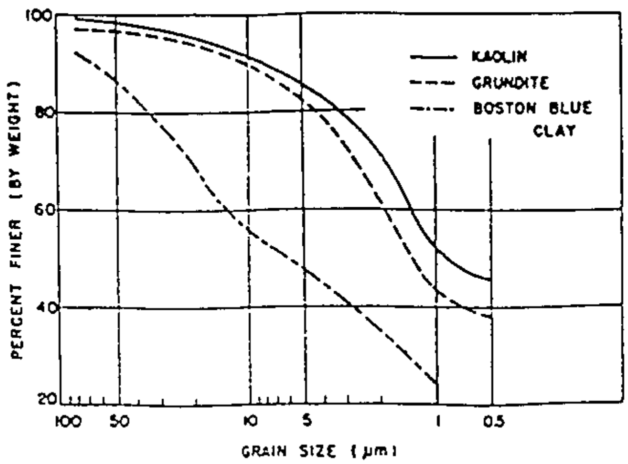


Figure 5.9 Grain-size distribution curves for soils used by Sridharan et al.(1971)

desorption effect during the sedimentation process.

## 5.7 Calculation of Desorption Effect

The rest of the clay particles are considered as closely compacted and consequently interacting at very close ranges. Nevertheless there are still some unknowns that hamper the modelling calculation:

(1) Quantitative information on patterns of grain orientation, i.e., the percentage figures on face-face, face-edge and edge-edge arrangements respectively.

(2) Quantitative information on clay grain surface irregularity, which ultimately determines the smallest separation distance of two grains.

However, experimenting on the DLI model with various particle orientation and surface irregularity has suggested that once the surfaces are within small distance, e.g., less than 100-200 angstroms, the DLI model becomes not so sensitive to these parameters. In other words, if the particles themselves are small enough to bring the surface into close range, orientation and surface irregularity of the particles becomes much less important. Particle size is therefore very important, since it determines the interaction range. Table 5.4 was composed based on the information of grain size from Figure 5.9.

**Table 5.4 Grain Size Distribution and Corresponding Desorption Percentage Predicted by DLI Model**

| Grain Size (μm) | | <100 | <50 | <10 | <5 | <1 | <0.5 |
|---|---|---|---|---|---|---|---|
| Cumulative % | | 100 | 98.5 | 91.5 | 80.1 | 52.3 | 46.1 |
| Breakdown % | | 1.5 | 7.0 | 11.4 | 27.8 | 6.2 | 46.1 |
| Desorption (%) | Ionic Strength $10^{-2}$ | 0 | 2 | 8 | 16 | 58 | 81 |
| | Ionic Strength $10^{-3}$ | 0 | 7 | 30 | 51 | 97 | 100 |

Calculation was carried out with the DLI model in an effort to estimate the desorption effect if suspended clay particles become consolidated sediment. Two ionic strengths were used in the modelling. The calculation indicates clearly that desorption effect will be very strong on particles smaller than 0.5 micron, nearly 81% to 100% of the adsorbed sorbates will desorb. The desorption effect decreases with increasing particle size. For particles of around 100 micron, there is virtually no desorption effect. Combining together all the data, also considering the 37% of pore-constructing clay particles that do not contribute to the double layer interaction, the desorption effect on this particular clay will be around 29% and 44 % at ionic strength of $10^{-2}$ and $10^{-3}$ respectively.

## 5.8 Concluding Remarks on DLI Model and Its Application

The demonstration of the application of the DLI model in this chapter, speculative as it is, bears significant environmental implication. It suggests a pathway that pollutants may be transported in the water column by means of adsorbing to particulate substances and then released into the solution phase at considerable percentage, as particles settle down to the bottom. Considering the huge amount of suspended particles existing in natural waters, under appropriate conditions, the desorption process may contribute significantly to the degree of pollutants partitioning between dissolved and adsorbed phases, altering the fate of pollutant species, including transportation, settling, resuspension, chemical transformation and biological uptake.

The accuracy of the prediction of the DLI model on the desorption effect in this particular case may be limited by many uncertainties. Among them, the lack of adequate mathematical description of the geometric characteristics of the clay is crucial. Also, as emphasized in previous chapters, mechanisms other than double layer interaction are likely to be present and interfere. More research is necessary on the phenomenon of the particle concentration effect to satisfy the demand of practical application.

## 6. SUMMARY AND CONCLUSIONS

1. The phenomenon of particle-particle interaction resulting in desorption with increasing particle concentration was investigated.

2. The hypothesis is made that columbic repulsion forces are developed by overlap of the double layer of small adjacent particles. The repulsion forces can cause the reduction of the adsorption energy, resulting in desorption effect. Depending on parameters such as ionic strength, particle size and concentration, this particle attributed force can be significant but small (less than a few hundred cal/mol) when compared to chemical binding forces.

3. Based on classical theory, a double layer interaction (DLI) model is developed for spheres of equal sizes and also approximated for a clay size distribution. Calculation showing the magnitude of change of adsorption are presented in Table 4.7, 4.8, 4.10, 4.11 and 5.4.

4. An experimental design was devised to test the theory. The setup (Figure 4.11) and testing process permitted ONLY change in particle concentration, thus minimizing experimental artifacts and ensuring that no change in surface chemical parameters and chemical binding occurred.

5. A Couette device was also used to quantitatively determine the particle-particle collision effect under laminar flow and defined shear. This experiment was designed to assess the possible effect of particle collisions.

6. The argument that the particle concentration effect is due to collisions is dismissed in the case of metal adsorption, because it has been found both experimentally and theoretically that collision energy is insignificant compared to adsorption energy.

7. The experimental results and the model calculations both exhibit a desorption effect for small particles in increasing concentration. The effect disappears at elevated ionic strength due to decrease of the double layer.

8. The calculations and the experimental results agree with each other within 10% on average under well-controlled experimental condition.

9. Particle size and ionic strength (salinity) are the two master variables. Particles greater than about 10 micron (silt) will evidence negligible desorption due to particle concentration. Similarly waters of ionic strength equal or greater than about 0.1 mol/l will show no particle concentration effect (See table 5.4 for summary).

10. Therefore this theory and experiments predict that all clay particles in fresh water environment can exhibit about 30% or more desorption effect upon particle concentration such as compaction and during diagenesis.

11. Although the DLI concept can explain the particle concentration effect, other mechanisms affecting adsorption/desorption may also prevail with respect to particle concentrations.

## APPENDIX A: MULTI-INTERACTIONS BETWEEN RINGS OF TWO SPHERICAL PARTICLES

Instead of only considering interactions between two rings of the same diameter, a general approach on the interactions between two spherical particles should consider interactions between every single ring and others.

### 1. Potential Produced by a Ring Elemnet of a Semisphere

As has been defined in Equition 2.13, the potential generated by the surface charge of the sorbent in the vicinity of the surface can be written as

$$\Delta\psi_x = 2\frac{RT}{zF}\cdot \ln\left(\frac{(P+1)+(P-1)\exp(-\kappa x)}{(P+1)-(P-1)\exp(-\kappa x)}\right) \qquad (2.13)$$

The surface of a spherical particle can be sliced into many co-axled rings. Consider the potential generated by a ring element on a spherical particle (Figure A.1). The projected area of the ring element in Figure A.1

$$ds = 2\pi r dr \qquad (A\text{-}1)$$

$$r = \sqrt{a^2 - u^2} \qquad (A\text{-}2)$$

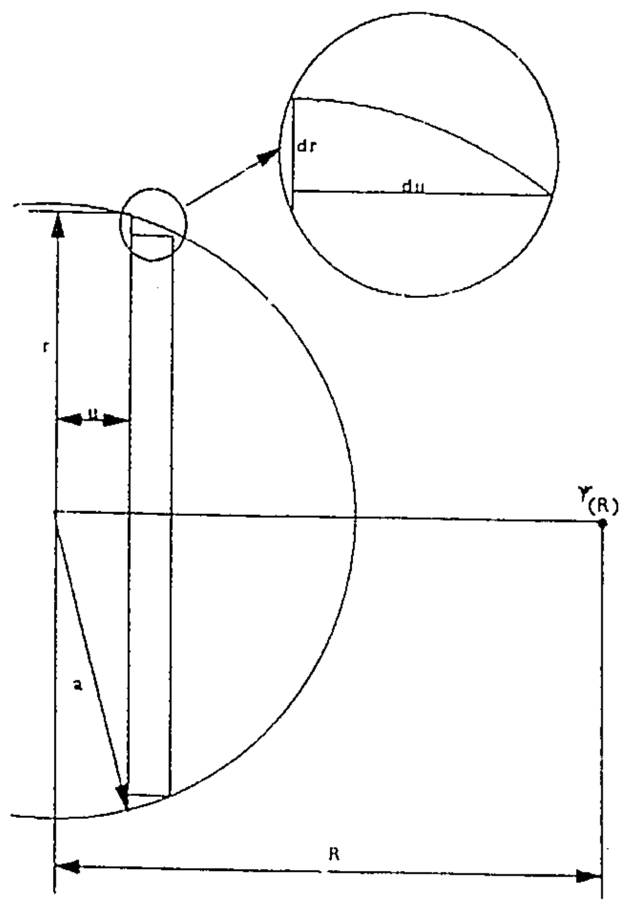


Figure A-1 potential generated by ring-shaped surface therefore

$$
\begin{aligned}
dr &= \frac{-2udu}{2\sqrt{a^2-u^2}} \\
&= -\frac{udu}{\sqrt{a^2-u^2}}
\end{aligned}
\tag{A-3}
$$

$$
\begin{aligned}
ds &= 2\pi\sqrt{a^2-u^2}\cdot\left(\frac{-udu}{\sqrt{a^2-U^2}}\right) \\
&= -2\pi udu
\end{aligned}
\tag{A-4}
$$

The potential generated by ds is $\Delta\psi(R,u)$

$$
\begin{aligned}
\Delta\psi\,(R,u) &\equiv \Delta\psi_x ds \\
&= \Delta\psi_{R-u}\cdot(-2\pi u)\,du
\end{aligned}
\tag{A-5}
$$

where x= R - u

## 2. Potential of the Whole Semisphere

The potential of the whole semisphere can be obtained by integrating over u from zero to a

$$
\begin{aligned}
\psi\,(R) &= \int_0^a -2\pi udu\cdot\Delta\psi_{R-u} \\
&= \int_0^a 2\pi udu\cdot\Delta\psi_{R-u}
\end{aligned}
\tag{A-6}
$$

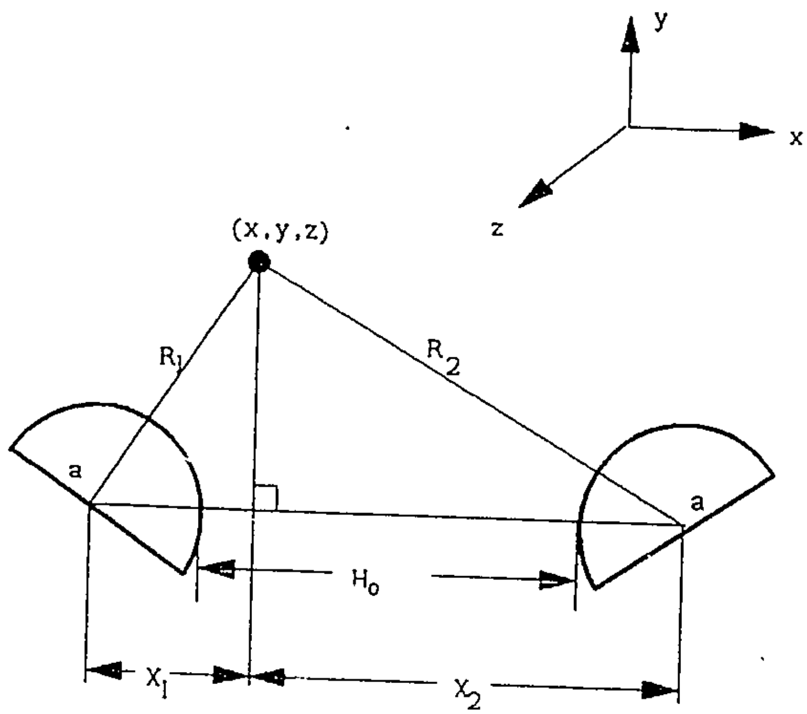


Figure A-2 The potential at any point in space generated by two semispheres

**3. Potential at Any Point in Space Generated by 2 Semispheres.**

Based on the above arguments, the potential at any point in space generated by sphere 1 and sphere 2 (Figure A.2) are $\psi(R_1)$ and $\psi(R_2)$ respectively. The total contribution from both spheres is

$$\psi_{(x,y,z)} = \psi_{(R1)} + \psi_{(R2)} \tag{A-7}$$

Choosing the center of sphere 1 as the origin (Figure A.2), the geometry of the system can be expressed in coordination terms

$$R_2 = \sqrt{(2a+H_o-x)^2+y^2+z^2} \tag{A-9}$$

$$R_1 = \sqrt{x^2+Y^2+z^2} \tag{A-8}$$

therefore

$$\Delta\psi_{(x,y,z)} = \int_0^a 2\pi u du \cdot (\Delta\psi_{R1-u} + \Delta\psi_{R2-u}) \tag{A-10}$$

where

$$\Delta\psi_{R1-u} = \frac{2Rz}{zF}\ln\left(\frac{(P+1)+(P-1)\exp(-k(\sqrt{x^2+y^2+z^2}-u)}{(P+1)-(P-1)\exp(-k(\sqrt{x^2+y^2+z^2}-u)}\right) \tag{A-11}$$

and

$$\Delta\psi_{R2-u} = \frac{2Rz}{zF}\ln\left\{\frac{(P+1)+(P-1)\exp(-k(\sqrt{(2a+H_o-x)^2+y^2+z^2}-u))}{(P+1)-(P-1)\exp(-k(\sqrt{(2a+H_o-x)^2+y^2+z^2}-u))}\right\} \qquad \text{(A-12)}$$

## APPENDIX B: IN SEARCH OF THE ANALYTICAL RESOLUTION FOR EQUATION

### 1. Manual Deduction

$$\int_0^\infty \Delta G_i dx = \int \Delta\psi_x dx \cdot Z\,F \tag{B-1}$$

$$\int_0^\infty \Delta G_i\, dx = \int_0^\infty Z\,F \Delta\psi_x dx$$

$$= Z\,F \int_0^\infty \Delta\psi_x dx$$

$$= 2RT \int_0^\infty \ln\left(\frac{(e^{ZF\psi_0/2RT}+1)+(e^{ZF\psi_0/2RT}-1)e^{-\kappa x}}{(e^{ZF\psi_0/2RT}+1)-(e^{ZF\psi_0/2RT}-1)e^{-\kappa x}}\right) dx \tag{B-2}$$

There is no rigorous analytical solution for Equation B-2. Careful examination of the equation however indicates

$$e^{ZF\psi_0/2RT} > 1$$

Thus equation B-2 can be simplified into

$$- 2RT \int_0^\infty \ln\left(\frac{e^{ZF\psi_0/2RT} + e^{ZF\psi_0/2RT} e^{-\kappa x}}{e^{ZF\psi_0/2RT} - e^{ZF\psi_0/2RT} e^{-\kappa x}}\right) dx$$

$$- 2RT \int_0^\infty \ln\left(\frac{1 + e^{-\kappa x}}{1 - e^{-\kappa x}}\right) dx$$

$$- 2RT \int_0^\infty \ln\frac{e^{\kappa x} + 1}{e^{\kappa x} - 1}\, dx$$

$$- \frac{2RT}{\kappa} \int_0^\infty \ln\frac{e^{\kappa x} + 1}{e^{\kappa x} - 1}\, d(\kappa x) \qquad \text{(B-3)}$$

In Equation B-3

$$\int_0^\infty \ln\frac{e^x+1}{e^x-1}\,dx = \frac{\pi^2}{4} \tag{B-4}$$

Substitute equation B-4 in to B-3

$$\int_0^\infty \Delta G_i dx = \frac{2RT}{\kappa}\cdot\frac{\pi^2}{4} \tag{B-5}$$

Note that two approximations were made before Equation B-5 can be obtained. Besides eliminating the "1" terms in Equation B-2, the integration is done from 0 to infinity instead of from zero to R.

## 2. Using Computer Software MAPLE

MAPLE is a software program that is capable of resolving integrating equations. In this case, the software failed to provide an analytical resolution. Note in the last equation, the function "gamma" is a special function generated by the program to accommodate the part of the equation that can not be resolved analytically.

```
                         top := P + 1 + (P - 1) exp(- k x)

                       bottom := P + 1 - (P - 1) exp(- k x)

                                    P + 1 + (P - 1) exp(- k x)
                            R T ln(----------------------------)
                                    P + 1 - (P - 1) exp(- k x)
            Xsi := Xsi0 - 2 --------------------------------------
                                              Z F

                                    P + 1 + (P - 1) exp(- k x)
                            R T ln(----------------------------)
                                    P + 1 - (P - 1) exp(- k x)
       DeltaG := Z F (Xsi0 - 2 --------------------------------------)
                                              Z F

words used=100032, alloc=49152, time=3.58
words used=200058, alloc=94208, time=7.48
Result :=

   .5000000000

      ((Xsi0 s k Z F + 2 Xsi0 gamma k Z F

         -2

            dilog(-2

                                               P + 1
               -------------------------------------------------------------)
                - P - 1 + P exp(- k (s + 2 gamma)) - exp(- k (s + 2 gamma))

               R T

         -2

                   P + P exp(- k (s + 2 gamma)) - exp(- k (s + 2 gamma)) + 1
            ln(- -------------------------------------------------------------)
                  - P - 1 + P exp(- k (s + 2 gamma)) - exp(- k (s + 2 gamma))
```

```
        ln(-2

                                            P + 1
           -----------------------------------------------------------------------
            - P - 1 + P exp(- k (s + 2 gamma)) - exp(- k (s + 2 gamma))
           )

        R T

    -2

      dilog(- (P + P exp(- k (s + 2 gamma)) - exp(- k (s + 2 gamma)) + 1)

         / (- P - 1 + P exp(- k (s + 2 gamma)) - exp(- k (s + 2 gamma))

         ))




       R T)

  / k

  - (Xsi0 s k Z F

                                       P + 1
     - 2 dilog(- 2 ---------------------------------------) R T
                     - P - 1 + P exp(- k s) - exp(- k s)

     -2

                P + P exp(- k s) - exp(- k s) + 1
       ln(- ---------------------------------------)
              - P - 1 + P exp(- k s) - exp(- k s)

                                      P + 1
          ln(- 2 ---------------------------------------) R T
                   - P - 1 + P exp(- k s) - exp(- k s)

                  P + P exp(- k s) - exp(- k s) + 1
     - 2 dilog(- ---------------------------------------) R T)
                   - P - 1 + P exp(- k s) - exp(- k s)

     / k)

 1 / gamma
```

## APPENDIX C: ESTIMATION OF COLLISION ENERGY

Recall Fig. 3.6, particles 1 and 2 are having an elastic collision. With a mass of $m_1$, particle 1 travels at a speed of $\upsilon_1$. Particle 2, with a mass of $m_2$, was stationary before the collision. Because the collision is not necessarily centre to centre, both particles could bounce to any direction after the collision. Suppose particle 1 will continue its motion with a speed of $\upsilon_1'$ along an angle of $\theta$. Particle 2 will gain a speed of $\upsilon_2'$ and a direction of angle $\phi$. Before and after the collision, the laws of conservation of momentum and kinetic energy must hold:

$$m_1 v_1 = m_1 v_1' + m_2 v_2'^2 \qquad \text{(C-1)}$$

$$\frac{1}{2} m_1 v_1^2 = \frac{1}{2} m_1 v_1'^2 + \frac{1}{2} m_2 v_1'^2 \qquad \text{(C-2)}$$

From Equation C-1, it can be derived:

$$m_1 v_1 = (m_1 v_1' \cos\phi + m_2 v_2' \cos\theta) + (m_1 v_1' \sin\phi - m_2 v_2' \sin\theta) \qquad \text{(C-3)}$$

The two parenthesizes in Equation C-3 represent the horizontal and vertical components of the vectors respectively. Let the original vertical component equal to zero. (i.e., particle 1 was travelling in a direction parallel to horizontal axis), then the second parenthesis should equal zero too, because the original vertical component is zero. Thus in the last parenthesis of Equation C-3

$$(m_1 v_1' \sin\phi = m_2 v_2' \sin\theta) \tag{C-4}$$

Then Equation C-3 becomes

$$m_1 v_1 = (m_1 v_1' \cos\phi + m_2 v_2' \cos\theta) \tag{C-5}$$

Equation C-2 can be simplified to

$$m_1 v_1^2 = m_1 v_1'^2 + m_2 v_1'^2 \tag{C-6}$$

$(C\text{-}4)^2 + (C\text{-}5)^2$ results

$$(m_1 v_1 - m_1 v_1' \cos\phi)^2 + (m_1 v_1' \sin\phi)^2 = m_2^2 v_2'^2 (\cos^2\theta + \sin^2\theta) \tag{C-7}$$

Note that the last parenthesis in Equation C-7 equals 1. Substitute Equation C-5 into Equation 4 and rearrange

$$(m_2 + m_1) v_1'^2 - 2 m_1 v_1 v_1' \cos\phi - (m_2 - m_1) v_1^2 = 0 \tag{C-8}$$

Equation C-8 is parabolic, with $v_1'$ as the only unknown. For our specific case of $m_1 = m_2$, the particular solution is

$$v_1' = v_1 \cos\phi \tag{C-9}$$

Since particle 2 is assumed as stationary before the collision, the last term on the right side of Equation C-2 represents the net kinetic energy gain of particle 2. The energy transfer may be expressed as

$$\Delta E = \frac{1}{2} m_2 v_2'^2 = \frac{1}{2} m_1 v_1^2 - \frac{1}{2} m_1 v_1'^2 \tag{C-10}$$

Substitute Equation C-9 into Equation C-10

$$\Delta E = \frac{1}{2} m_1 v_1^2 \sin^2\phi \tag{C-11}$$

In Fig.3.6, the travelling direction of particle 1, after collision, can be anywhere between 0 to 180 degrees. Statistically, the collision energy should be the average over that range, thus

$$\Delta E_m = \frac{1}{2} m_1 v_1^2 \frac{1}{\pi} \int_0^{\pi} \sin^2\phi \, d\phi \tag{C-12}$$

The resolution of equation C-12 is

$$\Delta E_m = \frac{1}{4} m_1 v_1^2 \tag{C-13}$$

namely, half of the original kinetic energy of particle 1.

## APPENDIX D: SPECIATION CHECKING OF ADSORBATE IN SOLUTION

The purpose of checking is to ensure that no precipitation develops under the given condition. Computer software MINEQL (v.1.1) was employed for the calculation. Upon the input of the total concentrations of the solutes in the solution, the software calculates solution equilibrium and out put speciation information including complexation and precipitation. The original printout of the MINEQL is rather complicated and can be confusing to outsiders. The results that are crucial to this study are therefore extracted and tabled below.

1. Cu Speciation

Table D.1 and D.2 are for the preliminary and glass beads experiments on Cu respectively.

Table D.1 Speciation of Cu and Ac at pH 5

| $Cu_{Total}$ (μmol) | $Cu_{total}$ | | $Ac_{total}$ | |
|---|---|---|---|---|
| | $CuAc^{+}$ | $Cu^{2+}$ | HAc | $Ac^{-}$ |
| 0.1 | 14.9% | 84.7% | 34.9% | 65.1% |
| 0.5 | 14.9% | 84.7% | 34.9% | 65.1% |
| 1.0 | 14.9% | 84.7% | 34.9% | 65.1% |
| 2.0 | 14.9% | 84.7% | 34.9% | 65.1% |

(HAc/NaAc buffer; ionic strength $10^{-3}$)

Table D.2 Speciation of Cu and Ac at pH 5.5

| $Cu_{Total}$ (μmol) | $Cu_{total}$ | | $Ac_{total}$ | |
|---|---|---|---|---|
| | $CuAc^+$ | $Cu^{2+}$ | HAc | $Ac^-$ |
| 0.1 | 18.7% | 80.4% | 12.7% | 87.3% |
| 0.5 | 18.7% | 80.4% | 12.7% | 87.3% |
| 1.0 | 18.7% | 80.4% | 12.7% | 87.3% |
| 2.0 | 18.7% | 80.4% | 12.7% | 87.3% |

(HAc/NaAc buffer; ionic strength $10^{-3}$)

The results of the calculations indicate that for both cases (preliminary and glass beads), no precipitation will occur in the applied sorbate concentration range. The sorbate copper exists in the solution only in two forms: hydrated $Cu^{2+}$ and $CuAc^+$. At pH 5, nearly 85% of the copper is in the form of $Cu^{2+}$, the balance $CuAc^+$. As pH raised to 5.5, the percentage of $CuAc^+$ has increased to 18.7%, with ca. 80% of Cu in the $Cu^{2+}$ form. Also, the percentages of species remain constant throughout the concentration range (from 0.1 to 2 μmol/l).

2. Ni Speciation

Listed in Table D.3 are results of the equilibrium calculation on nickel.

Table D.3 Speciation of Ni and B at pH 8.1 ($H_3BO_3$/$NaH_2BO_3$ buffer; ionic strength $10^{-3}$)

| $Ni_{Total}$ (µmol) | $Ni_{total}$ | | | $B_{total}$ | |
|---|---|---|---|---|---|
| | $NiOH^{+1}$ | $Ni(OH)_2^0$ | $Ni^{2+}$ | $B(OH)_4^-$ | $H_3BO_3 \cdot H_2O$ |
| 0.1 | 18.9% | 0.2% | 80.9% | 12.7% | 87.3% |
| 0.5 | 18.9% | 0.2% | 80.9% | 12.7% | 87.3% |
| 1.0 | 18.9% | 0.2% | 80.9% | 9.7% | 90.3% |
| 2.0 | 10.0% | 47.2% | 42.7% | 9.7% | 90.3% |

When the total concentration of Ni is equal or lower than 1 µmol/l, the given conditions, a large majority of nickel (>99.8%) is in the form of $Ni^{2+}$ and $NiOH^+$, but once the total concentration of Ni reaches 2 µmol/l, a large portion of the Ni becomes $Ni(OH)_2$, part of which is subject to precipitation.

3. Speciation of Cd

Listed in table D.4 are results on the equilibrium calculation on cadmium.

Table D.4 Speciation of Cd and B at pH 8 ($H_3BO_3$/$NaH_2BO_3$ buffer; ionic strength $10^{-3}$)

| $Cd_{Total}$ (µmol) | $Cd_{total}$ | | | $B_{total}$ | |
|---|---|---|---|---|---|
| | $CdOH^+$ | $CdCl^+$ | $Cd^{2+}$ | $B(OH)_4^-$ | $H_3BO_3 \cdot H_2O$ |
| 0.1 | 7.9% | 7.3% | 84.7% | 7.9% | 92.1% |
| 0.5 | 7.9% | 7.3% | 84.7% | 7.9% | 92.1% |
| 1.0 | 7.9% | 7.3% | 84.7% | 7.9% | 92.1% |
| 2.0 | 7.9% | 7.3% | 84.7% | 7.9% | 92.1% |

Under the given conditions, Cd will not precipitate from the solution.

## APPENDIX E: SPECIFICATIONS OF THE GLASS BEADS

### 1. Glass Microspheres from Duke Scientific (Fig. E-1)

Certified Mean Diameter: 1.6 µm 0.3 µm
Standard Deviation: 0.5 µm
Coefficient of variation: 31%
Microsphere composition: soda lime glass
Specific gravity: 2.42 g/cc
Index of refraction: 1.51 @ 589 nm
Dielectric constant 7.3 @ 1 KHz and 20 °C
Approximate number: $1.9 \times 10^{11}$/gram

### 2. Superbrite Glass Beads from 3 M (Fig. E-2)

Average diameter: 50 µm
Density: 2.5 gram/cc
Dielectric constant 7 @ 300M
Hardness: 6 (Mohs scale)
Composition: soda lime glass

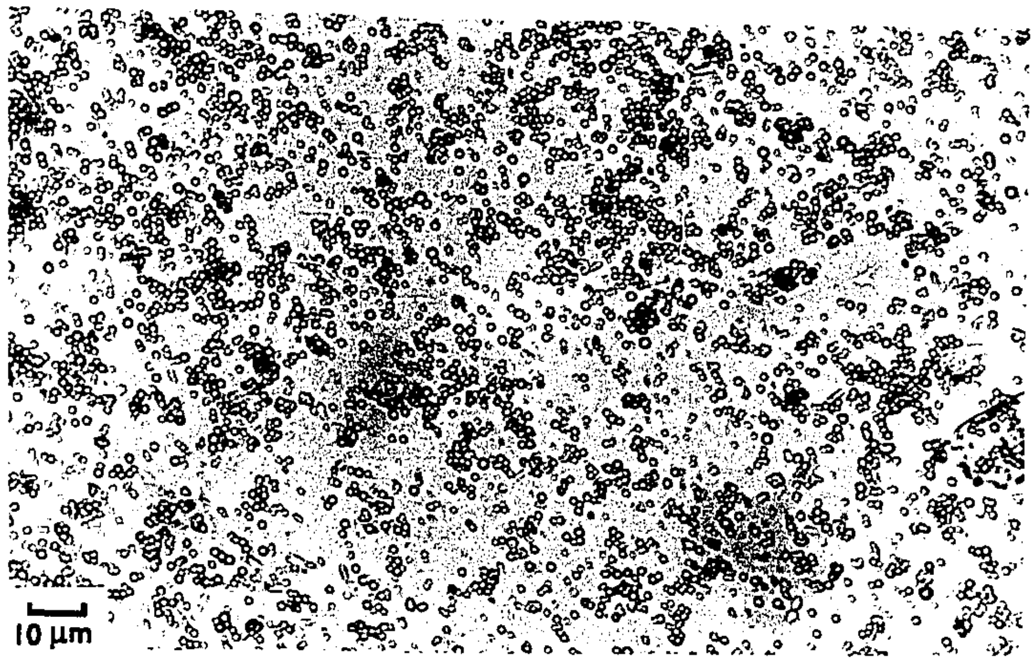


Figure E.1 $\phi$1.6 $\mu$m glass microspheres from Duke Scientific

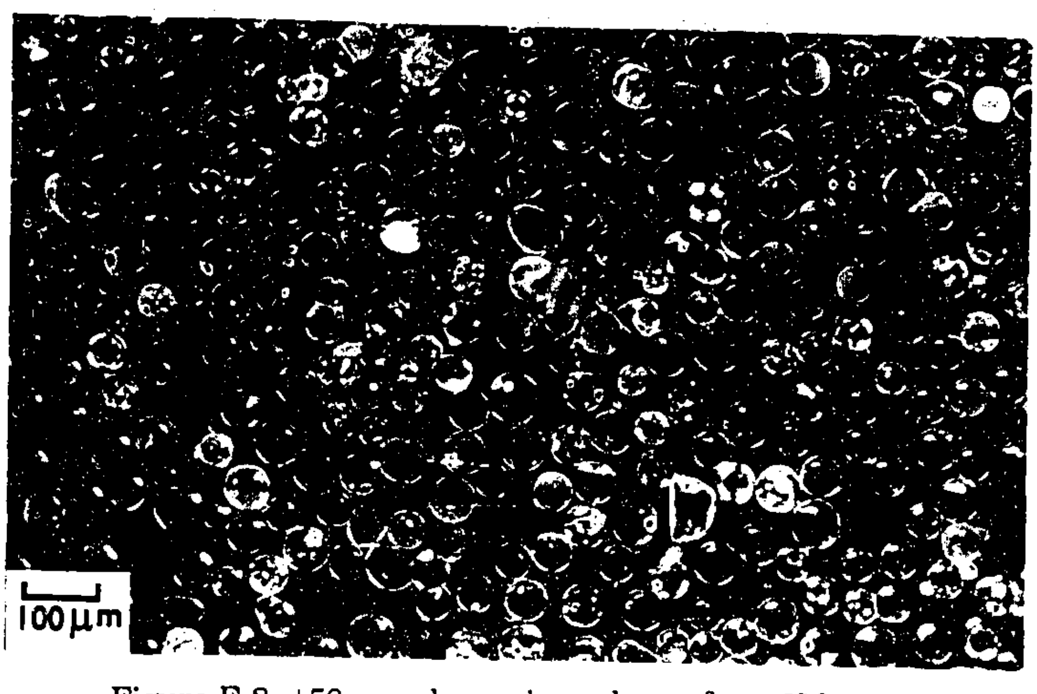


Figure E.2 $\phi$50 $\mu$m glass microspheres from 3M

## APPENDIX F. CALCULATION OF ADSORPTION ENERGY CHANGE WITH CLAY PARTICLES

### 1. Calculation of Interparticle Distance

Assume the shape and size distribution of the clay particles is that illustrated in Figure 4.5 (Pusch 1970), one may use brick-like rectangular parallelepipedons to approximate the irregular-shaped clay particles.

For a given weight of clay, the total number of particles can be readily calculated from their size distribution. The average space for each particle (particle space) can be obtained by dividing the total volume of the adsorption system (i.e., the total volume of the suspended solution) by the total number of particles. The geometry of the particle space is manipulated with computer so that it forms a rectangular parallelepipedon similar to the one (clay rectangular parallelepipedon) used to approximate a clay particle. Assuming particles in a suspension tend to distribute themselves at equal distance apart from one another. The rectangular parallelepipedon clay is then placed in the centre of the particle space with all its six surfaces apart equally from the corresponding surfaces of the particle space respectively (Fig. F.1).

Fit the smallest group of particles in Fig.4.5 into the particle space and obtain the interparticle distance (2 x d in Fig. 4.5). When fit the next group of particles (that is one size larger than the smallest ones) into the particle space, in order to maintain the same interparticle distance as that of the last group, all the three dimensions of the particle space need to be expanded by the dimensional differences between the two groups.

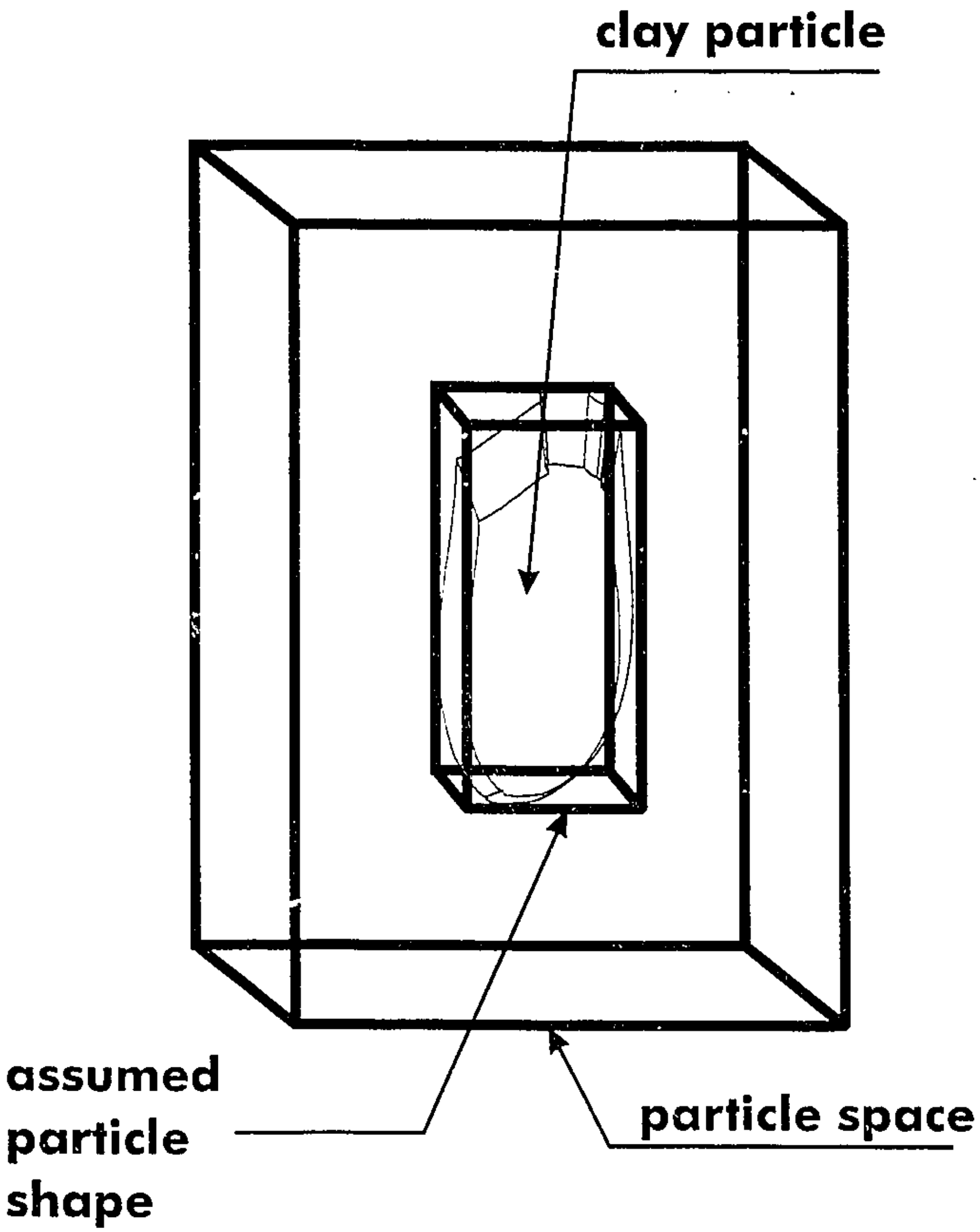


Fig. F.1 Calculation of particle space

Apply the same procedure on groups of all the size distribution. Thus the spaces are summed for all of the particle spaces. Because of the dimensional expansions of the particle spaces to maintain identical interparticle distance, the summed-up volume of all the particle spaces will be larger than the actual total volume of the adsorption system. Using a computer, the calculated total volume is reduced to that of the experimental adsorption system by shrinking all particle spaces proportionally.

A final interparticle distance is then obtained to be used for later calculation of the adsorption energy reduction.

**2. Calculation of Adsorption Energy Reduction**

(1) Calculate $\Delta G_0$ in Figure 2.7

Use Equation 2.12 through Equation 2.16 to calculate $\Delta G_0$. Here the distance x in equation 2.13 equals zero.

(2) Calculate $\Delta G_1$ in Figure 2.7

Use Equation 2.12 through Equation 2.16 to calculate $\Delta G_1$. Here the distance x in equation 2.13 equals 0.5x (interparticle distance calculated from section 1).

(3) Calculate $\Delta G_2$ in Figure 2.7

$\Delta G_2 = \Delta G_0 - (2 \times \Delta G_1)$

(4) Calculate Desorption Caused by the Adsorption Energy Change

Employ Equation 2.20 to calculate the amount of desorption caused by the adsorption energy change, using $\Delta G_2$ and $\Delta G_0$ obtained from (3) and (1). The result is the ratio of the amount of adsorption after and before the impact of the particle concentration effect (ratio of adsorption). The amount of desorption is thus:

original amount of adsorption x (1 - ratio of adsorption)

## REFERENCES


Ahmed, S. M. 1972 "Oxides and Oxide Films" (1) Chap.4.

Andersen, T. N., and Bockris, J. O. M. 1964 "Forces Involved in the "Specific" Adsorption of Ions on Metals From Aqueous Solution." Electrochim. Acta. (9):347-371.

Atkinson, R. J., Posner, A. M., and Quirk, J. P. 1972 J. Inorg. Nucl. Chem.. (34):2201.

Barclay, L., Harrington, A., and Ottewill, R. H. 1972 "The Measurement of Forces Between Particles in Disperse Systems." Kolloid-Z. U. Z. Polymere. (250):655-666.

Barlow, C. A., and Macdonald, J. R. 1967 "Theory of Discreteness of Charge Effects in Electrolyte Compact Double Layer." Advan. Electrochem. Eng.. (6):1-199.

Benjamin, M. M., and Leckie, J. O. 1981 Colloid Interface Sci. (79):209-221.

Bennett, R. H., Bryant, W. R., and Hulbert, M. H. 1991 "Microstructure of Fine-Grained Sediments." Springer-Verlag

Bennett, R. H., Fischer, K. M., Lavoie, D. L., Bryant, W.R., and Rezak, R. 1989 "Porometry and Fabric of Marine Clay and Carbonate Sediments: Determinants of ermeability." Marine Geology. (89):127-152.

Born, N. 1920 "Volumen und Hydratationswärme der Ionen" Z. Phys. (1):45-50

Carter, C. W., and Suffet, I. H. 1982 "Binding of DDT to Dissolved Humic Materials." Envi. Sci. Tech. (16):735-740.

Chandrasekhar, S. 1954 "The Stability of Viscous Flow Between Rotation Cylinders." Mathematika (1):5-13

Chase, R. R. P. 1979 "Settling Behavior of Natural Aquatic Particulates." Limnology & Oceanography, 417-426

Cornet, K., and Burwell, R. L.,Jr. 1968 "Chromium Compount on Silica Gel." J. Amer. Chem. Soc. (90):2489-2494.

Curl, R. L., and Keolelan, G. A. 1984 "Implicit Adsorbate Model for Apparent Anomalies with Organic Adsorption on Natural Adsorbents." Envi. Sci. Tech. (18):916-922.

Davis, J. A., James, R. O., and Leckie, J. O. 1978 "Surface Ionization and Complexation at the Oxide/Water Interface: 1. Computation of Electrical Double Layer Properties in Simple Electrolytes." J. Colloid Interface Sci.. (63)3:480-499.

Davis, J. A., and Leckie, J. O. 1978 "Surface Ionization and Complexation at the Oxid/Water Interface: 2. Surface Properties of Amorphous Iron Oxyhydroxide and Adsorption of Metal Ions." J. Colloid Interface Sci. (67)1:90-107.

Davis, J. A., and Leckie, J. O. 1978 "Surface Ionization and Complexation at the Oxide/Water Interface: 3. Adsorption of Anions." J. Colloid Interface Sci. (67):90-107

Delage, P. and Lefebvre, G. 1984 "Study of the Structure of a Sensitive Champlain Clay and its Evolution During Consolidation." Canadian Geotechnical J. (21):21-35

Derjaguin, B. 1940 "On the Repulsive Forces Between Charged Colloid Particles and on the Theory of Slow Coagulation and Stability of Lyophobe Sols." Trans. Faraday Soc. (36):203-215.

Derrah, R. I., and Ruthven, D. M. 1975 "Sorption of the Inert Gases (Ar, Kr, and Xe) in

Type A Zeolites." Can. J. Chem. (53):996-1005.

Di Toro, D. M., Horzempa, L. M., Casey, M. M., and Richardson, W. 1985 "Reversible and Resistant Components of PCB Adsorption-Desorption Effects." Great Lakes Res. (8):336-349.

Di Toro, D. M., Mahony, J. D., Kirchgraber, P. R., O'Byrne, A. L., Pasquale, L. R., and Piccirilli, D. C. 1986 "Effects of Nonreversibility, Particle concentration, and Ionic Strength on Heavy Metal Sorption." Envi.Sci.Tech. (20):55-61.

Donelly, R. J. 1968 "Experiments on the Stability of Viscous Flow Between Rotatin Cylinders." Proc. Roy. Soc. (246A):312-325

Dugger, D. L., Stanton, J. H., Irby, B. N., McConnell, B.L., Cummings, W. W. and Maatman, R. W. 1964 "The Exchange of Twenty Metal Ions with the Weakly Acidic Silanol Group of Silica Gel" J. Phys. Chem. (68):757-767

Enfield, C. E., Harlin, C. C., Jr., and Bledsoe, B. E. 1976 "Comparison of Five Kinetic Models for Orthophosphate Reactions in Mineral Soils." Soil Sci. Soc. Am. J. (40):243-249

Everett, K. H., and Radke, C. J. 1975 "Thermodynamics of Adsorption and Interparticle Forces." in "Adsorption at Interfaces" Mittal, K. L. ed. Am. Chem. Soc.

Garcia-Bengochea, I., Lovell, C. W., and Altschaeffl, A. G. 1979 "Pore Distribution and Permeability of Silty Clays." J. Geotechnical Engineering Division. 839-855.

Grahame, D. C. 1947 "The Electrical Double Layer and the Theory of Electrocapillarity." Chem. Rev. (41):441-501.

Griffin, R. A., and Au, A. K. 1977 "Lead Adsorption by Montmorillonite Using a Competitive Langmuir Equation." Soil Sci. Soc. (41):880-882.

Grover, R., and , R. J. 1970 "Effect of Ratio of Soil to Water on Adsorption of Linuron and Atrazine." Soil Sci. (109):136-138.

Gschwend, P.M., and Wu, S. 1985 "On the Constancy of Sediment-Water Partition Coefficientsof Hydrophic Organic Pollutants" Environ. Sci. Technol. (19)1:90-96

Hathaway, B. J., and Lewis, C. E. 1969a "Electronic Properties of Transition-Metal Complex Ions Adsorbed on Silica Gel: Part I. Nickel (II) Complexes." J. Chem. Soc. London. 1176-1183.

Hathaway, B. J., and Lewis, C. E. 1969b "Electronic Properties of Transition-Metal Complex Ions Adsorbed on Silica Gel: Part II. Cobalt (II) and Cobalt (III)." J. Chem. Soc. London. 1183-1188.

Healy, T. W., Yates, D. E., White, L. R., and Chan, D. 1977 "Nernstian and Non-Nernstian Potential Differences at Aqueous Interfaces." J. Electroanal. Chem. (80):57-66.

Hingston, F. J. 1981 in "Adsorption of Inorganics at Solid-Liquid Interfaces" chapter 3. Anderson, M. A. & Rubin ed., Ann Arbor Science.

Honeyman, B. D. 1984 Ph. D. thesis. Stanford University.

Hunter, R. J., and Wright, H. J. L. 1971 "Dependence of Electrokinetic Potential on the Concentration of Electrolyte." J. Colloid Interface Sci. (37):564-574.

Ives, K. J. and Bhole, A. G. 1975 "Study of Flowthrough Couette Flocculators-I. Design for Uniform and Tapered Flocculation" Water Research (9):1085-1092

Ives, K. J. and Bhole, A. G. 1977 "Study of Flowthrough Couette Flocculators-II. Laboratory Studies of Flocculation Kinetics" Water Research (11):209-215

James, R. O., and Healy, T. W. 1972a "Adsorption of Hydrolyzable Metal Ions at the Oxide-Water Interface: (I) Co(II) Adsorption on $SiO_2$ and $TiO_2$ as Model Systems." J. Colloid Interface Sci. (40):42-52.

James, R. O., and Healy, T. W. 1972b "Adsorption of Hydrolyzable Metal Ions at the Oxide-Water Interface: (II)Charge Reversal of $SiO_2$ and $TiO_2$ Colloids by Adsorbed Co(II), La(III) and Th(IV) as Model Systmes." J. Colloid Interface Sci. (40):53-64.

James, R. O., and Healy, T. W. 1972c "Adsorption of Hydrolyzable Metal Ions at the Oxide-Water Interface: (III) A Thermodynamic Model of Adsorption." J. Colloid Interface Sci. (40):65-81.

Karickhoff, S. W. 1984 "Organic Pollutant Sorption in Aquatic Systems." J. Hydrau. Eng. 110:707-735.

Kurbatov, M. H., and Wood, G. B. 1952 J. Phys. Chem. (56):698-701.

Laidler, K. J. and Muirhlad-Gould, J. S. 1967 "Continuous Dielectric Model for Hydration of Monotomic Ions" Trans. Faraday Soc. (63):953-957

Laidler, K.J. and Pegis, C. 1957 "The Influence of Dielectric Saturation on the Thermodynamic Properties of Aqueous Ions" Proc. Roy. Soc. Ser.A (241):80-92

Lal, D. 1977 "The Oceanic Microcosm of Particles" Science (198):997-1009

Lambe, T. W. and Asce, M. 1958 "The Engineering Behavior of Compacted Clay" J. Soil Mechanics & Foundations Div., Proc. Am. soc. Civil Eng. Paper 1655.

Levine, S., Mingins, J., and Bell, G. M. 1967 "The Discrete-Ion Effect in Ionic Double Layer." J. Electroanal. Chem. Interfacial Electrochem. (13):280-329.

Li, Y. H., Burkhardt, L., Buchholtz, M., O'Hara, P., Santschi, P. H., " Partition of Radiotracers between Suspended Particles in Sea Water" 1984 Geochim. Cosmochim. Acta. 48:2011-2019.

Liebau, F. 1985 "Structural Chemistry of Silicates." Spring-Verlag

Lotse, E. G., Graetz, D. A., Chesters, G., Lee, G. B., and Newland, L. W. 1968 "Lindane Adsorption by Lake Sediments."Envi. Sci. Tech. (2):353-357.

Lyklema, J. 1971 "The Electrical Double Layer on Oxides." Croat. Chim. Acta. 43:249-274.

Mackay, D. and Powers, B. 1987 "Sorption of Hydrophobic Chemicals From Water: A Hyppothesis for the Mechanism of the Particle Concentration Effect." Chemosphere (16):745-757.

McGrail, B. P., Pederson, L. R., and Petersen, D. A. 1986 "The Influence of Surface Potential and pH on the release of Sodium from Na2O.3SiO2 Glass." Physics and Chemistry of Glasses. 27 No.2:59-64.

McKinley, J. P. and Jenne, E. A. 1991 "An Experimental Investigation and Review of the Solids Concentration' Effect." Environ. Sci. & Tech. (25):2082-2087

Mehta, A. J., Hayter, E. J., Parker, W. R., Krone, R. B. and Teeter, A. M. 1989 "Cohesive Sediment Transport. I: Process Description." J. Hydr. Eng. (115)8:1076-1094.

Migniot, C. 1986 "A Study of the Physical Properties of Different Very Fine Sediments and Their Behavior Under Hydrodynamic Action." La Houille Blanche (7):591-620

Morel, F. M. M., and Gschwend, P. M. 1987 in "Aquatic Surface Chemistry." Stumm, W. ed., John Wiley & Sons

Muirhead-Gould, J.S. and Laidler, K. J. 1967 "Continuous Dielectric Model for Hydration of Dipolar Molecules" Trans. Faraday Soc. (63):958-965

Nyffeler, U. P., Li, Y. H., and Santschi, P. H. 1984 "A Kinetic Approach to Describe Trace-

Elemnt Distribution Between Particles and Solution in Natural Aquatic Systems" Geochim. Cosmochim. Acta. (48):1513-1522.

Nyffeler, U. P., Li, Y. H., and Santschi, P. H. 1986 "The Relevance of Scavenging Kinetics to Modeling of Sediment-Water Interactions in Natural Waters" Limnol.Oceanogr. (31):227-292.

O'Connor, D. J., and Connolly, J. P. 1980 "The Effect of Concentration of Adsorbing Solids on the Partition Coeffficient." Water Res. (14):1517-1523.

Ottewill, R. H. 1985 "Didpersed Systems: Recent Developments." Bunsenges Phys. Chem. (89):517-525.

Parker, W. R. and Kirby, R. 1977 "Fine Sediment Studies Relevant to Dredging Practice and Control." Proc., 2nd Int. Symp. on Dredging Tech., Paper B2, British Hydraulic Research Association-Fluid Engineering, Texas A & M University, College Station, Tex, 15-26

Parks, G. A. 1975 "Adsorption in the Marine Environment." Chemical Oceanography. 2nd ed.:Chap.4.

Partheniades, E. 1965 "Erosion and Deposition of Cohesive Soils." J. Hydr. Div. 91(1):105-139.

Penrose, W. R., Karttunen, J. O., and Mehlhaff, P. 1985 "Effects of Dissolved Organic Carbon on the Adsorption Properties of Plutonium in Natural Waters." Envi. Sci. Tech. (19):127-131.

Pusch, R. 1970 "Microstructural Changes in Soft Quick Clay at Failure." Canadian Geotechnical Journal. (7):1-7.

Rayleigh, L. 1917 " On the Dynamics of Revolving Fluids" Proc. Roy. Soc. (93A):148-154.

Ross, S., and Olivier, J. P. 1964 "On Physical Adsorption." Interscience Publishers

Ruthven, D. M. 1984 "Principles of Adsorption and Adsorptin Processes" John Wiley & Sons

Sacher, E. and Laidler, K. J. 1964 in Modern Aspects of Electrochemistry (J. O. Bockris and B. E. Conway ed.) Vol.3. Butterworths, London.

Santschi, P. H. 1984 "Particle Flux and Trace Metal Residence Time in Natural Waters." Limnol. Oceanogr. (29):1100-1108.

Schindler, P., Fürst, B., Dick, R., and Wolf, P. 1976 "Ligand Properties of Surface Silanol Groups." J. Colloid Interface Sci. (55):469-475.

Schindler, P., Fürst, Wälti, E., and Furst, B. 1976 "The Role of Surface Hydroxyl Groups in the Surface Chemistry of Metal Oxides." Chimia. (30)2.

Sridharan, A., Asce, A. M. Altschaeffl, A. G., Asce, M. and Diamond, S. 1971 "Pore Size Distribution Studies" J. Soil Mechanics & foundations Div., Proc.Am. Soc. Civil Eng. 771-787

Stewart, R. F., Whitehead, M. A., and Donnay, G. 1980 "The Ionicity of the Si-O Bond in Low-Quartz." Am. Miner. 65:324-326.

Stumm, W., Huang, C. P., and Jenkins, S. R. 1970 "Specific Chemical Interaction Affecting the Stability of Dispersed Systems." Croat. Chem. Acta. (42):223-245.

Stumm, W. and Morgan, J. J. 1981 "Aquatic Chemistry" 2nd ed. John Wiley & Sons.

Taylor, G. I. 1923 "Stability of a Vicous Liquid Contained Between Two Rotation Cylinders" Phil. Trans. Roy. Soc. (223A):289-343

Taylor, G. I. 1935 "Distributiion of Velocity and Temperature Between Concentric Rotation

Cylinders." Proc. Roy Soc. (151A):494-512
Taylor, G. I. 1923 "Fluid Friction Between Rotation Cylinders." Proc. Roy. Soc. (157A):546-578
Van Duuren, F. A. 1968 "Defined Velocity Gradient Model Flocculator." J. sanit. Engng. Div. Am. Soc. Civ. Engrs. (94 SA4): 671-682
Van Olphen 1977 "An Introduction to Clay Colloid Chemistry" 2nd ed. John Wiley & Sons.
Verwey, E. J. W., and Overbeek, J. T. G. 1948 "Theory of the Stability of Lyophobic Colloids."
Voice, T. C., Rice, C. P., and Webger, W. J., Jr. 1983 "Effect of SolidsContion on the Sorptive Partitioning of Hydrophobic Pollutants in Aquatic Systems." Envi. Sci. Tech. 513-518.
Washburn, E. W. 1921 "A Note on a Method of Determining the Distribution of Pore-Size in a Porous Material." Proc. National Academy of Science (7):115-118
Yates, D. E. 1975 "The Structure of the Oxide/Aqueous Electrolyte Interface." Ph.D. Thesis. University of Melbourne:Australia.